AD-A154 039 MEASUREMENT OF MODE INTERACTION DUE TO WAVEGUIDE SURFACE ROUGHNESS(U) NAVAL POSTGRADUATE SCHOOL MONTEREY CA S R KASPUTIS ET AL. DEC 84 1/2

UNCLASSIFIED F/G 9/1 NL

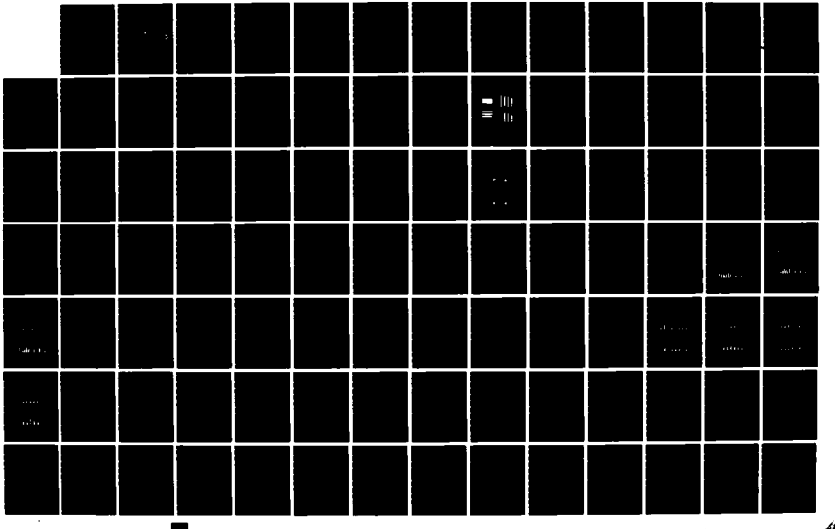

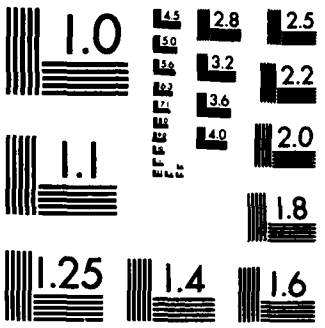

(2)

NAVAL POSTGRADUATE SCHOOL

Monterey, California

THESIS

MEASUREMENT OF MODE INTERACTION DUE TO
WAVEGUIDE SURFACE ROUGHNESS

by

Stephen R. Kasputis

and

Paul D. Hill

December 1984

Thesis Advisor: H. Medwin

Approved for public release; distribution unlimited

UNCLASSIFIED

SECURITY CLASSIFICATION OF THIS PAGE (When Data Entered)

REPORT DOCUMENTATION PAGE	READ INSTRUCTIONS BEFORE COMPLETING FORM
1. REPORT NUMBER	2. GOVT ACCESSION NO. AD-A154 039	3. RECIPIENT'S CATALOG NUMBER
4. TITLE (and Subtitle) Measurement of Mode Interaction Due to Waveguide Surface Roughness	5. TYPE OF REPORT & PERIOD COVERED Master's Thesis (December 1984) 6. PERFORMING ORG. REPORT NUMBER
7. AUTHOR(s) Stephen R. Kasputis Paul D. Hill	8. CONTRACT OR GRANT NUMBER(s)
9. PERFORMING ORGANIZATION NAME AND ADDRESS Naval Postgraduate School Monterey, California 93943	10. PROGRAM ELEMENT, PROJECT, TASK AREA & WORK UNIT NUMBERS
11. CONTROLLING OFFICE NAME AND ADDRESS Naval Postgraduate School Monterey, California 93943	12. REPORT DATE December 1984 13. NUMBER OF PAGES 164
14. MONITORING AGENCY NAME & ADDRESS(if different from Controlling Office) Naval Postgraduate School Monterey, California 93943	15. SECURITY CLASS. (of this report) UNCLASSIFIED 15a. DECLASSIFICATION/DOWNGRADING SCHEDULE
16. DISTRIBUTION STATEMENT (of this Report) Approved for public release; distribution unlimited	
17. DISTRIBUTION STATEMENT (of the abstract entered in Block 20, if different from Report)	
18. SUPPLEMENTARY NOTES	
19. KEY WORDS (Continue on reverse side if necessary and identify by block number) Waveguide, mode coupling, scattering, dispersion	

20. ABSTRACT (Continue on reverse side if necessary and identify by block number)

A laboratory experiment was conducted examining the effects of large slope surface roughness on mode propagation in a rigid walled waveguide. A waveguide hundreds of depths in length was developed, as well as a mode transduction system comprised of electret type mode transducers, and an amplitude and phase selectable amplifier. A device for automatically measuring surface roughness was also built. The interaction of modes with two types of surface roughness, deterministic and random, is compared to propagation in the smooth

DD FORM 1 JAN 73 1473 EDITION OF 1 NOV 65 IS OBSOLETE

S N 0102-LF-014-6601

UNCLASSIFIED

SECURITY CLASSIFICATION OF THIS PAGE (When Data Entered)

waveguide. The results demonstrate coupling between modes and difference of this coupling in the presence of either a deterministically rough surface or a randomly rough surface. A significant change in modal phase speed due to roughness is demonstrated at selected frequencies.

Keywords included

19

Approved for Public Release, Distribution Unlimited

Measurement of Mode Interaction Due to Waveguide Surface Roughness

by

Stephen R. Kasputis
Lieutenant, United States Navy
B.S., Pennsylvania State University, 1977

and

Paul D. Hill
Lieutenant, United States Navy
B.S., Miami University, 1978

Submitted in partial fulfillment of the
requirements for the degree of

MASTER OF SCIENCE IN ENGINEERING ACOUSTICS

from the

NAVAL POSTGRADUATE SCHOOL
December 1984

Author: Stephen R Kasputis
Stephen R. Kasputis

Author: Paul D Hill
Paul D. Hill

Approved by: _____
Herman Medwin, Thesis Advisor

Lawrence J. Ziomek
Lawrence J. Ziomek, Second Reader

James V. Sanders
James V. Sanders, Chairman,
Engineering Acoustic Academic Committee

John Dyer
John Dyer, Dean of Science and Engineering

ABSTRACT

A laboratory experiment was conducted examining the effects of large slope surface roughness on mode propagation in a rigid walled waveguide. A waveguide hundreds of depths in length was developed, as well as a mode transduction system comprised of electret type mode transducers, and an amplitude and phase selectable amplifier. A device for automatically measuring surface roughness was also built. The interaction of modes with two types of surface roughnesses, deterministic and random, is compared to propagation in the smooth waveguide. The results demonstrate coupling between modes and difference of this coupling in the presence of either a deterministically rough surface or a randomly rough surface. A significant change in modal phase speed due to roughness is demonstrated at selected frequencies.

TABLE OF CONTENTS

LIST OF TABLES

LIST OF FIGURES

III. MEASUREMENT THEORY

For simplicity, consider propagation of a single frequency. The method for measuring modes is based upon the observation that the pressure at any point in the waveguide is a superposition of each of the modes present in the waveguide at that point [Ref. 4]. At a fixed range, the observed pressure varies with depth as the sum of all the modes varies. This is shown for an example of three modes at a fixed instant in time. (Fig. 6) If measurements are taken at as many depths as there are modes, a system of linear equations is obtained such as the following:

$$P(z_0) = a_{00} P_0 + a_{01} P_1 + a_{02} P_2$$
$$P(z_1) = a_{10} P_0 + a_{11} P_1 + a_{12} P_2$$
$$P(z_2) = a_{20} P_0 + a_{21} P_1 + a_{22} P_2$$

The terms on the left hand side of each equation are the pressures observed in the waveguide at the corresponding depths. The P_n terms on the right hand side are the pressure amplitudes of the modes assumed present in the waveguide. The transformation that relates these two quantities is contained in the coefficients a_{ij}, where i is the depth coordinate and j is the mode contribution. The notation employed relates directly to the modes. Mode 0 is the plane wave mode and it has the j subscript 0. Mode 1 is the next higher mode, having pressure maxima at the walls but going through one minimum at mid depth. Mode 1 has the j subscript 1. Logical extension shows that the j subscript,

4. The Timing Simulator

The Interface Technology model RS-648 timing simulator triggers the signal generator, OPHELEA, and the wave analyzer at the intervals required to provide coordination between the system components. It has a rated timing resolution of 50 nanoseconds.

A detailed listing of the equipment settings is contained in Appendix C.

Table 1

Filtering and Monitoring Equipment

Component	Description
Oscilloscope	Kikusui COS5060 dual trace
Frequency synthesizer	General Radio, 1162A decade frequency synthesizer
Frequency counter	Hewlett Packard, model 5223L
Bandpass filter	Krohn-Hite frequency filter, model 3550
Voltage amplifier	Princeton Applied Research Amplifier, model 113

a. OPHELEA

OPHELEA is a computer designed especially for data acquisition and analog/digital conversion. It was designed by the Special Projects Section of the Naval Air Development Center with its primary component an Interdata model 70 computer that is programmable in both FORTRAN and BASIC. It has a 64 thousand byte core memory and magnetic disk drives. Data is stored in 12 bit words. The computer is connected to a Phoenix analog to digital converter, model ADC 712. This A/D converter is capable of encoding input signals of up to 10 volts into digital form with an accuracy of one part in 4000. The system is extremely fast, with a maximum data sampling rate of 450,000 samples per second. Output from the system is through a Texas Instruments data terminal which is a combined keyboard and line printer.

b. Nicolet FFT Wave Analyzer

The Nicolet Scientific Corporation model 660B wave analyzer is programmable and performs its own analog to digital conversion. The sampling rates are limited to manufacturer selected values and a maximum of 250,000 samples per second. It has a built-in CRT screen that allows real time observation of either the received signal or its spectrum.

c. Input Filters, Amplifiers, and Monitors

A summary of the other instruments used in received signal filtering and monitoring is included in Table 1.

b. Wavetek Arbitrary Waveform Generator

The Wavetek Arbitrary Signal Generator, model 175, is a multifunction, programmable signal generator that is crystal oscillator controlled. The crystal oscillator provides excellent frequency stability and phase locking, but enables periodic transmission at discrete frequencies only. The programmable feature allows the user to drive the source with a signal of arbitrary shape. This is used to drive the source with a signal of several strong Fourier components, though all the harmonics are still limited to multiples of the crystal oscillator fundamental.

2. The Receive System

The receiver system employs Bruel and Kjaer 1/2" microphones as the primary detection device. The pre-amplifiers are Bruel and Kjaer, model 2619. To take measurements of the pressure inside the waveguide, the microphone is attached to a vertical probe made of 4 mm outside diameter and 3 mm inside diameter steel tubing. This introduces significant viscous losses from the tubing walls, but these are minimized by tuning the probe length to the fundamental frequency. Prior to signal processing, the signal is amplified by an HP voltage amplifier to reduce the effects of line noise entering the system through transmission lines.

3. The Signal Processing System

The signal processing system is composed of input filters and two separate analysis subsystems: OPHELEA, a special purpose computer and a Nicolet FFT Wave Analyzer.

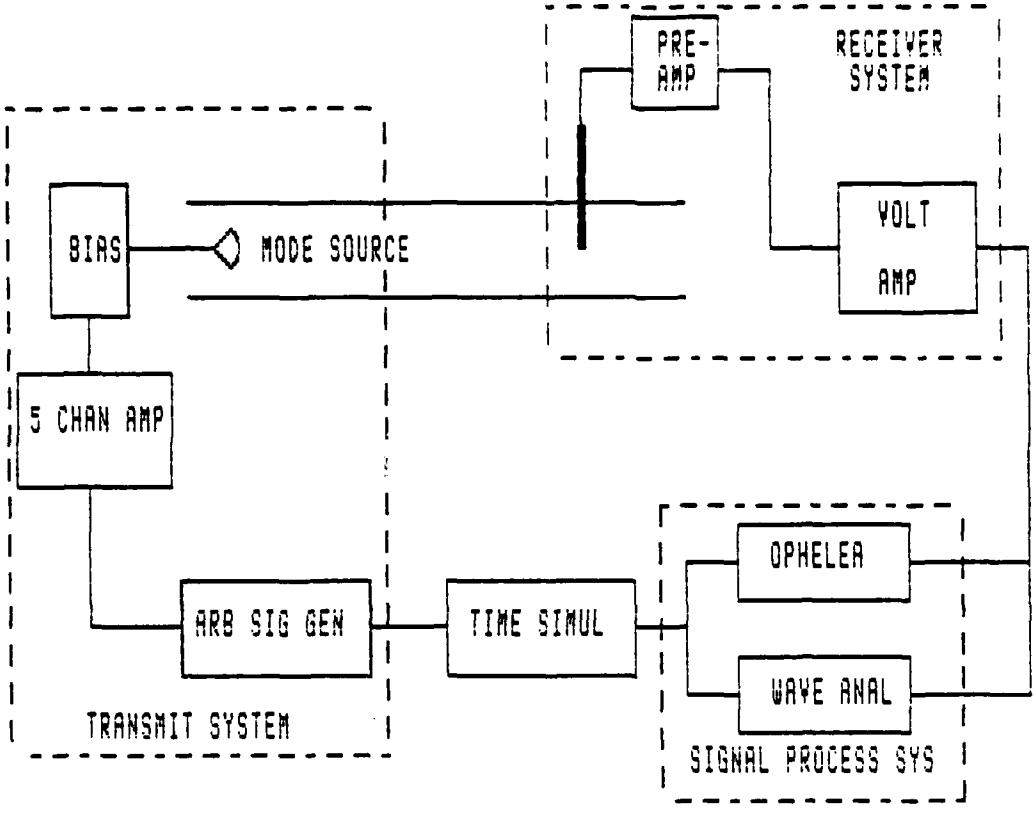

Figure 5. Experimental Setup.

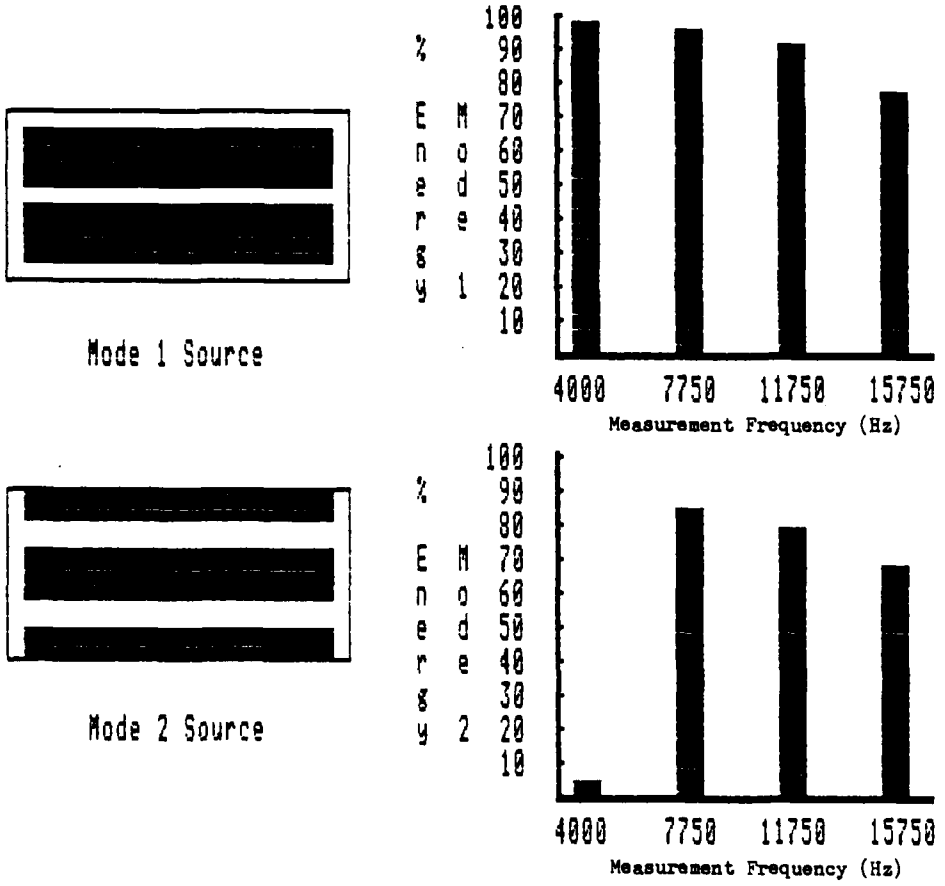

Figure 4. Mode Sources and Source Frequency Response.

frequencies up to 12000 Hertz (Hz) and 73 percent for frequencies up to 16000 Hz (Fig. 4). This simplifies the analysis of data for frequencies that would otherwise have high modal densities.

3. Random Surface Measuring Device

The Random Surface Measuring device (RSM) allows the accumulation of a large data base for statistics on a given surface. It is capable of taking 1,200 samples of the surface per hour and with a depth discrimination of 20 micrometers. This large sampling provides meaningful statistics and the resolution provides a high degree of accuracy. Details of its construction and operation are included in Appendix B.

B. OCEAN PHYSICS LABORATORY

The experiment was conducted in the Ocean Physics Laboratory at the Naval Postgraduate School. A diagram of the experimental set-up is shown in Figure 5 and is described below:

1. Transmit System

The mode sources and multichannel amplifier have already been discussed in section II-A-2. For point sources, Bruel and Kjaer microphones are used. In all cases, the driving signal is from either a Wavetek Signal Generator or a Wavetek Arbitrary Waveform Generator (ARB).

a. Wavetek Signal Generator

The Wavetek Phaselock Signal Generator, model 186, provides selectable output signal forms, such as a square wave or sinusoidal wave. Its primary advantage over the ARB is that it covers a continuous frequency spectrum.

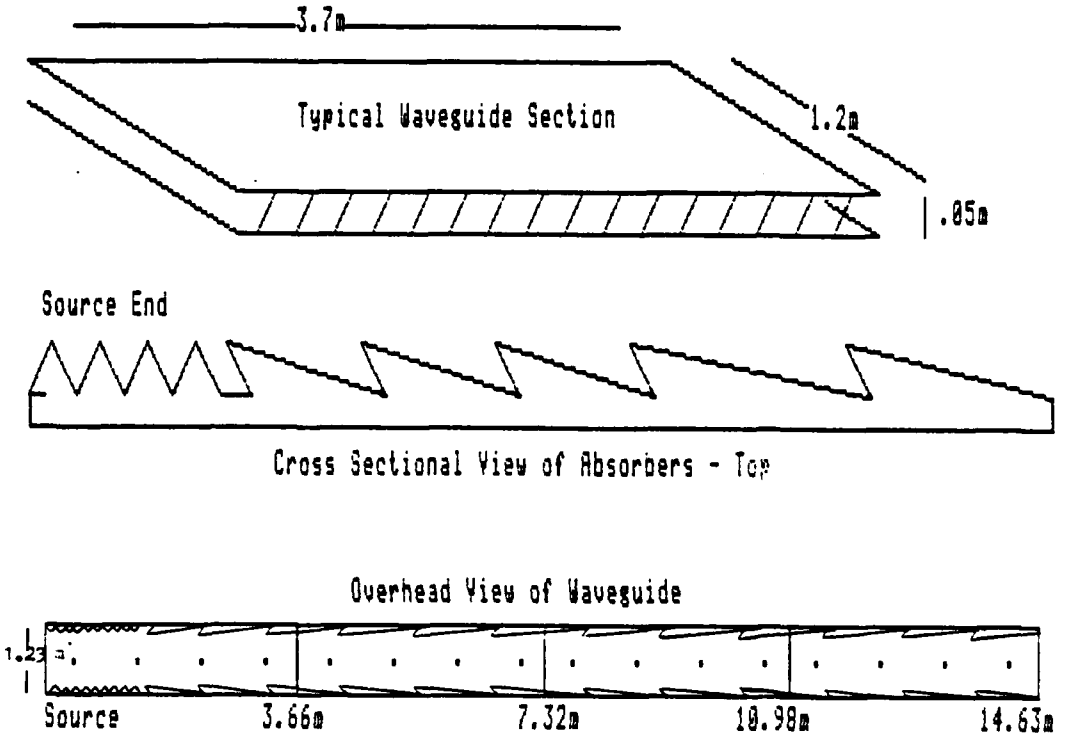

Figure 3. Waveguide Design Overview.

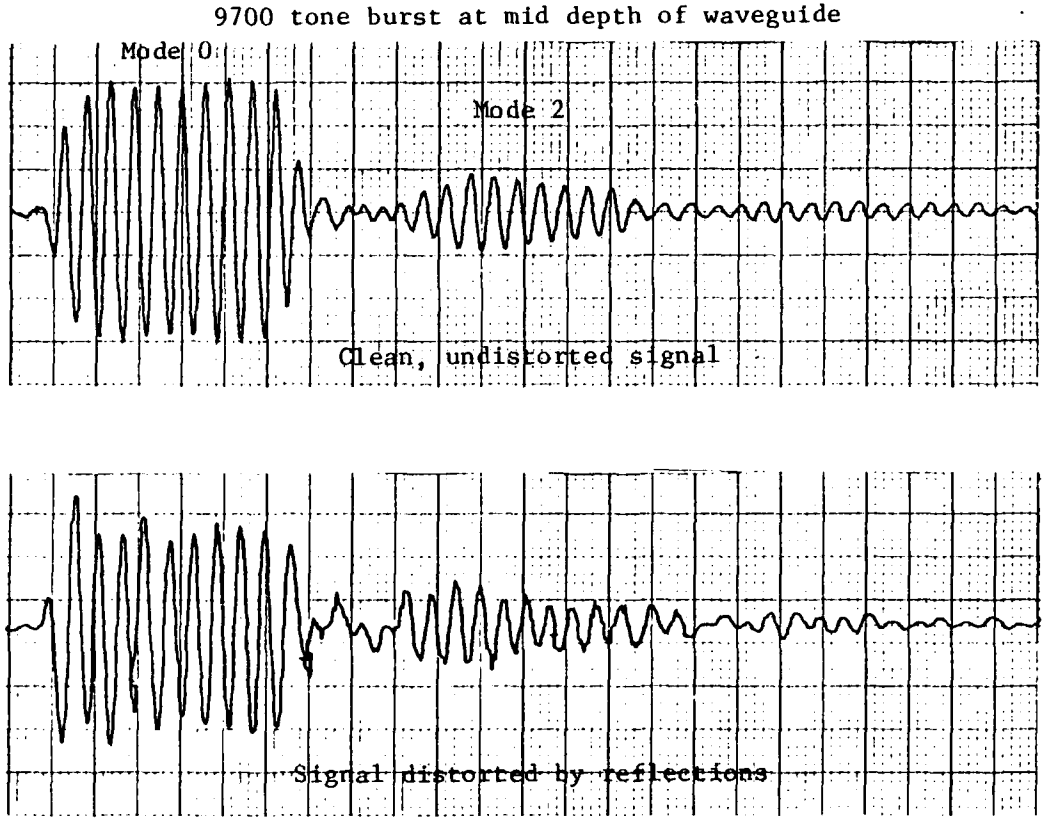

Figure 2. Analysis of Absorber Shape.

At A, over half of wedge face is shadowed
from the wave front by the preceding wedge.

At B, over half the sawtooth is shadowed;
relocating the sawtooth to C reduces shadowing.

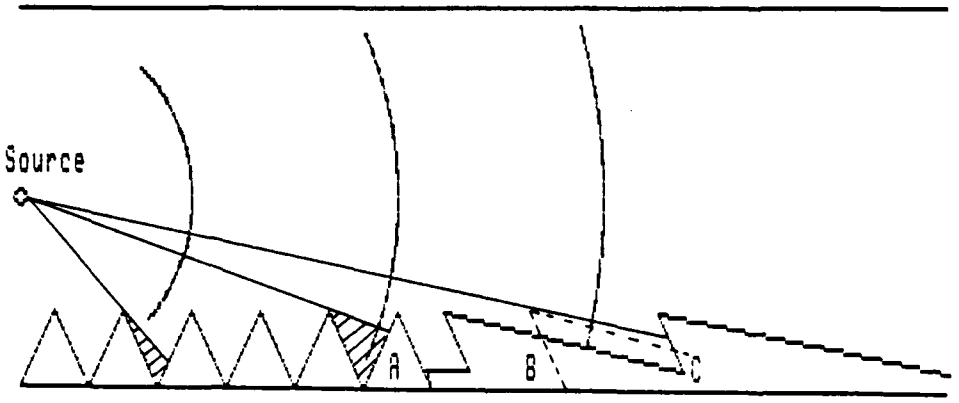

Figure 1. Shadowing of Absorbers.

b. Final Design

Controlled by these constraints, a final design for the waveguide evolved. The resultant waveguide is 14.6 meters long, 1.23 meters wide and 0.05 meters in depth. It is constructed of aluminum plates and gypsum board. Four aluminum plates, each 3.66 meters long by 1.23 meters wide and 0.0095 meters thick are used for the top surface of the waveguide. These plates are reinforced with aluminum channel to minimize their sagging. They are suspended from the ceiling by wires and turnbuckles and joined together to make the 14.6 meter by 1.23 meter top surface. By adjusting the turnbuckles, the height of the waveguide is maintained at 5.19 $\pm$ .14 cm. The top plates are mass loaded by a layer of sand to damp shear waves which may propagate along them. Holes are drilled in these plates every 0.91 meters starting 0.405 meters from one end. These holes accommodate a microphone probe tube of 5 mm diameter which samples the sound field in the waveguide at these intervals. The bottom surface of the waveguide is made of gypsum board sections 2.46 meters long by 1.23 meters wide by 0.013 meters thick. The gypsum board is used since it provides a smooth rigid surface and does not support shear waves.

To achieve the desired cylindrical spreading of the sound field, fiberglass absorbers are placed along the sides of the waveguide. Common dense duct insulation of 5 pounds per cubic foot scatters more than it absorbs at shallow grazing angles of less than 15 degrees. Therefore, low density fiberglass of one pound per cubic foot is used. Signal interference from side reflections in the initial experiments showed the need to increase the distance between wedges

The experiment conducted for this thesis provides some preliminary data in this area. A cylindrical laboratory waveguide was chosen in that it provided a prototype of real ocean ducts, yet it was simple and sufficiently controlled to allow examination of the mechanism of mode interactions. The experiment was designed to examine the effects of both deterministically rough surfaces and randomly rough surfaces.

I. INTRODUCTION

The purpose of this thesis is to examine mode interaction due to surface roughness in a rigid walled waveguide. Of particular interest are roughnesses with large slopes and sharp edges. Though much theoretical and experimental work has been done for gentle roughnesses, where the Kirchhoff approximation is applicable, development of a theory for surfaces with large slopes only began in the 1950's with independent work by Twersky [Ref. 1] and Biot [Ref. 2] Biot treated roughness elements as monopole and dipole scatterers and summed the effects of these scatterers over the surface. Most notably this work has been continued by I. Tolstoy [Ref. 3] who has extended the ideas of Biot. From Tolstoy's work [Ref. 4] for example, decreases in phase velocities and the existence of boundary waves are predicted for grazing, low frequency propagation over a rough surface.[1] L. Dozier [Ref. 5] has studied the problem for sonar applications by using the parabolic equation and S. McDaniel [Ref. 6] has written about the effects of roughness on mode coupling in a waveguide. Yet, developement of a cohesive understanding of roughness effects in a confined channel has been hindered by a lack of experimental data.

---

[1]Tolstoy's waveguide development is for a rigid bottom and a pressure release surface. Therefore, his predictions do not apply directly to this thesis, but the general phenomena he predicts provide insight into the effects being investigated.

ACKNOWLEDGEMENT

The writers wish to express their appreciation to Professor Herman Medwin of the Physics Department, U.S. Naval Postgraduate School for his guidance and encourgement during the preparation of this thesis; to Dr. Jorge Novarini for the sharing of his knowledge on waveguides; to Mr. Gerald D'Spain for his physical insight and computer programming; and to Mr. Bob Moeller for his invaluable assistance in the construction of the necessary special purpose equipment; and to our wives for their infinite patience and immeasurable assistance in the preparation of this thesis.

The Modes Present at A Fixed Time, t, and the Observed Vertical Pressure Distribution

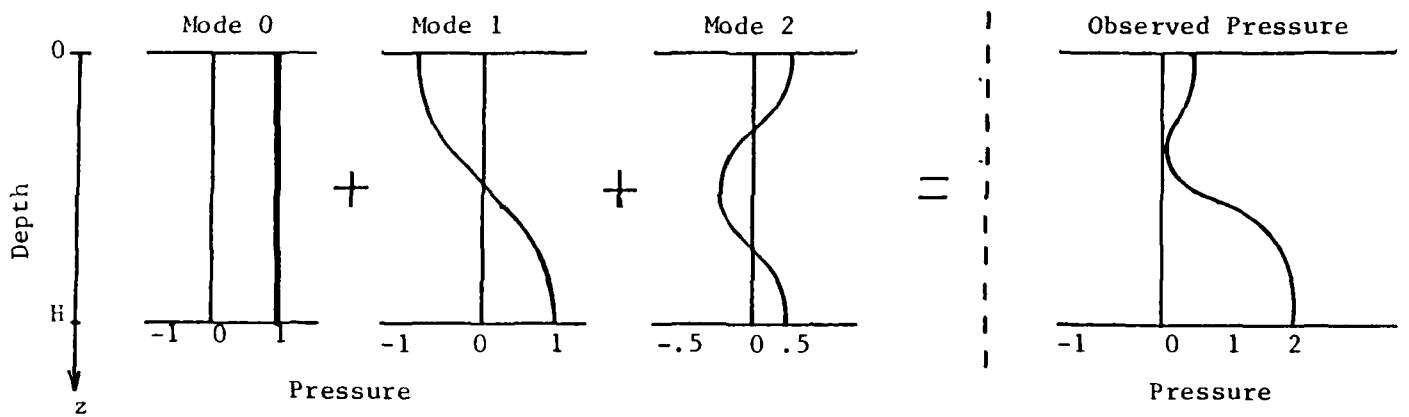

Figure 6. Pressure as Mode Superposition.

or mode number, corresponds to the number of minimums that mode has in a rigid-rigid waveguide. Examining the a_{ij}'s, the method of this becomes clear. For example, $a_{00}=a_{10}=a_{20}=1$; however, $a_{01}=-a_{21}=1$ and $a_{11}=0$. For a fixed second subscript, j, the a_{ij}'s correspond to the eigenfunction of the mode j. Recall that for a rigid-rigid waveguide, the normalized eigenfunctions for each mode j are $\cos(jzk_z)$ where k_z is pi divided by the waveguide height, h. Direct comparison of this form of the eigenfunction with the a_{ij}'s will show exact agreement when z takes on values of 0, h/2, and h.

In order to obtain the modal distribution in the waveguide then, it suffices to take measurements of the pressure at each depth and solve the linear system $P(z)=A\ P_m$, where A is the matrix of coefficients a_{ij} (Fig. 7).

This simple model is slightly complicated because the P(z) column vector is complex. It contains both phase and amplitude data, but this is a bonus. Solving the linear system yields amplitude information about the mode distribution as well as the relative phase relations of the modes present at the measurement frequency.

The above description is most easily understood for a single frequency. In practice, a non-sinusoidal signal is propagated and the FFT of the received signal is analyzed. Take as an example a triangular pulse; multiplying its frequency spectrum by the frequency response of the electret transducers results in a transmitted signal spectrum with strong components up to 24,000 Hz (Fig. 8). For the smooth waveguide, this one data run provides information about many frequencies and with a signal to noise ratio greater than 20 dB. This

depth	mode 0	mode 1	mode 2	mode 3	mode 4	mode 5
top	1.0	1.0	1.0	1.0	1.0	1.0
1 cm	1.0	0.8	0.3	-0.3	-0.8	-1.0
2 cm	1.0	0.3	-0.8	-0.8	0.3	1.0
3 cm	1.0	-0.3	-0.8	0.8	0.3	-1.0
4 cm	1.0	-0.8	0.3	0.3	-0.8	1.0
bottom (5 cm)	1.0	-1.0	1.0	-1.0	1.0	-1.0

Figure 7. Matrix A for Six Depths and Six Modes.

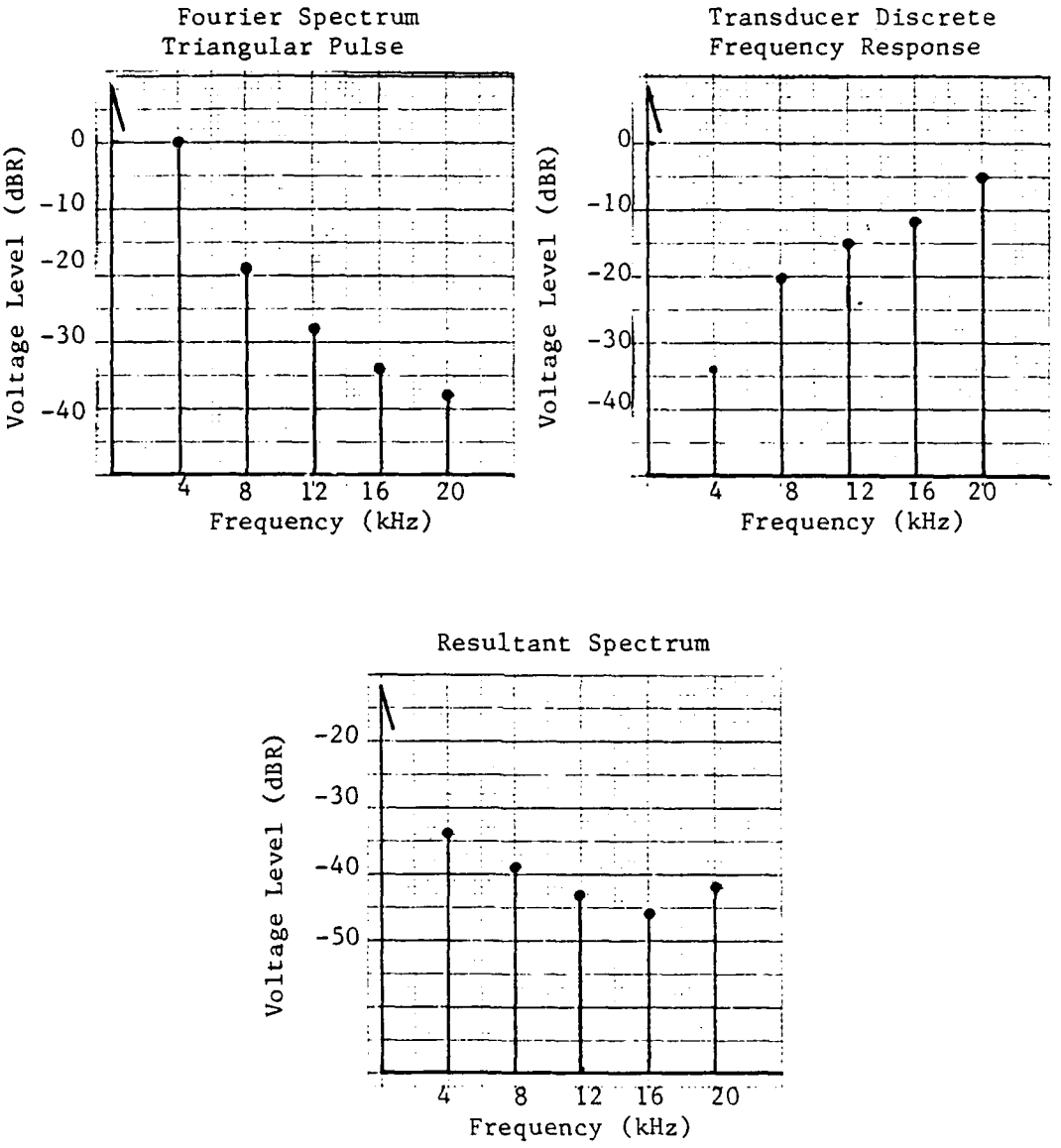

Figure 8. Transmit Signal Spectrum.

composite waveform can still be transmitted with the primary mode pressure distribution desired by using the mode source. That is to say, propagating a single mode is not constrained to sinusoidal signals only. The received data can then be processed in the frequency domain.

Processing in the frequency domain is done by the "Modes" progam (APP. D). The real and imaginary parts of the FFT are transformed by matrix multiplication with the inverse of the matrix A. This solves for modal distributions of both the real and imaginary parts. For a given mode, the square root of the sum of the squares of these two parts is the mode's amplitude and the inverse tangent of the ratio of the imaginary to the real part is the phase.

The percent energy in a mode at any fixed range is calculated from the ratio of the pressure squared in that mode to the sum of the pressures squared in all modes. This sum of pressures squared in all modes is proportional to the total energy and is used when total energy is referenced.

The phase information can be used to determine the phase speeds of the modes and any change of phase shift due to roughness. The absolute phase speeds are calculated from the phase change between measurement stations. This change, $\Delta\phi_n$ (the subscript n is the measurement station number), between stations is taken to be

$$\Delta\phi_n = \phi_n - \phi_{(n-1)}$$

and

$$\Delta\phi_n = \omega\Delta r/c_p$$

where Δr is the 0.91 meters between measurement positions and c_p is the

phase speed. Since ω, $\Delta\phi$, and Δr are known, a value for c_p can be obtained. The phase speed of mode m can also be used to solve for the free field speed of sound c_o, using the equation below.

$$c_o = [\ c_p^{-2} + (n/2c_p fh)^2\ ]^{-1/2}$$

This equation is obtained from the theoretical expression for the phase speed of mode n in a rigid walled waveguide of height h and frequency f in the absence of absorption. (Absorption is considered later in Section V.)

The phase shift induced by the roughness can be calculated from the phase speeds for both the smooth and rough waveguide. Since the phase is given by the term $\phi = \omega t - kr$ and $k = \omega/c_p$, the roughness induced phase shift can be calculated from

$$\Delta\phi = \omega \Delta r[(1/c_{ps})-(1/c_{pr})]$$

where the s subscript denotes the smooth surface and the r subscript the rough surface.

IV. EXPERIMENTAL PROCEDURE

A. MEASUREMENTS IN THE SMOOTH SURFACED WAVEGUIDE

Mode distribution in the smooth waveguide is the reference for all other measurements. Therefore, prior to making any meaningful evaluations of roughness effects, it is necessary to develop base line data of the mode distributions in the smooth waveguide. Two points of key interest are the reproducibility of the data and the attenuation of the sound field due to absorption and divergence.

1. Preliminary Validation

A series of pulsed experiments was run with the receiver at mid-depth. Part of this experiment was to confirm the divergence of the sound field observed during the continuous wave experiments (Fig. 9). Evaluation of the effects of repeatedly removing the side absorbers and then re-inserting them was also made during these pulsed trials. This is considered critical in that the absorbers are removed and replaced several times while placing the rough surfaces in the waveguide. No received signal variations, other than those caused by background noise, were observed due to movement of the fiberglass absorbers (Fig. 10). The effects of absorber movement were also analyzed for the case continuous wave transmission and showed the same results. The variations in the frequency spectrum were not greater than those caused by background noise, and this was less than 0.5 dB re 1 volt (Table 2).

Data obtained from 9700 Hz, 10 cycle tone burst.

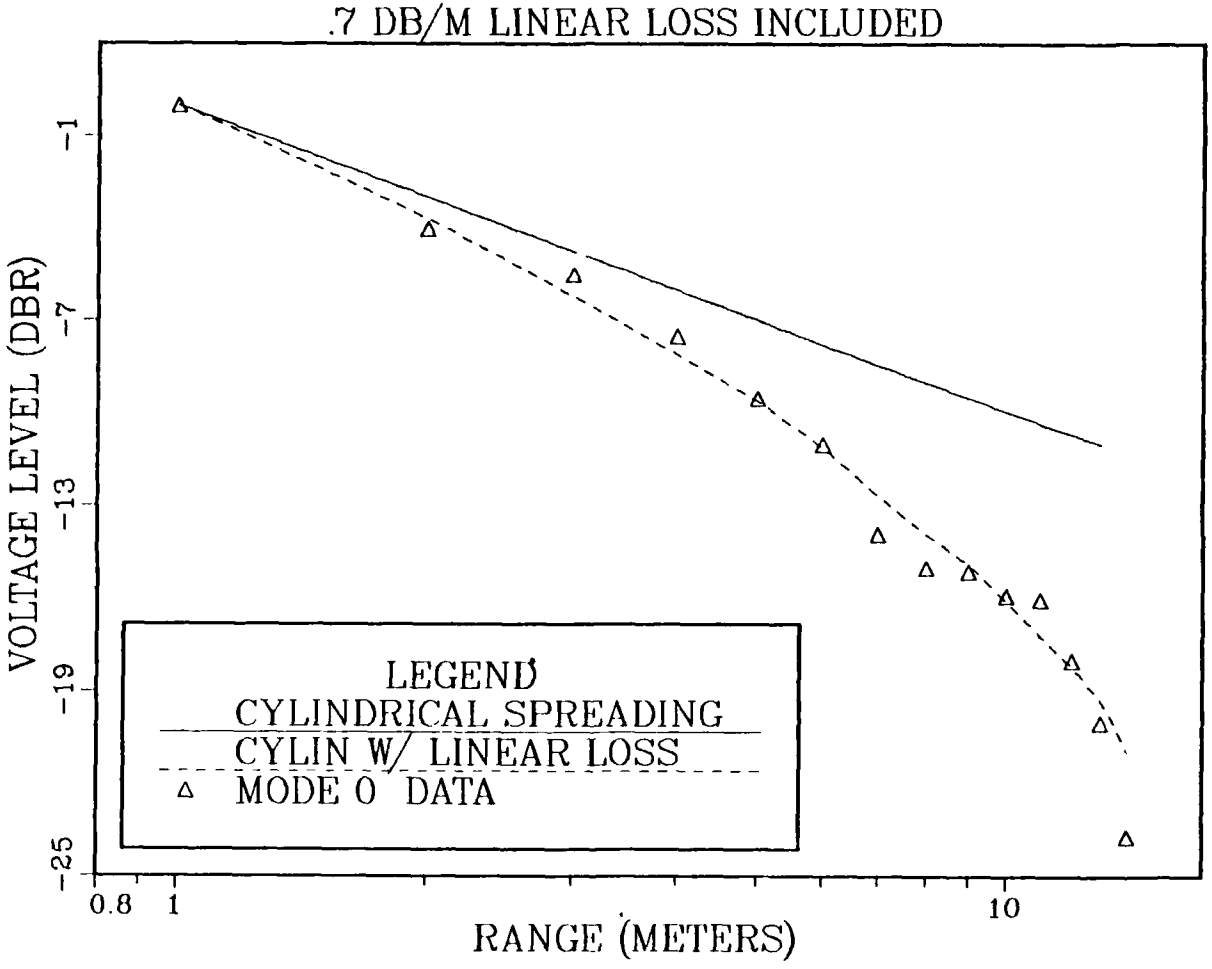

Figure 9. Sound Attenuation in Smooth Waveguide.

The received time signal of 7813 Hz tone burst for four distinct data runs. Absorbers have been removed and re-inserted between runs.

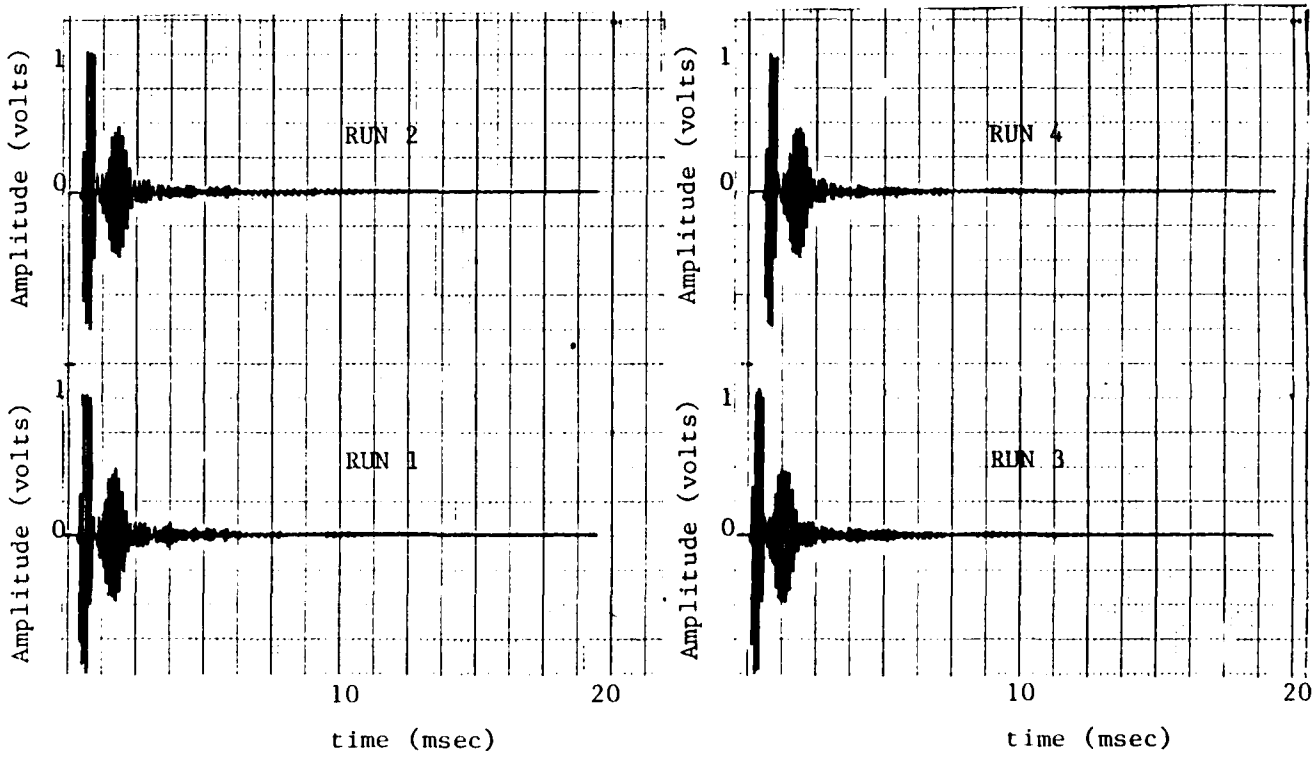

Figure 10. Effect of Absorber Movement.

Table 2

Effects of Absorber Movement on Frequency Spectrum
for 4 Data Runs.

Spectrum level (dB re 1 V) for selected frequencies (Hz)

Run #	7750	11750	15750	23500	31250
1	-17.4	-16.3	-27.0	-36.7	-52.0
2	-17.6	-16.6	-27.0	-36.9	-51.8
3	-17.4	-16.3	-27.0	-36.6	-51.7
4	-17.2	-16.0	-26.5	-36.2	-51.2

Standard deviation in spectrum level (dB re 1 V)

	7750	11750	15750	23500	31250
due to movement (4 run average)	0.16	0.24	0.25	0.29	0.33
due to noise (10 run average)	0.15	0.23	0.21	0.12	0.39

2. Continuous Wave Measurements in the Smooth Waveguide

The continuous wave data runs consist of data sets taken every 0.91 meters. A data set is comprised of six or ten data pairs, which are the real and imaginary parts of the FFT of 100 time averages of the received signal. The number of data pairs corresponds to the number of depths at which the sound field was measured at each range. Whether six or ten depth measurements were used depended on the highest frequency a data run examined. For frequencies below 16,000 Hz, six depths are sufficient, but for frequencies up to 31250 Hz, ten depths are needed because of the additional modes which can propagate.

The signal for these measurements is a triangular pulse with a fundamental frequency component of 3906.6 Hz and strong harmonics up to 31250 Hz. For frequencies below 16,000 Hz, only four modes propagate in a waveguide of 5 centimeters height. Hence, six equally spaced depth measurements provide sampling for more modes than is required. For the smooth waveguide, the energy that is detected in these non-propagating modes is a measure of the accuracy of the measurements. Consider mode 5 which is non-propagating for frequencies below 17,000 Hz. With a 15,750 Hz signal, the fifth mode is theoretically down 110 dB one meter from the source. Hence, it is reasonable to assume that any energy detected in this non-propagating mode is due to measurement inaccuracy. This provides a qualitity check for each data run and since there is typically less than one percent energy in these modes, the method is considered accurate enough to observe the variations in amplitude caused by surface roughnesses.

By repeating these data runs several times, it is possible to show that the smooth waveguide amplitude observations are quite reproducible. The standard deviation, over several days of measurements, in the percent energy present in a mode at a given range is typically less than three percent, and seven percent in the worst case. This is demonstrated (Table 3) by tabulation of the energy distribution in the smooth waveguide for several different data runs. Table 4 demonstrates reproducibility of data runs at the same location on the same day. At 7813 Hz and 15625 Hz, the standard deviation in the observed percent energy in any mode is three percent or less. At 11719 Hz, the standard deviation for the driven mode, mode 1, is seven percent, but it is less than three percent for all other modes at this frequency. For frequencies up to 32000 Hz, similar arguments can be made for ten depth measurements.

Additional monitoring for erratic or unexpected systematic response of the electret sources is achieved by using a 1/2" Bruel and Kjaer microphone placed 60 centimeters from the source. The greatest effect observed by this monitor was a monotonic decrease of six percent in the source amplitude over a four hour period.

B. MEASUREMENTS IN THE ROUGH SURFACED WAVEGUIDE

1. Surface Roughness Elements

Two types of surface roughnesses are used. The first is a deterministic, periodic surface of wedges. The other surface is randomly rough, but of known statistics.

Table 3

Reproducibility of Smooth Waveguide Results.

Energy distributions by percent for four data runs, six depths and processing by OPHELEA

7813 Hz - Smooth Waveguide (CW)

e	Mode 0 Energy (%)				Mode 1 Energy (%)			
	A	B	C	D	A	B	C	D
	0	1	1	-	99	97	99	-
	0	1	0	1	98	98	98	98
	1	1	1	-	98	97	96	-
	3	0	0	1	97	98	98	98
	1	0	0	-	98	100	99	-
	-	6*	0	-	-	71*	99	-
	-	10*	3	4	-	82*	97	90

e	Mode 2 Energy (%)				Mode 3 Energy (%)			
	A	B	C	D	A	B	C	D
	1	2	0	-	0	0	0	-
	1	2	1	1	0	0	0	0
	1	3	2	-	0	0	0	-
	0	1	2	0	0	0	0	1
	1	0	1	-	0	0	0	-
	-	8*	1	-	-	6*	0	-
	-	0*	0	1	-	2*	0	3

Table 3 (Cont'd)

11719 Hz - Smooth Waveguide (CW)

Range (m)	Mode 0 Energy (%) A	B	C	D	Mode 1 Energy (%) A	B	C	D
0.9	4	3	1	-	72	73	73	-
1.8	2	1	0	1	93	93	93	83
2.7	4	0	1	-	88	92	92	-
3.7	1	2	2	2	91	92	89	62
4.6	7	7	7	-	85	90	81	-
5.5	-	3	4	-	-	68	94	-
6.4	-	5	1	4	-	93	94	89

Range (m)	Mode 2 Energy (%) A	B	C	D	Mode 3 Energy (%) A	B	C	D
0.9	1	1	5	-	26	19	20	-
1.8	0	1	2	2	5	5	4	13
2.7	2	2	6	-	5	5	1	-
3.7	1	3	4	4	7	3	4	31
4.6	1	0	2	-	7	3	7	-
5.5	-	9*	2	-	-	6*	0	-
6.4	-	1*	4	5	-	1*	1	1

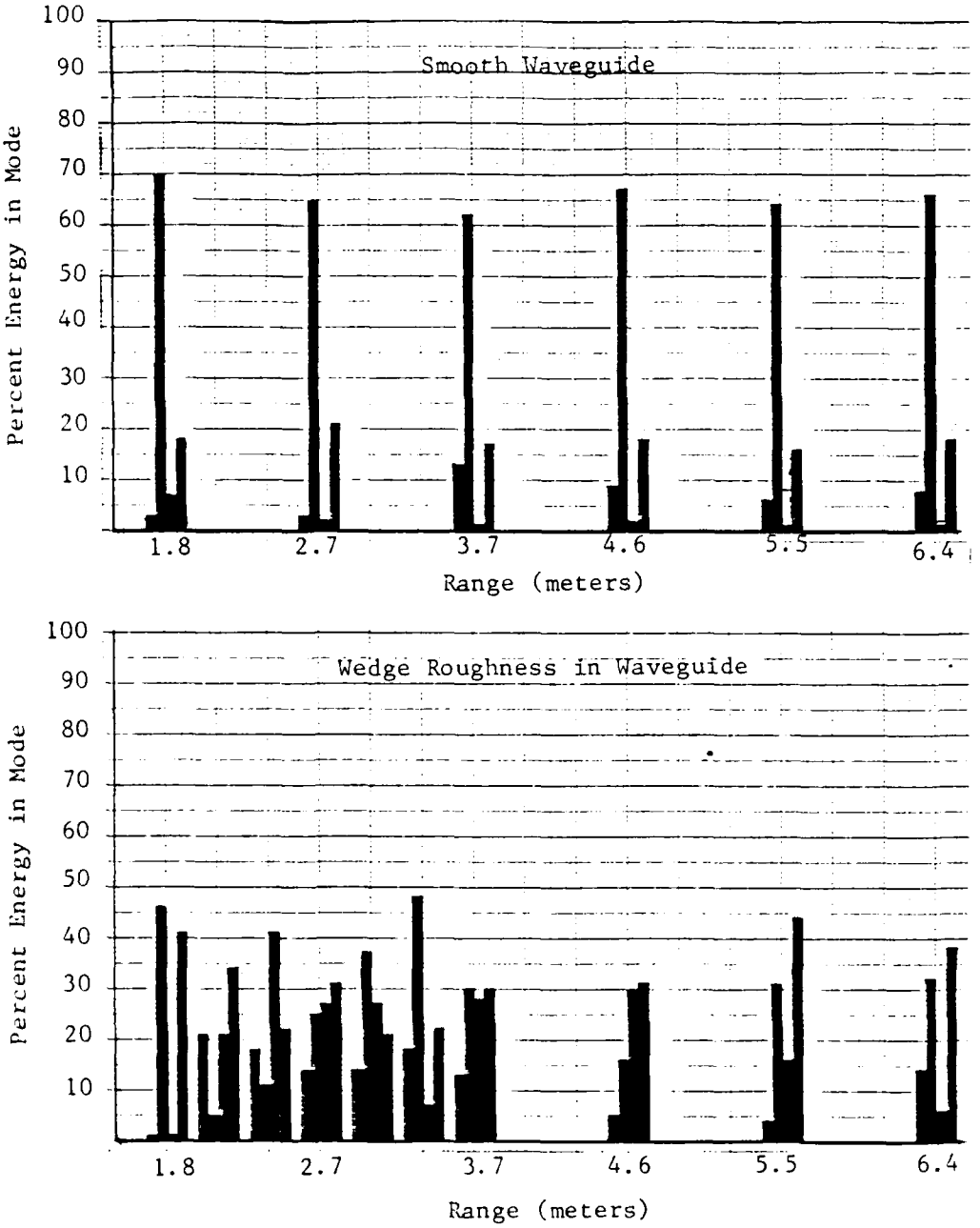

Figure 13b. Energy Distribution vs. Range at 23500 Hz, Mode 1 Driven.

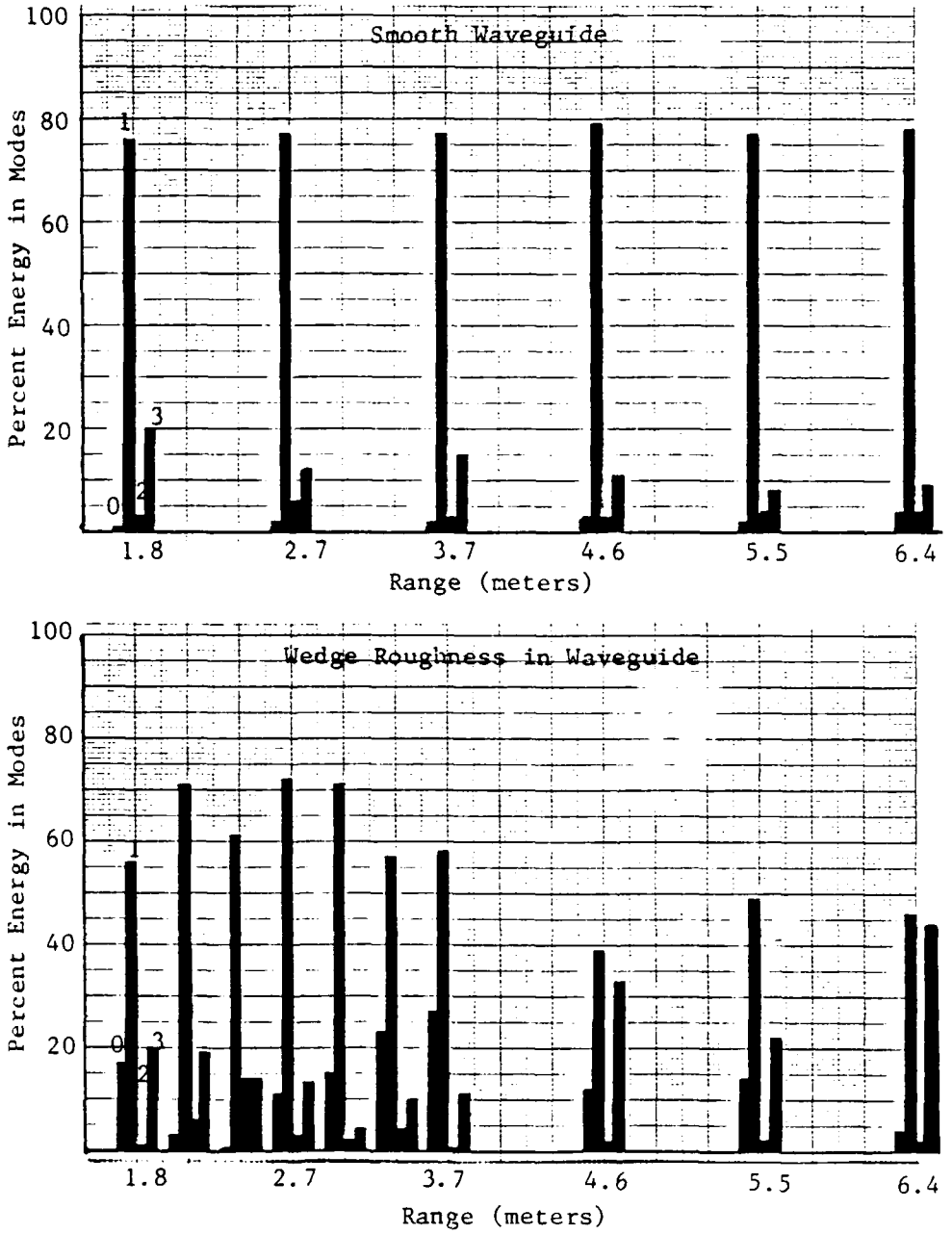

Figure 13a. Energy Distribution vs. Range at 15750 Hz, Mode 1 Driven.

Table 7 (Cont'd)

Mode 1 at 31250 Hz

Range (m)	Smooth energy in mode (%) 0	1	2	3	oth	Rubber Wedges energy in mode (%) 0	1	2	3	4	oth
1.8	6	62	1	29	2	23	2	12	51	5	7
2.1	-	-	-	-	-	22	52	0	26	0	0
2.4	-	-	-	-	-	41	5	5	34	6	9
2.7	4	66	9	19	2	10	48	6	10	16	10
3.0	-	-	-	-	-	17	14	52	10	1	6
3.3	-	-	-	-	-	34	32	18	10	1	5
3.7	2	69	3	21	5	9	27	16	38	7	3
4.6	-	-	-	-	-	29	11	20	25	3	12
5.5	10	72	3	10	5	23	24	18	24	3	8
6.4	13	53	2	29	3	33	26	5	22	5	9
7.3	S/N < 10 dB					34	30	13	14	3	6

Table 7

Energy Distribution for Mode 1 Driven System.

Modal energy distributions by percent.
Smooth data taken at six depths with OPHELEA processing.
Rough data taken at ten depths with Nicolet processing.
Signal-to-noise ratio greater than 20dB for all data.

Mode 1 at 15750 Hz

	Smooth energy in mode (%)					Rubber Wedges energy in mode (%)				
Range (m)	0	1	2	3	oth	0	1	2	3	oth
1.8	1	76	3	20	0	17	56	1	20	6
2.1	-	-	-	-	-	3	71	6	19	-
2.4	-	-	-	-	-	0	61	14	14	-
2.7	2	77	6	12	3	11	72	3	13	1
3.0	-	-	-	-	-	15	76	2	4	-
3.3	-	-	-	-	-	23	57	4	10	-
3.7	2	77	3	15	3	27	58	0	11	4
4.6	3	79	3	11	4	12	39	2	33	14
5.5	2	77	4	8	9	14	49	2	22	2
6.4	-	-	-	-	-	4	46	2	42	6
7.3	-	-	-	-	-	23	39	4	29	15

Mode 1 at 23500 Hz

	Smooth energy in mode (%)					Rubber Wedges energy in mode (%)				
Range (m)	0	1	2	3	oth	0	1	2	3	oth
1.8	3	70	7	18	2	1	46	1	41	11
2.1	-	-	-	-	-	26	5	26	34	9
2.4	-	-	-	-	-	18	11	41	22	8
2.7	3	65	2	21	5	14	25	27	31	3
3.0	-	-	-	-	-	14	37	27	21	1
3.3	-	-	-	-	-	18	48	7	22	5
3.7	13	62	1	17	7	13	30	27	30	0
4.6	9	67	2	18	4	5	16	30	31	18
5.5	6	64	8	16	6	4	31	16	44	5
6.4	8	66	2	18	8	14	32	6	38	10
7.3	-	-	-	-	-	12	14	33	34	7

V. RESULTS AND CONCLUSIONS

A. DETERMINISTIC SURFACE

1. Amplitude Analysis

Typical results for the mode 1 driven system are tabulated in Table 7 and graphically depicted in figure 13. Several qualitative observations can be made from a cursory look at this data. First, the average percent energy in modes, other than the driven mode, increases with frequency when roughness is present. This average is the arithmetic mean of the percent energy over all ranges. Second, the variability of the percent energy in a mode is greater in the presence of a rough surface than in the smooth waveguide. Third, energy is not only removed from the driven mode when roughness is present, but it may reappear in that mode at a greater range.

The average percent energy of modes in the smooth waveguide is compared to that in the wedge roughness waveguide as a function of frequency and kh (Fig. 14a). The strength of interaction is evaluated by the percent energy in modes adjacent to the driven mode and is seen in this figure to be dependent on frequency. To examine the cause of this frequency dependent behaviour, consider the roughness of the corrugated rubber surface as expressed in terms of the Rayleigh roughness parameter, $kh \sin\Theta_n$ (Table 8).

For a rigid walled waveguide, the Rayleigh roughness parameter is nearly constant with frequency. This is because the grazing angle of the mode, Θ_n, decreases at the same rate the wavelength decreases when

Table 6

Mode Cycle Distances (meters)
as a Function of Mode Number, n and Frequency, f (Hz)

n \ f	7750	11750	15750	31250
1	.20	.34	.46	.74
2	.06	.14	.22	.46
3	X	.06	.12	.30
4	X	X	.06	.22

all distances are in meters
X - denotes a non-propagating mode

It is structurally infeasible to place probe holes this close on the waveguide because of interference with cross supports. The alternative is to add roughness elements to the leading edge of the roughness and move the source a distance equal to the width of the added roughness. This has the same affect as moving the probe farther from the source; the only change is the length of rough surface the sound interacts with before reaching the receiver. Therefore any changes in the phases and mode distributions is due to this greater rough surface interaction.

Another question with a rough surface is determining the plane from which the waveguide height is measured. The reference plane selected was the statistical mean height of the roughness elements. A priori, this appears to be as good a selection as any and is chosen in many texts discussing scattering from a rough surface.

Table 5

Randomly Rough Surface Statistics

RMS height	0.150 cm
RMS slope	80
Correlation length	0.148 cm
Average height	0.255 cm

2. Continuous Wave Measurements in the Rough Waveguide

The data runs consist of 100 time average sets, as for the smooth waveguide, Section IV.2, but the signal used is dependent on the type of surface roughness. For the deterministically rough surface, a triangular pulse with a fundemental frequency of 3906.6 Hz produces a signal with a signal-to-noise ratio greater than 20 dB for all ranges. However, for the randomly rough surface, single frequency signals must be used to obtain a signal-to-noise ratio greater than 20 dB for ranges out to 9 meters. The higher attenuation caused by the random roughness scattering both transversely and along the waveguide axis makes the pure tone signal necessary.

Measurements must be taken at short intervals if the evolving mode interactions are to be tracked. One gauge of the required interval comes from ray theory. In ray theory, the cycle distance indicates how frequently a ray interacts with the surface. The cycle distances, as predicted by ray theory, for several modes at various frequencies are given in Table 6. From the entries of this table, a suggested sampling distance can be determined. An interval of 30 cm is selected. Though this is greater than the interval suggested by Table 6, it allows a complete data run to be made in two to three hours.

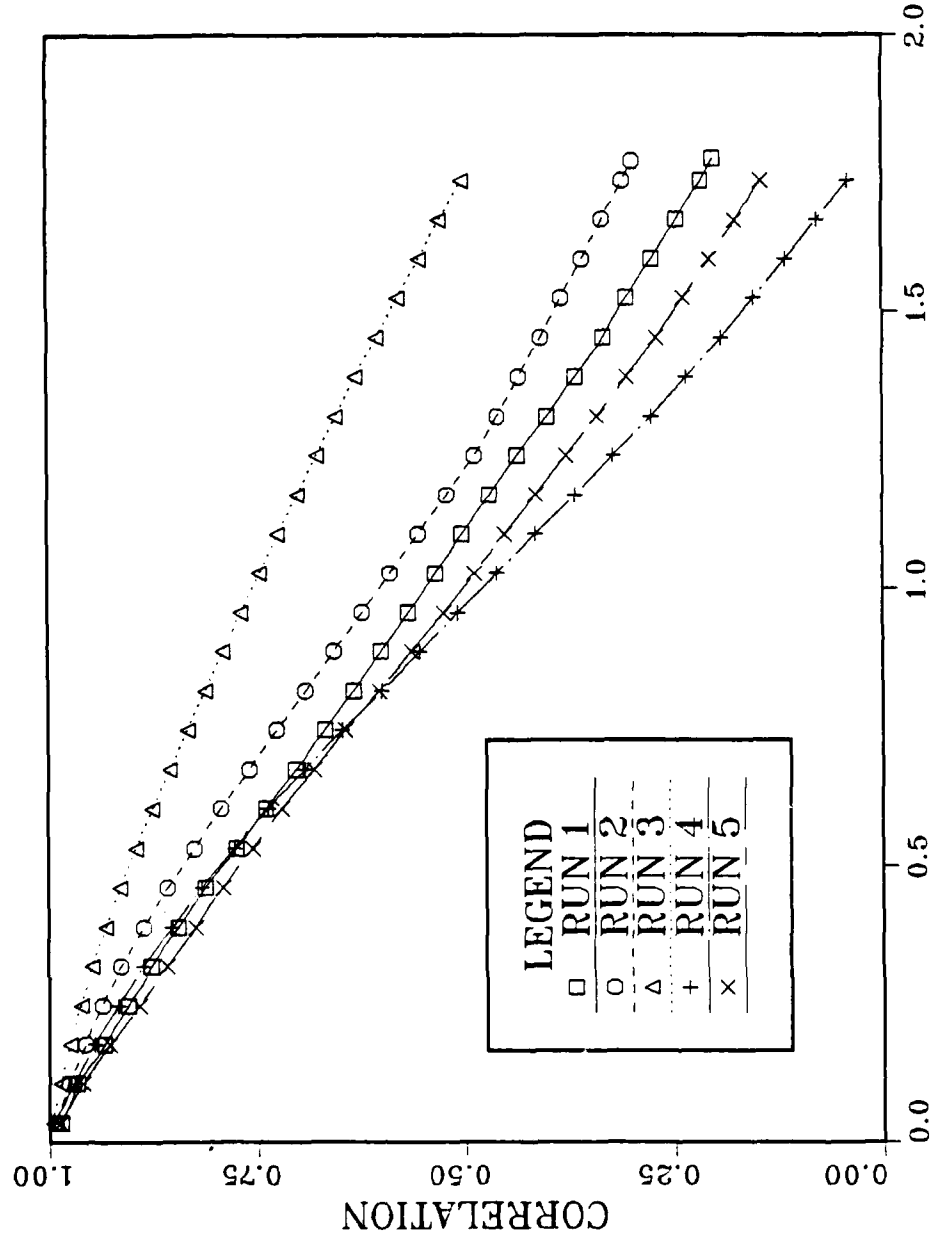

Figure 12c. Correlation Functions for Randomly Rough Surface.

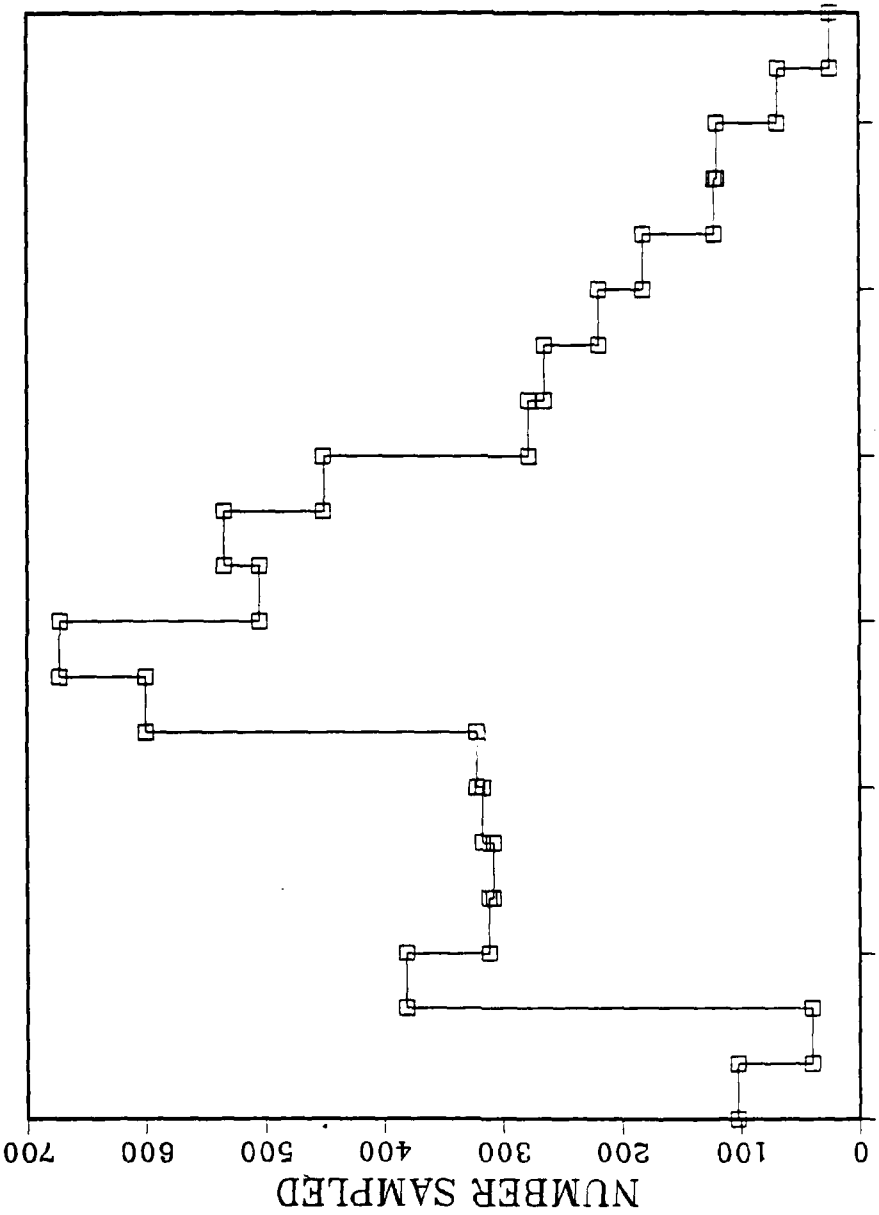

Figure 12b. Height Histogram of Randomly Rough Surface.

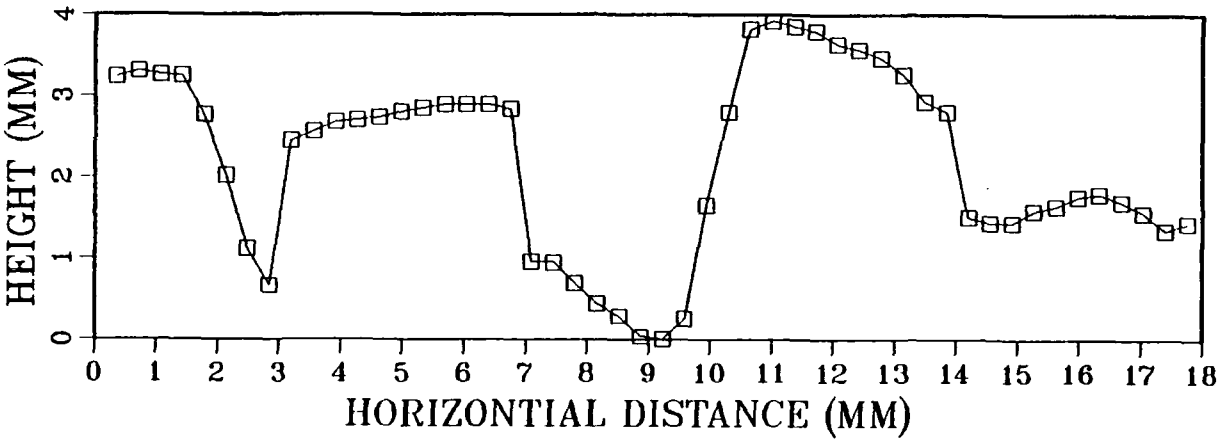

Figure 12a. Randomly Rough Surface Profile.

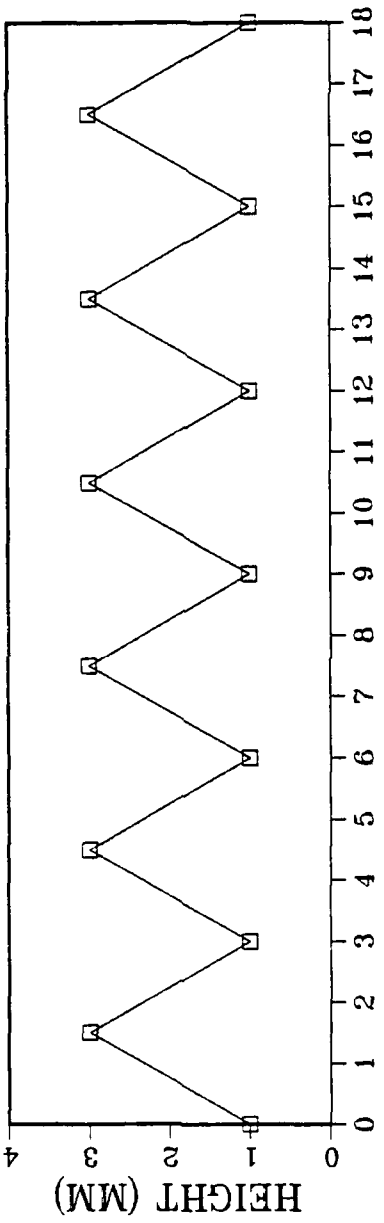

Figure 11. Deterministic Rough Surface Profile.

a. Deterministic Surface

The deterministic surface is made of wedge corrugated, hard rubber matting. The height of these wedges is 2 mm and the spacing between wedges is 3 mm (Fig. 11). To put the roughness to wavelength ratio in perspective, at 3800 Hz kh=0.14 and at 32150 Hz kh=1.18; "k" is the wave propagation constant and "h" is the height of the roughness element. The matting is placed on the bottom of the waveguide in contiguous one meter sections aligned so that the wedges lie perpendicular to the long axis of the waveguide.

b. Random Surface

This surface is obtained by using #2 aquarium sand spread on the bottom plate of the waveguide. The statistics are determined from samples made by the RSM. A profile of the surface is shown in Figure 12a. This surface data is processed to determine the RMS height and correlation length. These two numbers are then used to describe the surface. The probability density function (pdf) of the surface, which is obtained from a histogram of the surface heights, is shown in Figure 12b. The best fit obtained to this pdf is indeterminate, but not Gaussian. The correlation functions for five of the six data runs taken on this surface are shown in Figure 12c. The statistics of this surface averaged over the six runs is shown in Table 5.

Table 4

Measurement Reproducibility.

Continuous wave transmission

Six data runs conducted at the same range, on the same day.
(S/N > 20db for all cases)

7813 Hz

	Energy in Mode (%)					
Trial	0	1	2	3	4	5
1	6	84	8	1	1	0
2	1	92	6	0	0	0
3	1	94	3	1	1	0
4	1	92	5	1	1	0
5	1	91	7	0	0	0
6	3	91	5	0	0	0

11719 Hz

	Energy in Mode (%)					
Trial	0	1	2	3	4	5
1	11	64	8	15	2	0
2	3	81	2	12	0	1
3	5	79	3	12	1	0
4	6	83	0	8	2	1
6	7	80	0	12	1	0

15625 Hz

	Energy in Mode (%)					
Trial	0	1	2	3	4	5
1	13	54	2	19	11	1
2	10	54	1	26	9	0
3	10	53	4	28	6	0
4	7	53	2	27	10	1
5	8	57	5	23	7	0
6	7	59	5	25	4	0

Table 3(Cont'd)

15625 Hz - Smooth Waveguide (CW)

Range (m)	Mode 0 Energy (%) A	B	C	D	Mode 1 Energy (%) A	B	C	D
0.9	2	0	1	-	66	73	67	-
1.8	1	1	2	-	72	77	78	-
2.7	7	0	1	-	72	79	80	-
3.7	6	4	1	-	76	78	78	-
4.6	8	5	0	-	74	81	84	-
5.5	-	12	1	-	-	71	82	-
6.4	-	9	2	-	-	42	49	-
8.2	-	2	9	-	-	82	73	-

Range (m)	Mode 2 Energy (%) A	B	C	D	Mode 3 Energy (%) A	B	C	D
0.9	1	0	9	-	30	25	22	-
1.8	2	5	0	-	23	16	18	-
2.7	9	4	7	-	10	17	10	-
3.7	0	0	9	-	18	17	10	-
4.6	1	0	9	-	14	13	7	-
5.5	-	2	6	-	-	4	10	-
6.4	-	1	4	-	-	43	42	-
8.2	-	0	9	-	-	11	7	-

Date of run: A - 9/17 B - 9/29 C - 9/30 D - 10/28

* - S/N < 20 dB

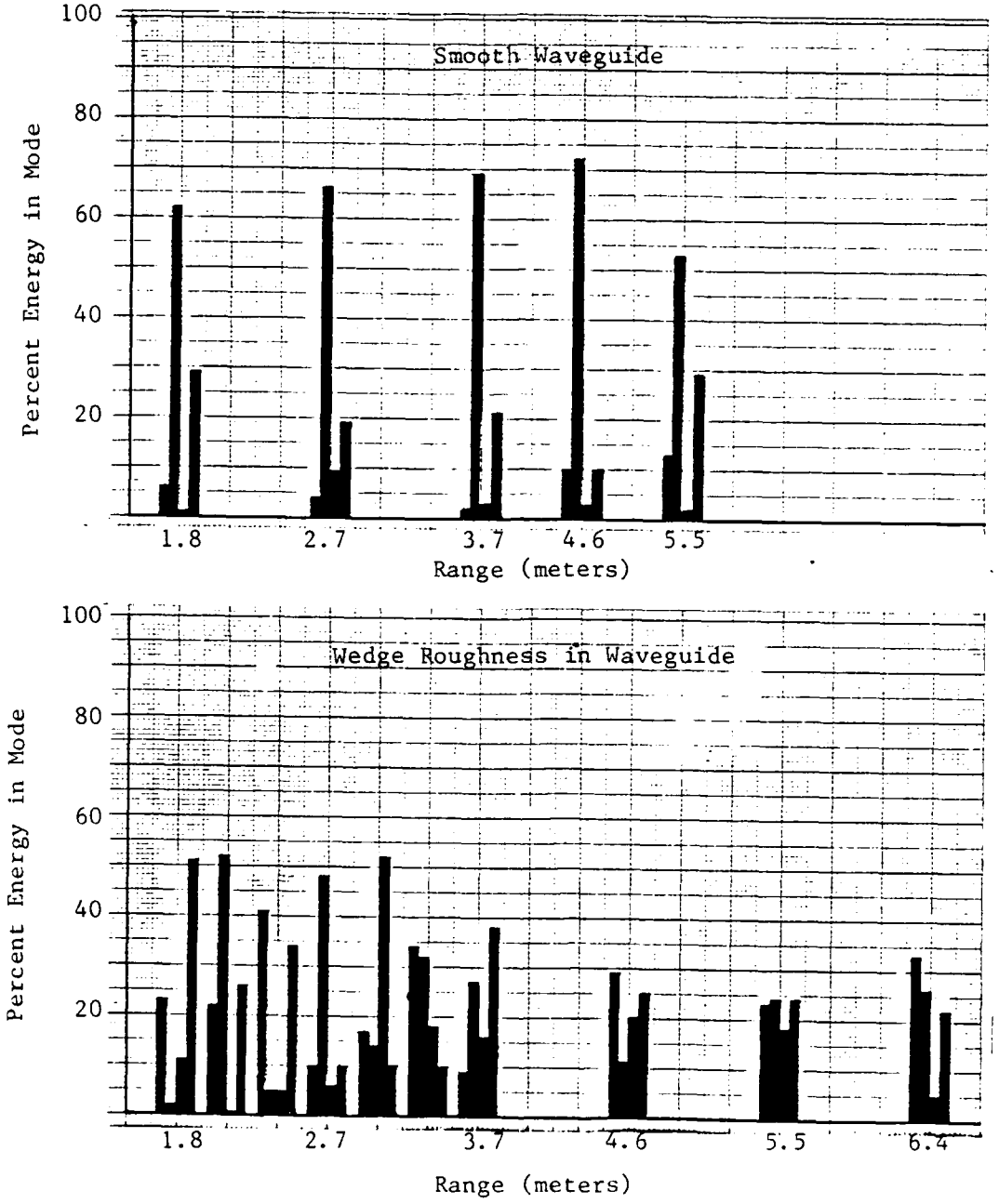

Figure 13c. Energy Distribution vs. Range at 31250 Hz, Mode 1 Driven.

The average percent energy is the arithmetic mean over all ranges for that frequency.

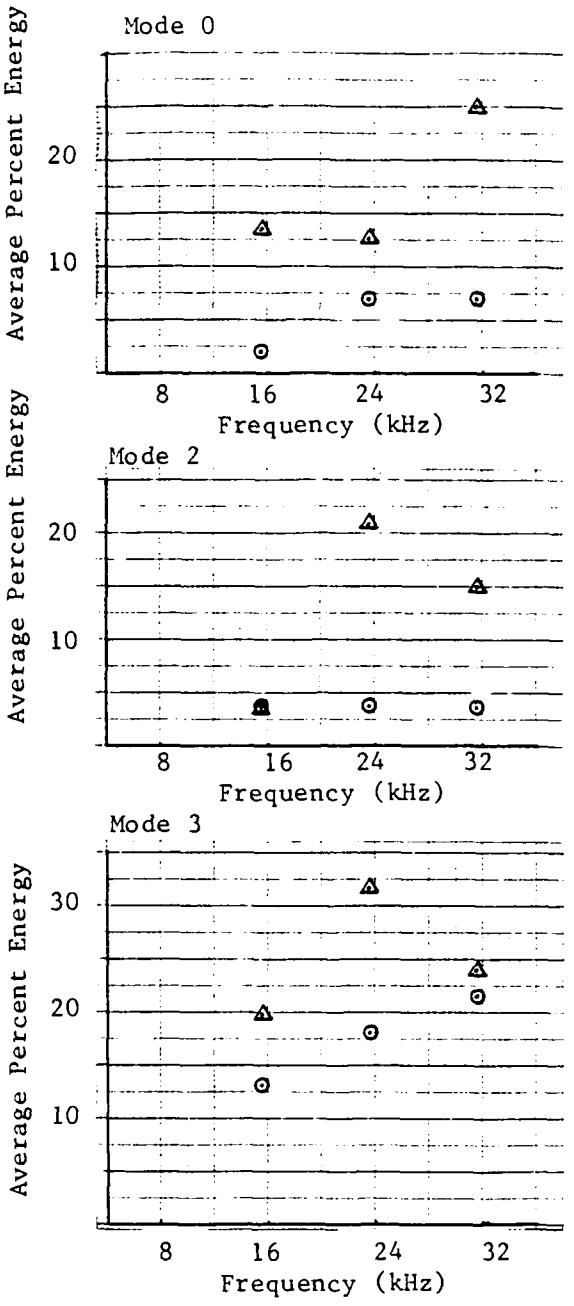

Figure 14a. Average Percent Energy in Modes Adjacent to Mode 1 (Mode 1 Driven).

frequency increases. Therefore, the Rayleigh roughness parameter is not helpful

Table 8

Rayleigh Roughness Parameter, R, h = 2 mm

	Mode			
	1	2	3	4
R	0.13	0.25	0.38	0.55

in accounting for the correlation between increasing frequency and increasing internal energy transfer due to the surface roughness. This is expected because the Rayleigh roughness parameter was developed for the special case of small slopes and specular scatter. However, as noted in section IV, $0.12 < kh < 1.10$ is in the region of Rayleigh scatter within which scattered power increases as the fourth power of the frequency. It is noted that the variation of energy in modes adjacent to the driven mode, as measured by the standard deviation about the average percent energy for all ranges at a given frequency, is also a strong function of frequency (Fig. 14b).

An interesting effect is the apparent oscillation of energy from one mode to another. At 31250 Hz. for example, energy is removed from mode 1 and distributed to closely adjacent modes as compared to the energy distribution in the smooth waveguide at 2 meters (Fig. 13c). By 3 meters, the energy distribution has returned to one more like the smooth waveguide. Oscillations like this continue throughout the ranges of observation.

It is noted that the attenuation rate for the corrugated surface is slighty less than for the smooth surface (Fig. 15). A

Deviation is about the arithmetic mean of Figure 14a.

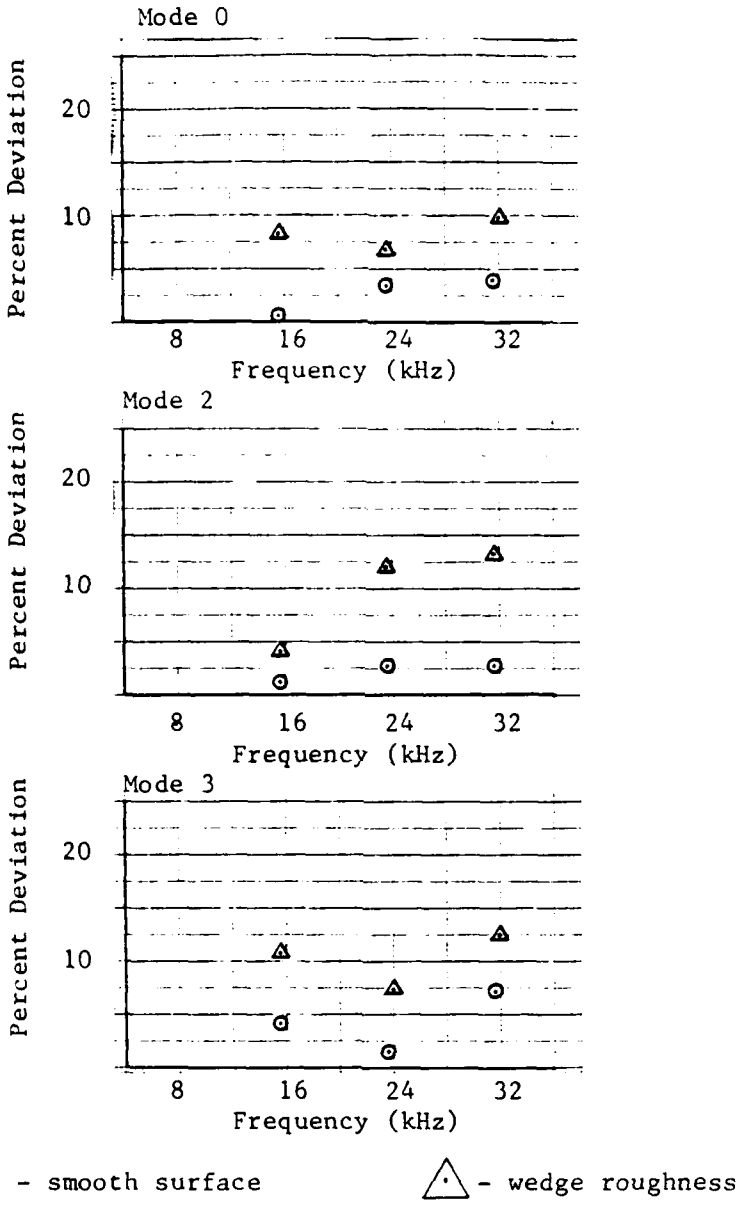

Figure 14b. Standard Deviation of Percent Energy in Modes Adjacent to Mode 1 (Mode 1 Driven).

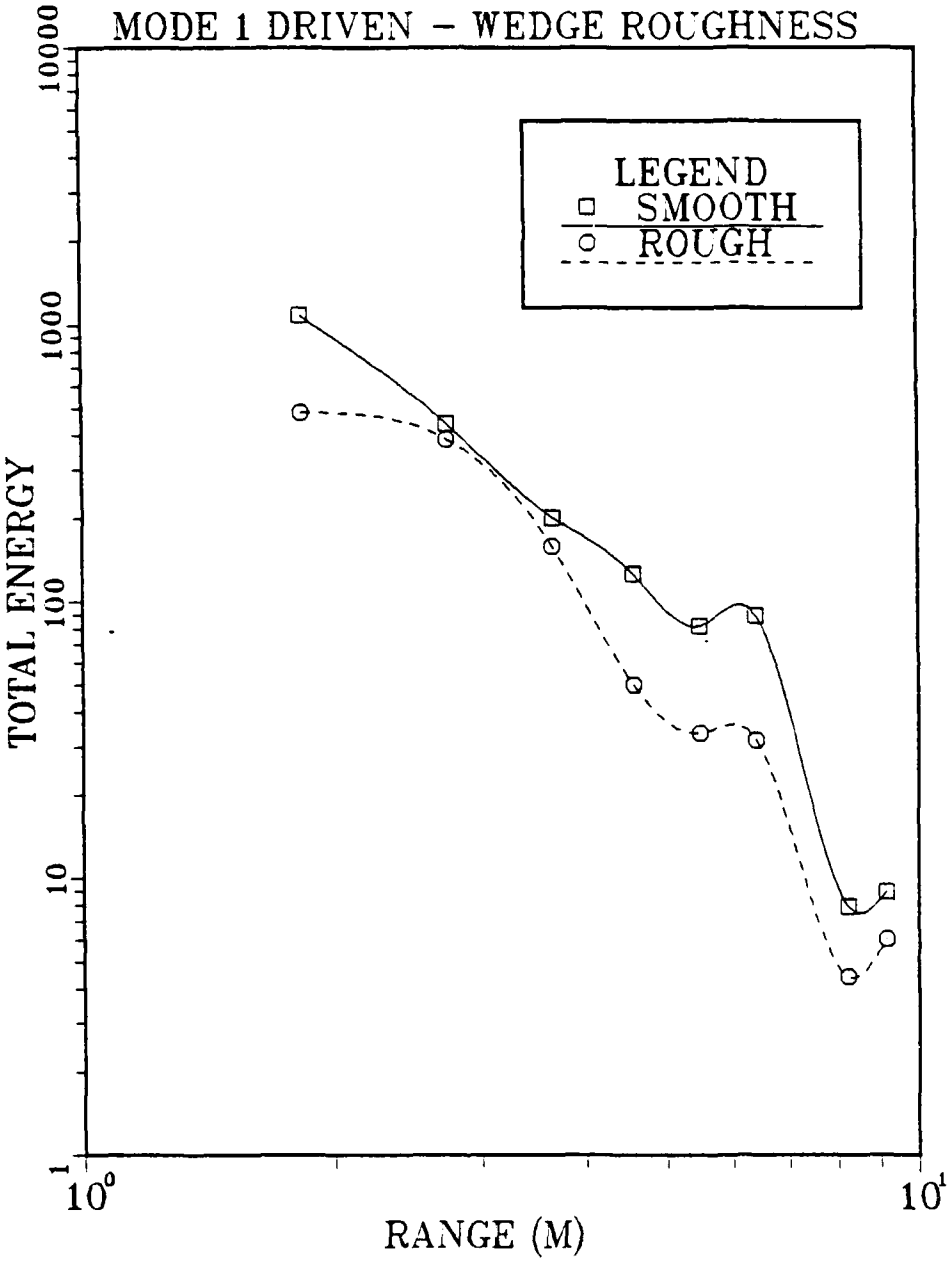

Figure 15a. Total Energy Attenuation at 15750 Hz, Mode 1 Source, Smooth vs. Deterministic Roughness.

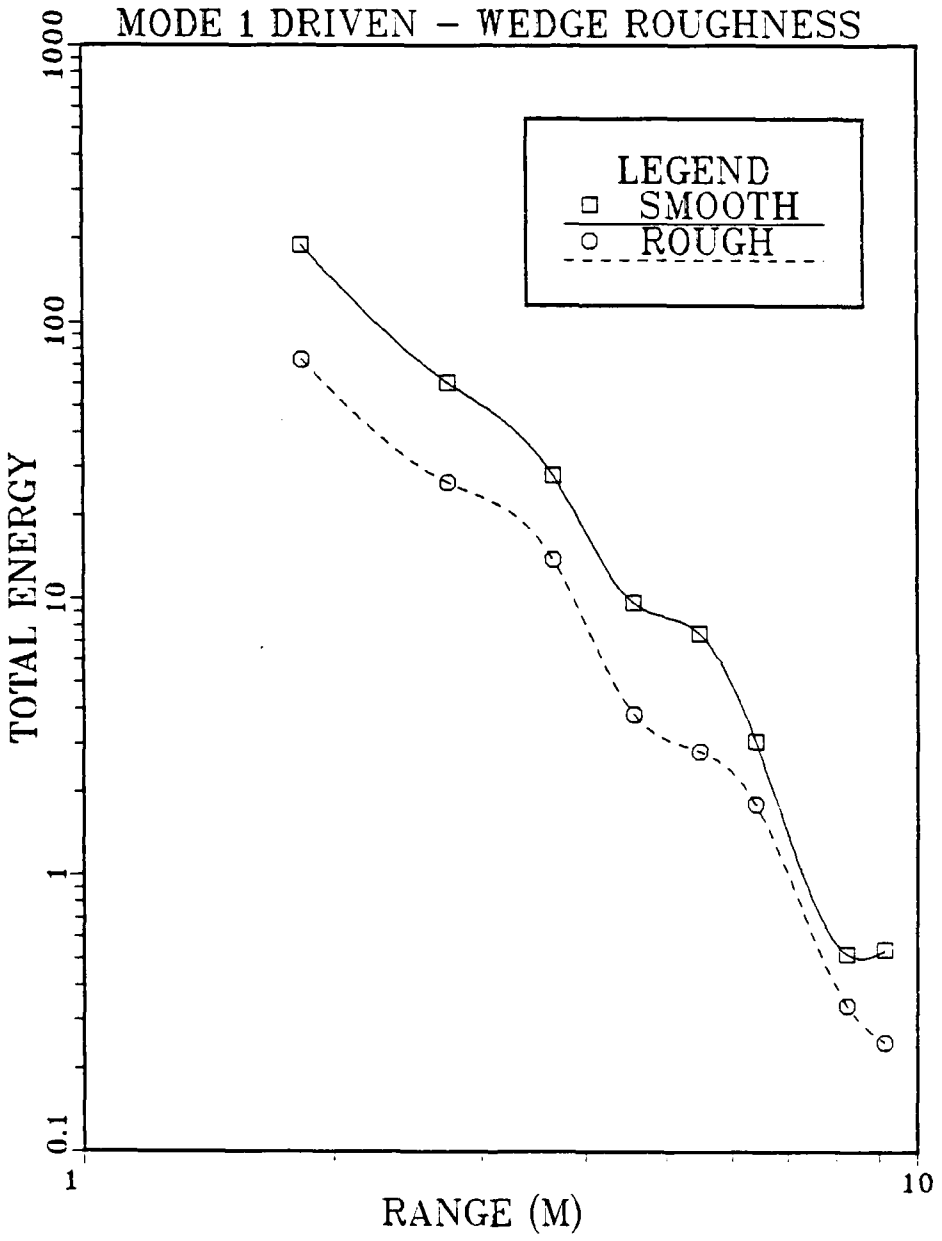

Figure 15b. Total Energy Attenuation at 23500 Hz, Mode 1 Source, Smooth vs. Deterministic Roughness.

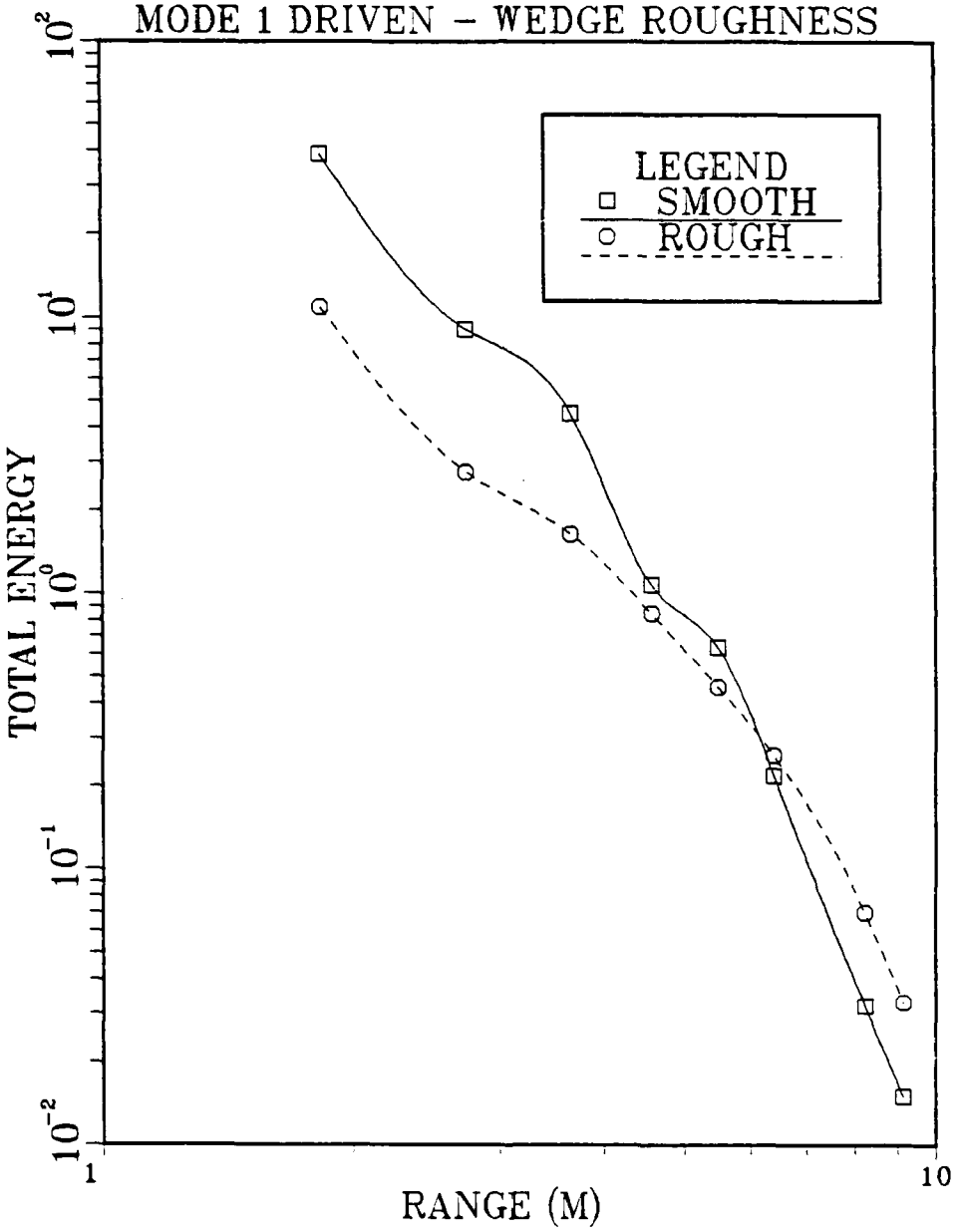

Figure 15c. Total Energy Attenuation at 31250 Hz, Mode 1 Source, Smooth vs. Deterministic Roughness.

possible explanation may be that the viscous losses caused by the gypsum board surface may be greater than the effects of the rubber wedges. A future experiment to test this would be to use smooth rubber of the same material as the wedges for the bottom surface in the smooth waveguide reference runs. Regardless, the corrugated wedges can be described as a one dimensional roughness and thus there is minimal scattering of sound to the sides of the waveguide. Thus a large change in the energy attenuation rate is not expected and is not observed. The remaining energy attenuation (dB/m), after subtracting out attenuation due to geometrical speading, for mode 1 driven in both the rough and smooth walled waveguide is given in Table 9. The energy attenuation for a given run is the average of the incremental attenuations, AI,

$$AI = \frac{-10}{\text{Distance}} \log\left[\left(\frac{\text{Total Energy}}{\text{Total Energy first range}}\right)\left(\frac{\text{first range}}{\text{range}}\right)\right]$$

where distance = range - first range. In table 9, the values are the averages over three runs.

Similar results are observed for the mode 2 driven system as are observed for the mode 1 driven system (Table 10 and Figure 16). The average energy in modes immediately adjacent to mode 2 and their variation in energy, as measured by the standard deviation of the energy about its mean, increase with frequency (Fig. 17). This comparison reveals no clear information about mode 0 though.

Oscillations of the energy in modes is also observed. To determine if this is a real phenomenon or due to different attenuation rates for each mode, the modal amplitudes are compared as a function of range (Fig. 18, 19, 20). In these figures, the rough waveguide

Table 9

Energy Attenuation
in Smooth and Wedge Roughness Waveguide,
Mode 1 Driven (dB/m).

Freq (Hz)	7813	11719	15626	19531	23438	27344	31250
Smooth Waveguide	1.66	2.21	2.67	3.06	3.27	3.88	4.15
Wedge Roughness	1.37	2.11	2.27	2.36	3.43	2.85	2.60

Table 10

Energy Distribution for Mode 2 Driven System,
Smooth and Deterministically Rough Surfaces.

Modal energy distribution by percent for ten depth measurements taken by the Nicolet wave analyzer and processed on the IBM 3030.
Signal-to-noise ratio greater than 20 dB for all data.

Mode 2 at 8000 Hz

	Smooth energy in mode (%)				Rubber Wedges energy in mode (%)			
Range (m)	0	1	2	3	0	1	2	3
1.8	23	1	76	0	17	1	81	0
2.7	24	4	72	0	11	4	80	0
3.7	11	3	85	0	16	3	79	0
4.6	22	20	57	0	19	6	74	0
5.5	31	13	54	0	10	6	74	1
6.4	40	9	51	0	40	18	38	1

Mode 2 at 13000 Hz

	Smooth energy in mode (%)				Rubber Wedges energy in mode (%)			
Range (m)	0	1	2	3	0	1	2	3
1.8	20	3	74	4	15	2	79	2
2.7	23	5	71	1	37	2	42	18
3.7	24	1	75	0	21	1	77	1
4.6	27	4	68	0	46	1	43	8
5.5	23	2	75	0	18	7	66	8
6.4	31	3	64	1	7	2	73	18
7.3	15	4	80	1	1	4	95	0
8.2	20	3	75	1	7	12	78	1

Table 10 (cont'd)

Mode 2 at 15750 Hz

Range (m)	Smooth energy in mode (%) 0	1	2	3	Rubber Wedges energy in mode (%) 0	1	2	3
1.8	13	2	83	2	5	11	76	6
2.7	11	1	84	0	14	12	68	2
3.7	11	6	79	1	17	19	58	6
4.6	12	7	80	1	11	13	61	12
5.5	12	3	83	1	6	19	73	1
6.4	16	1	81	0	1	23	74	0

Mode 2 at 23500 Hz

Range (m)	Smooth energy in mode (%) 0	1	2	3	Rubber Wedges energy in mode (%) 0	1	2	3
1.8	7	4	79	5	4	6	80	4
2.7	11	6	77	3	5	5	66	13
3.7	11	19	67	2	6	14	76	0
4.6	18	4	74	1	11	7	68	12
5.5	14	6	74	4	5	3	88	1
6.4	20	2	70	6	6	18	65	4

Mode 2 at 31250 Hz

Range (m)	Smooth energy in mode (%) 0	1	2	3	4	oth	Rubber Wedges energy in mode (%) 0	1	2	3	4	oth
1.8	11	1	72	5	6	5	8	32	17	3	21	19
2.7	11	8	72	2	4	3	4	13	52	7	14	10
3.7	3	5	68	12	5	7	2	30	34	2	17	15
4.6	3	6	76	8	4	5	4	34	22	6	12	22
5.5	8	17	66	1	3	1	11	3	49	14	12	11
6.4	22	4	55	7	4	8	15	3	20	24	8	30

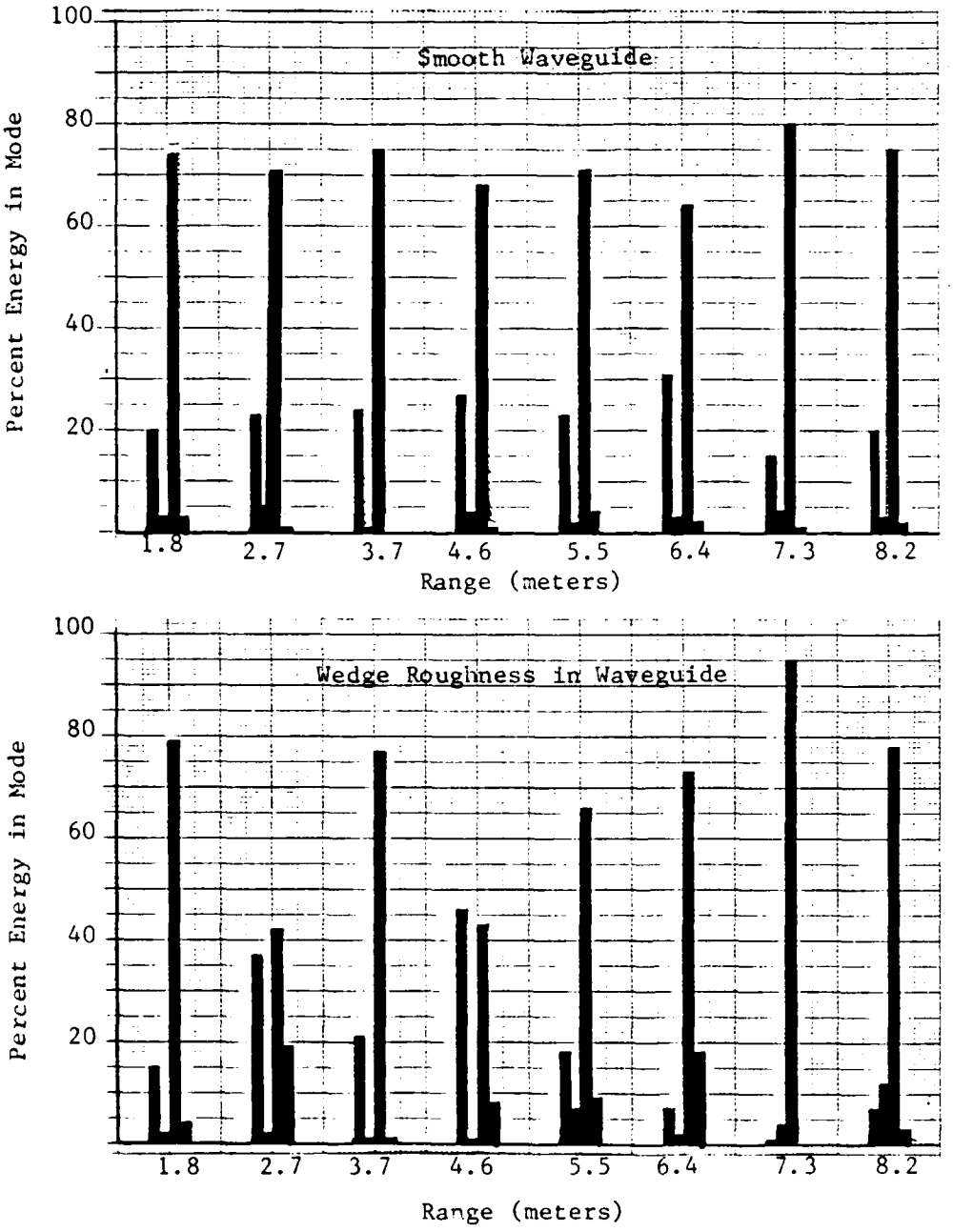

Figure 16a. Energy Distribution vs. Range at 13000 Hz, Mode 2 Driven.

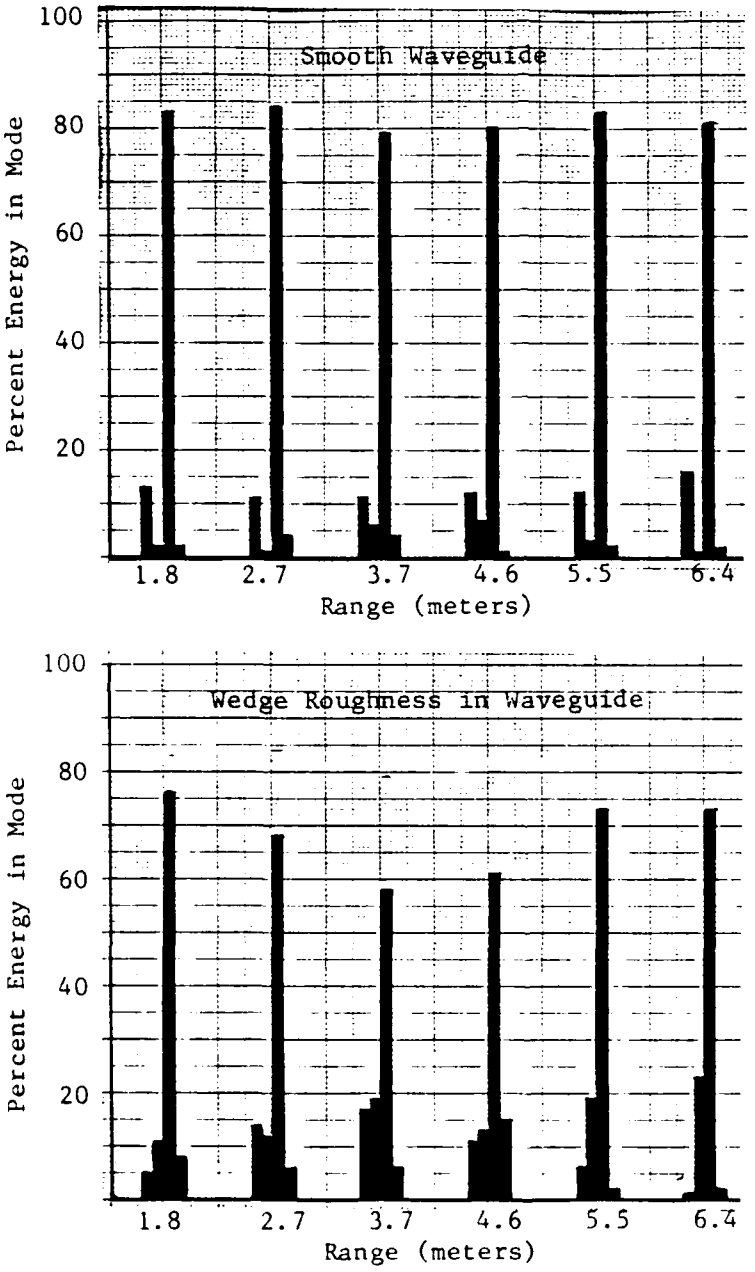

Figure 16b. Energy Distribution vs. Range at 15750 Hz, Mode 2 Driven

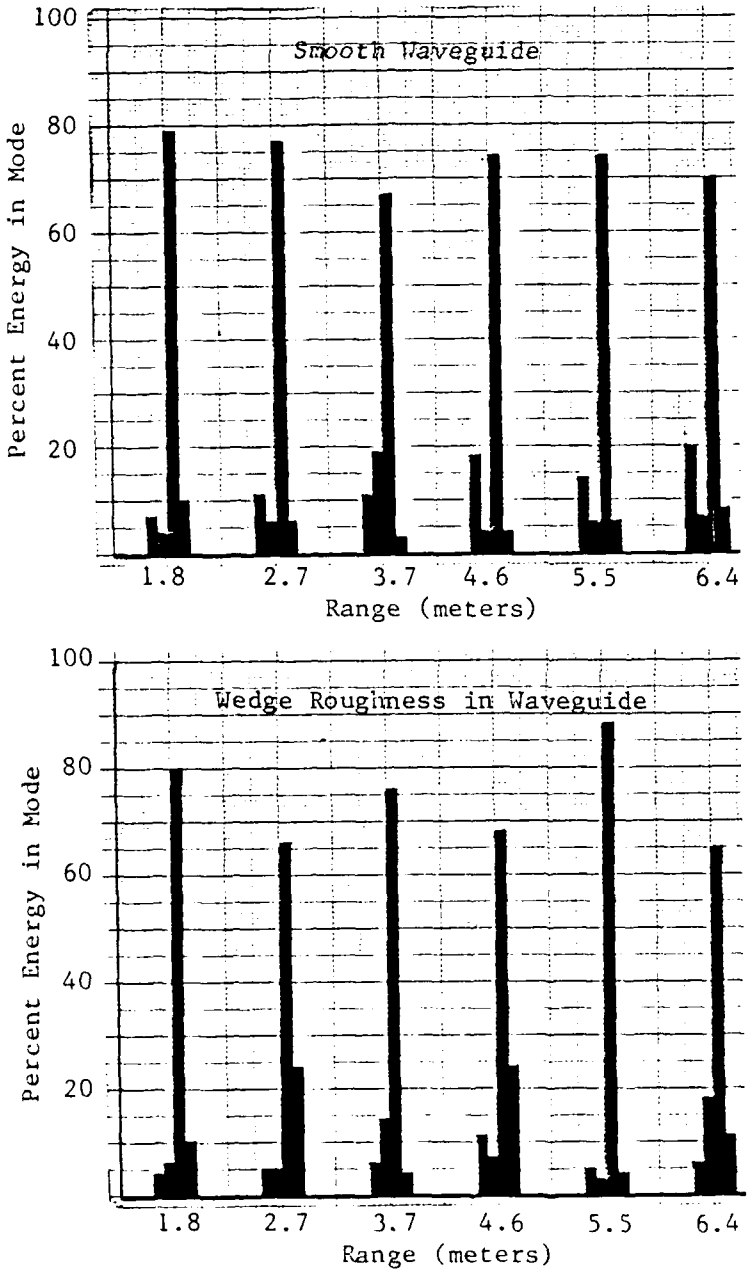

Figure 16c. Energy Distribution vs. Range at 23500 Hz, Mode 2 Driven.

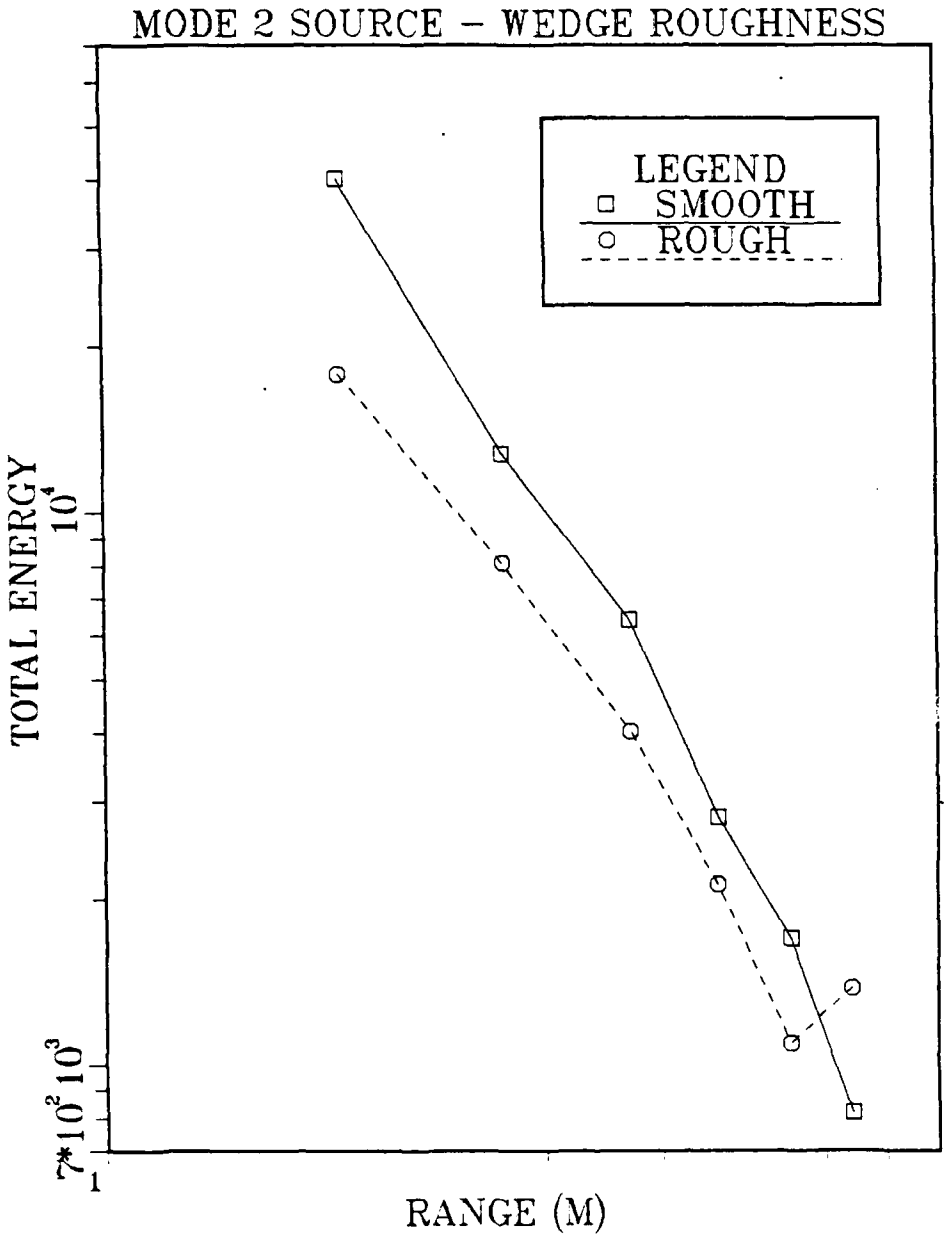

Figure 21a. Total Energy Attenuation at 15750 Hz, Mode 2 Source, Smooth vs. Deterministic Roughness.

amplitudes have been normalized. The normalization factor is the square root of the ratio of total energy energy present in the smooth waveguide to total energy present in the rough waveguide at that range. This compensates for any amplitude variations, as much as 2 dB, caused by the direction the probe tube faces. In both the smooth and rough walled waveguide, the rate of attenuation for different modes is not the same. As this does not affect the distribution of energy among modes in the smooth waveguide, it does not explain oscillations observed in the rough waveguide. The data suggests that there is oscillatory mode coupling in the presence of a deterministically rough surface.

The rate of total energy attenuation in the mode 2 driven system for the deterministically rough waveguide (Fig. 21) is less than for the smooth waveguide, as in the case of the mode 1 driven system. This is seen in Table 11 which lists the same information as Table 9 except mode 2 is driven. The values listed are averaged over 2 runs for the rough data and one run for the smooth data. It is noted that these attenuation rates are slightly different from those listed in Table 9 for mode one driven. Since the driven mode contains most of the energy present, this difference can be interpreted as a difference in attenuation for modes one and two. From a ray point of view and assuming the same loss per bounce, this is to be expected because mode two has a shorter skip distance and therefore interacts with the surface more often per unit distance. The difference in energy levels observed on these two sets of figures is because a different scaling

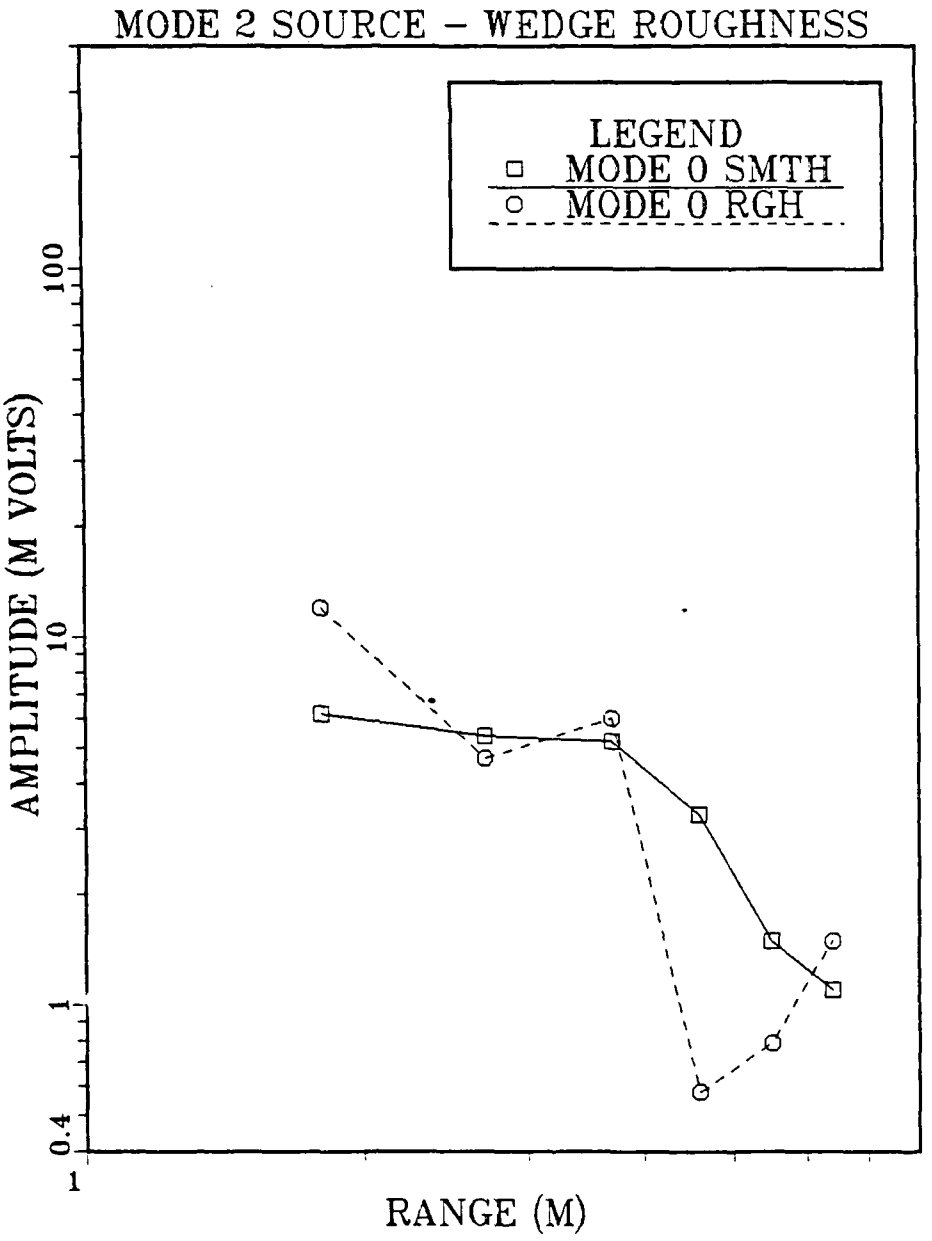

Figure 20c. Mode 0 Amplitude at 31250 Hz, Mode 2 Source, Smooth vs. Deterministic Roughness.

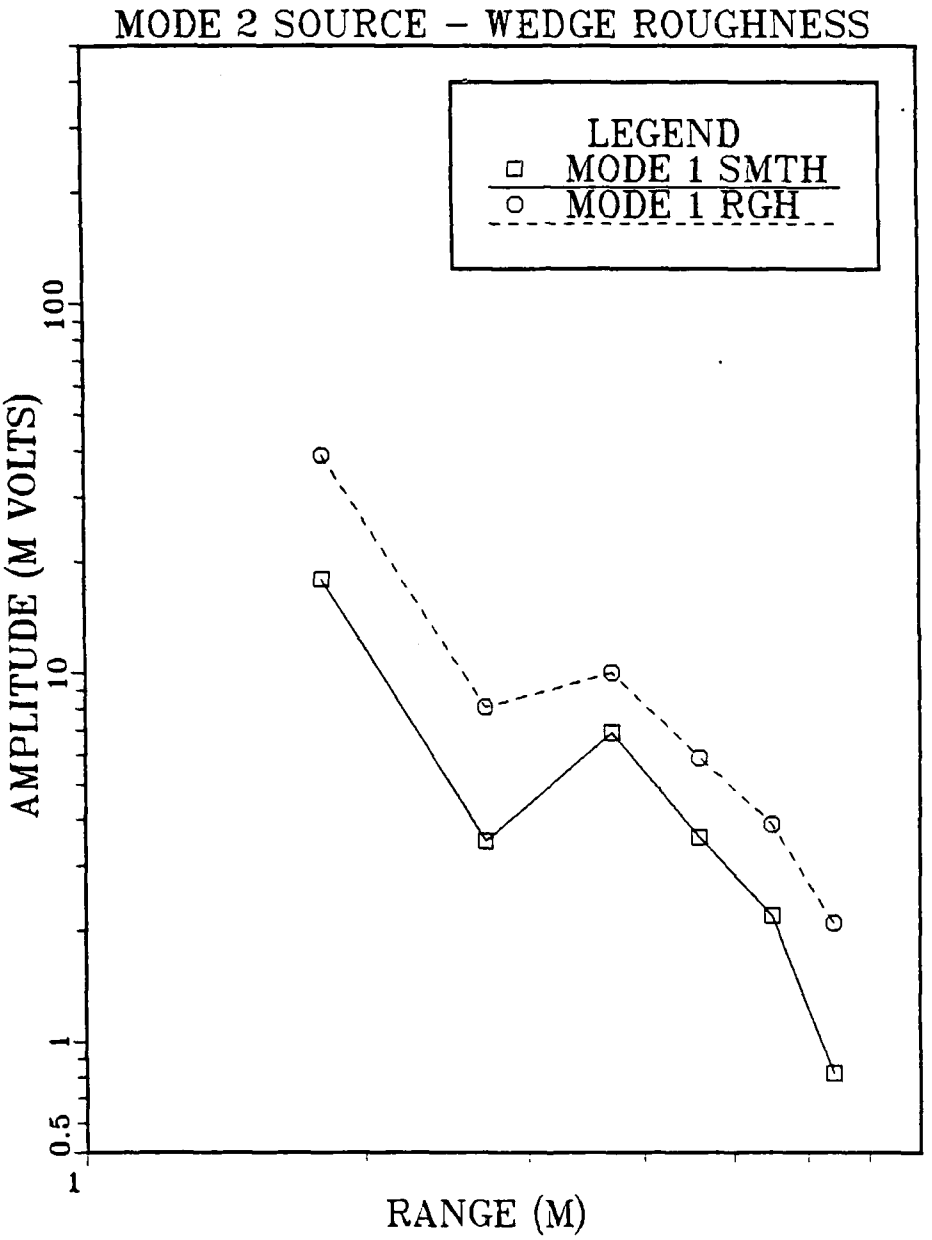

Figure 20b. Mode 1 Amplitude at 31250 Hz, Mode 2 Source, Smooth vs. Deterministic Roughness.

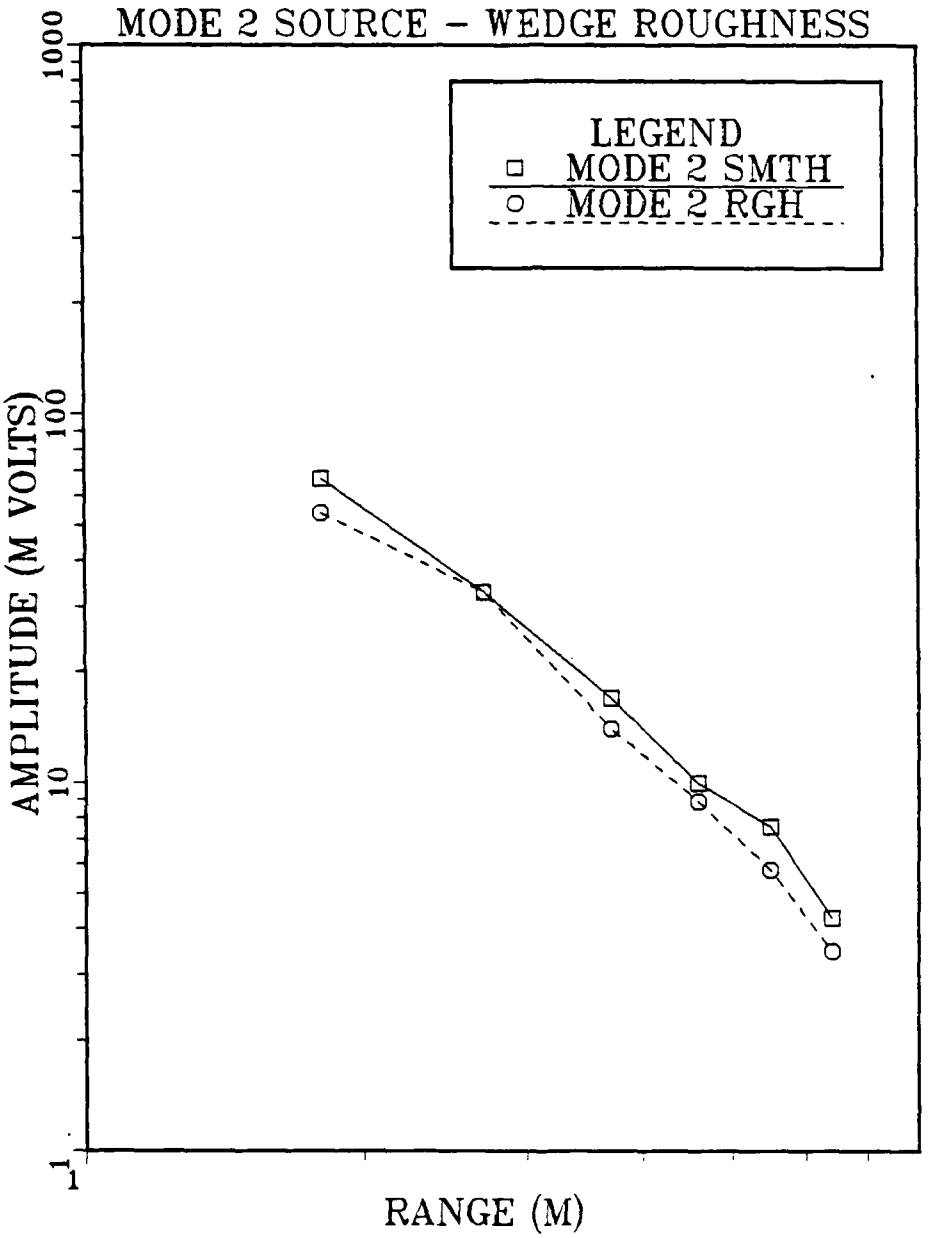

Figure 20a. Mode 2 Amplitude at 31250 Hz, Mode 2 Source, Smooth vs. Deterministic Roughness.

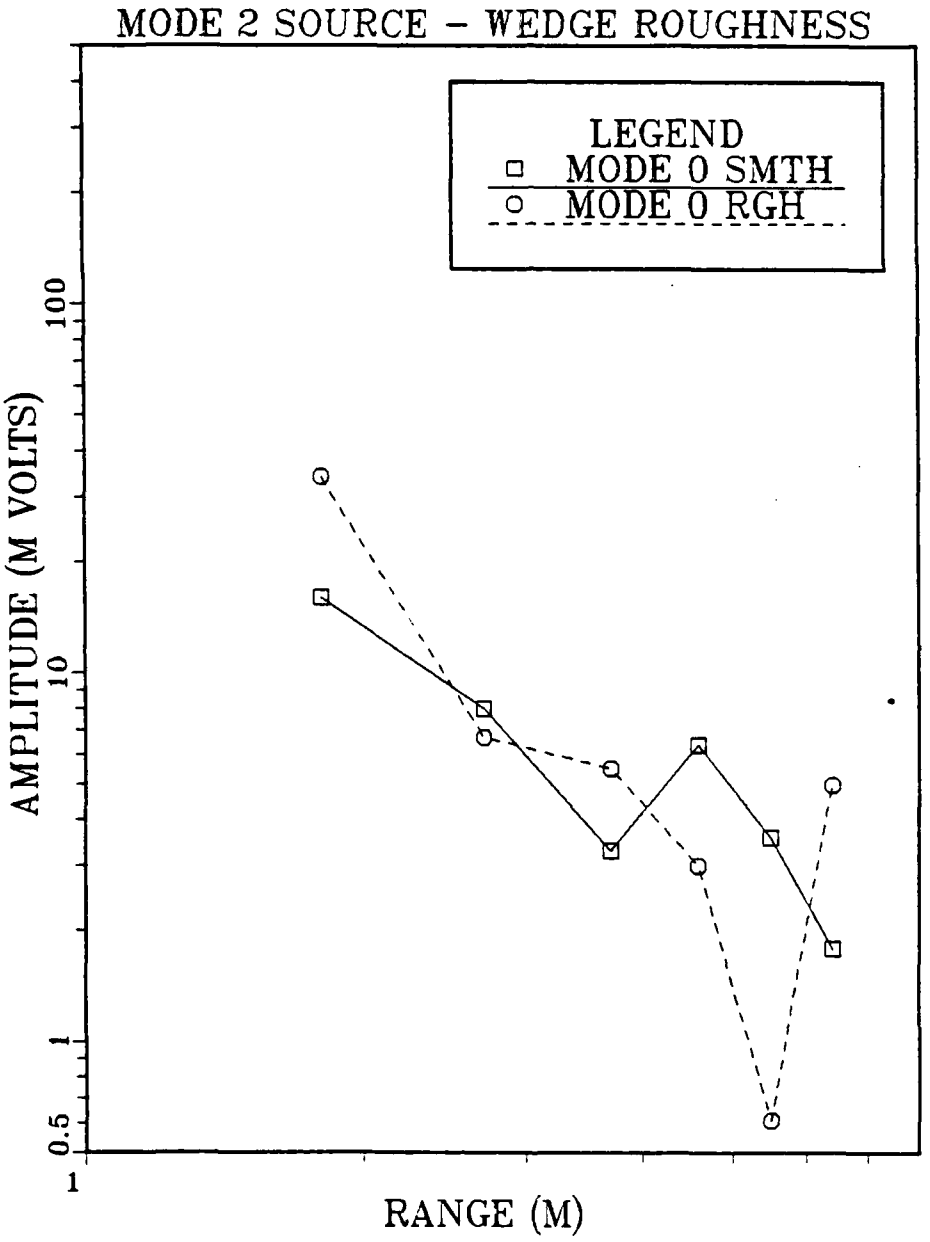

Figure 19c. Mode 0 Amplitude at 23500 Hz, Mode 2 Source, Smooth vs. Deterministic Roughness.

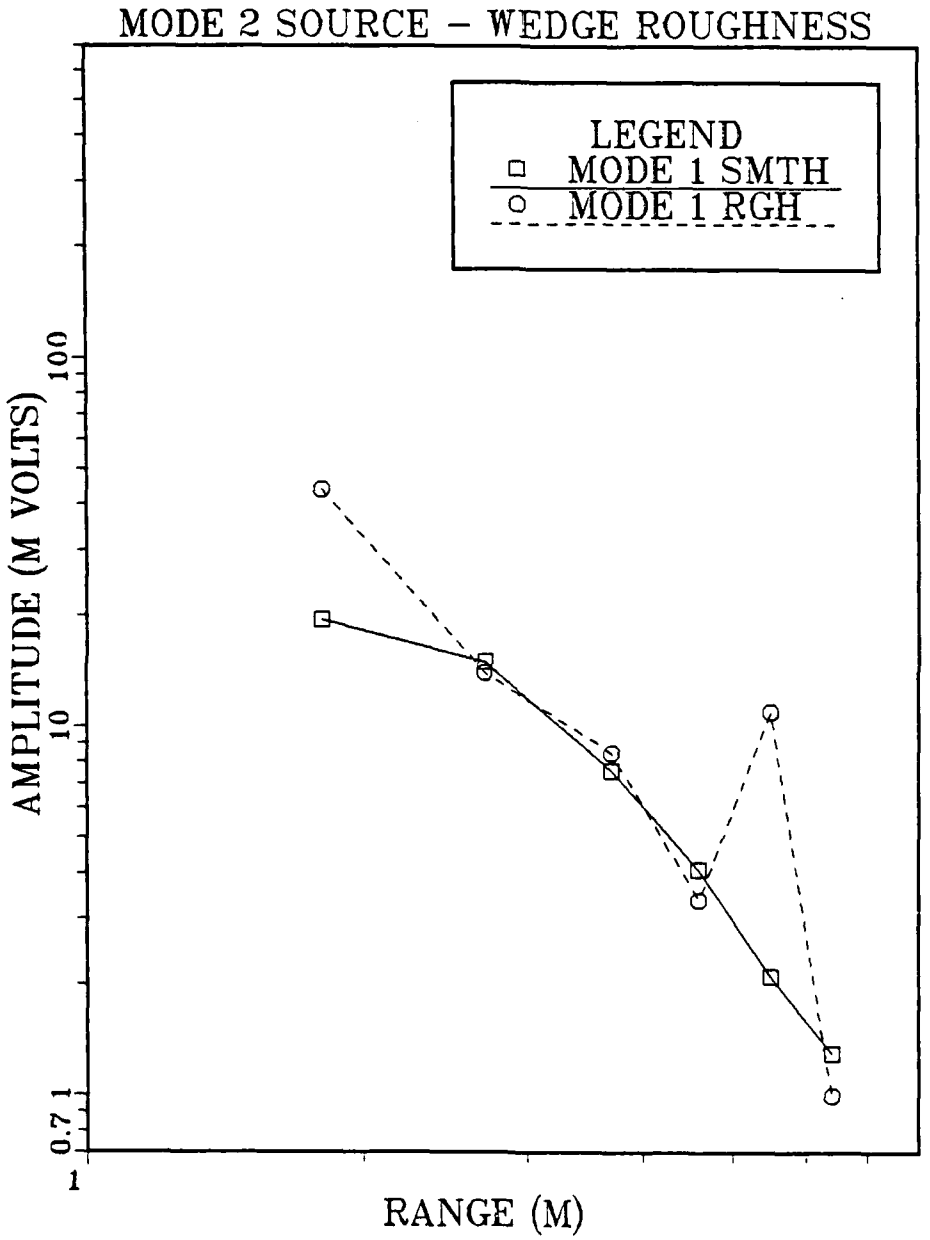

Figure 19b. Mode 1 Amplitude at 23500 Hz, Mode 2 Source, Smooth vs. Deterministic Roughness.

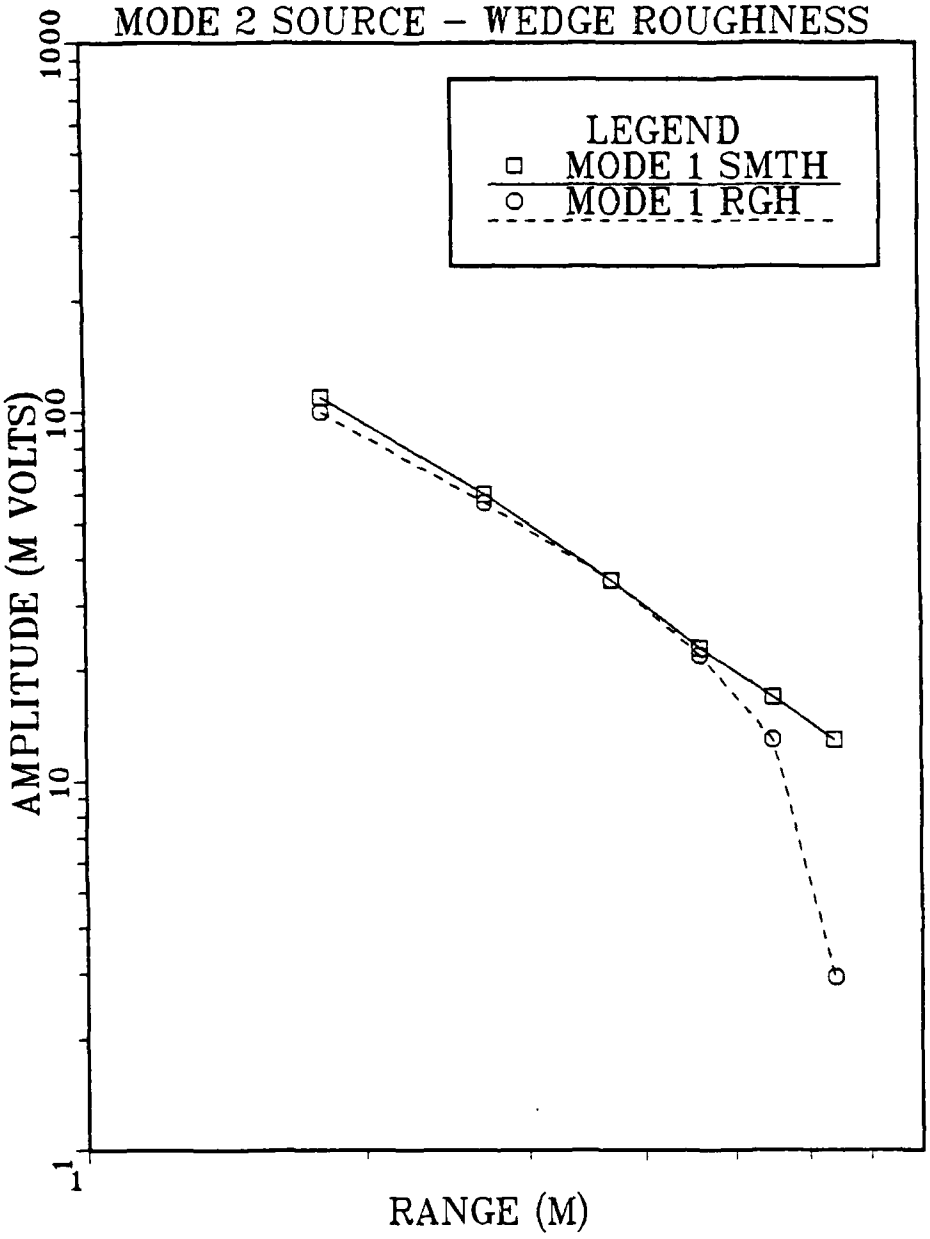

Figure 19a. Mode 2 Amplitude at 23500 Hz, Mode 2 Source, Smooth vs. Deterministic Roughness.

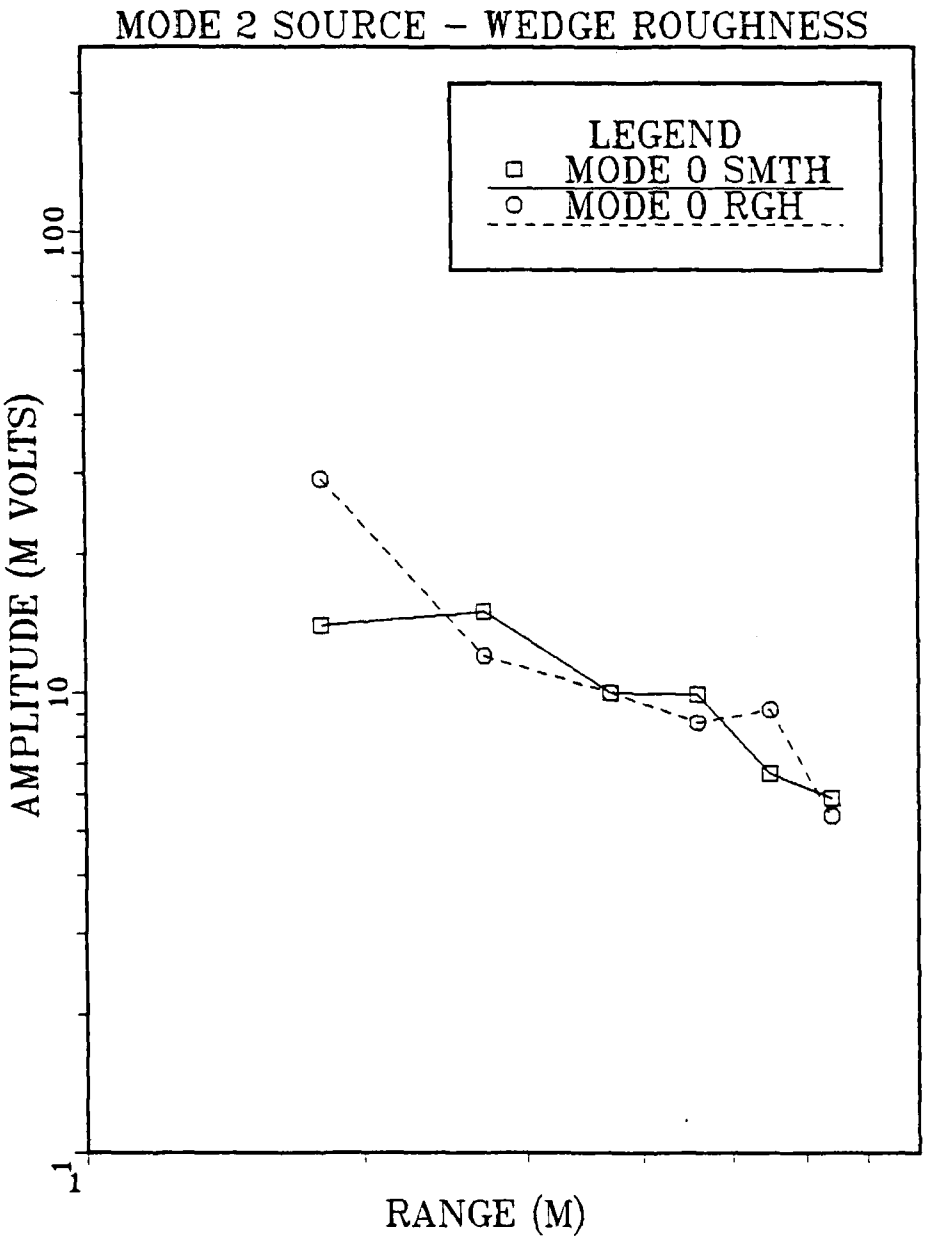

Figure 18c. Mode 0 Amplitude at 15750 Hz, Mode 2 Source, Smooth vs. Deterministic Roughness.

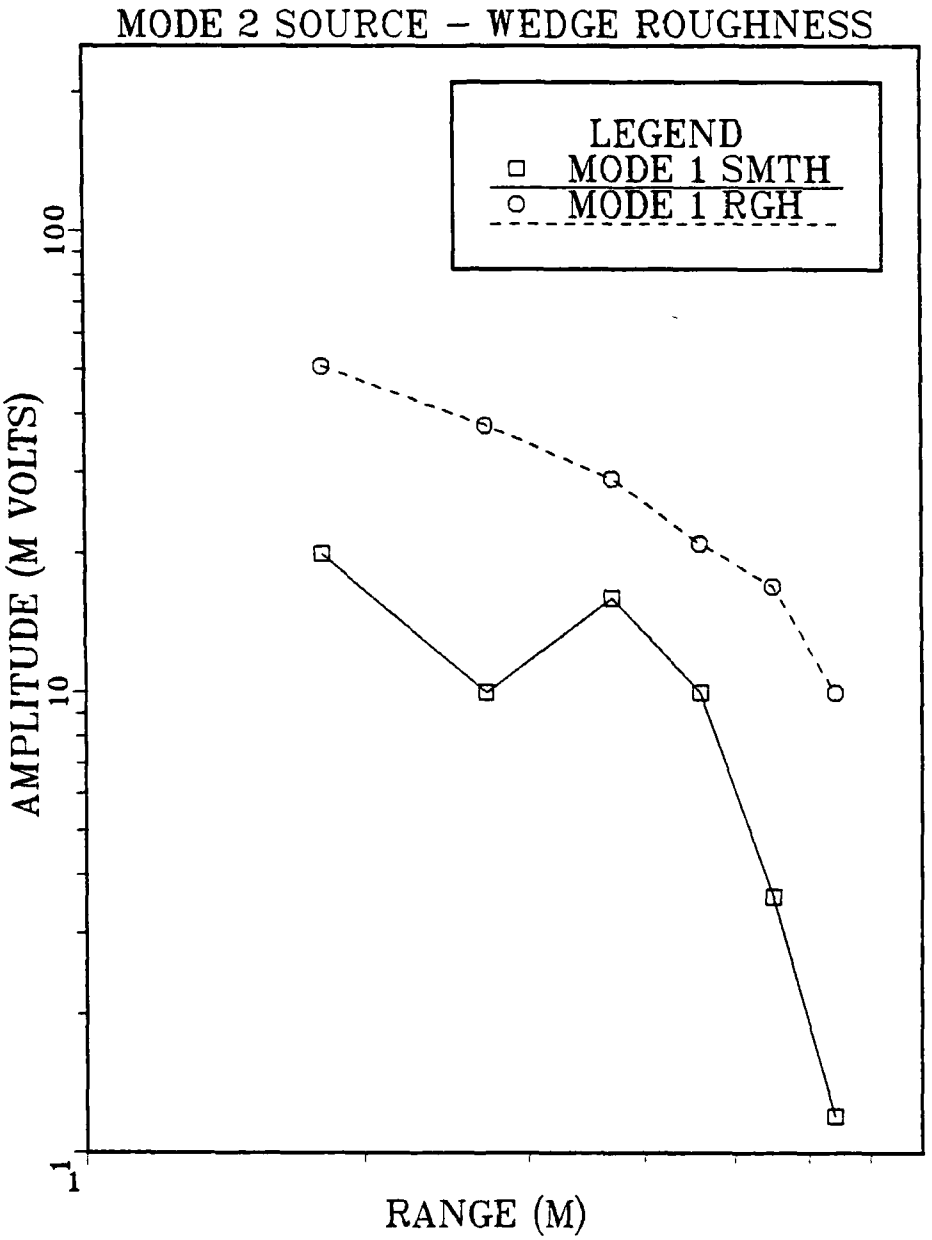

Figure 18b. Mode 1 Amplitude at 15750 Hz, Mode 2 Source, Smooth vs. Deterministic Roughness.

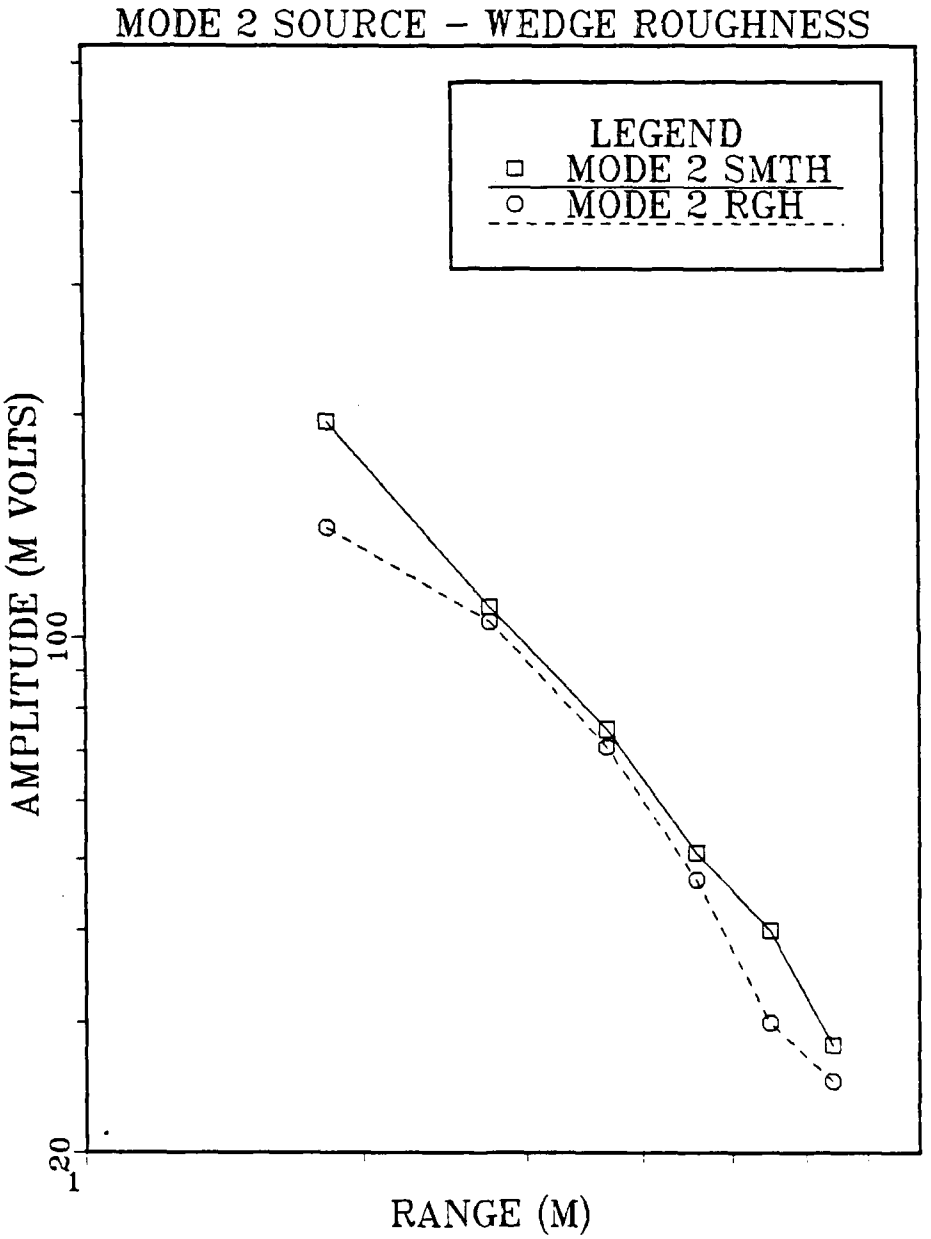

Figure 18a. Mode 2 Amplitude at 15750 Hz, Mode 2 Source, Smooth vs. Deterministic Roughness.

Deviation is about the arithmetic means of Figure 17a.

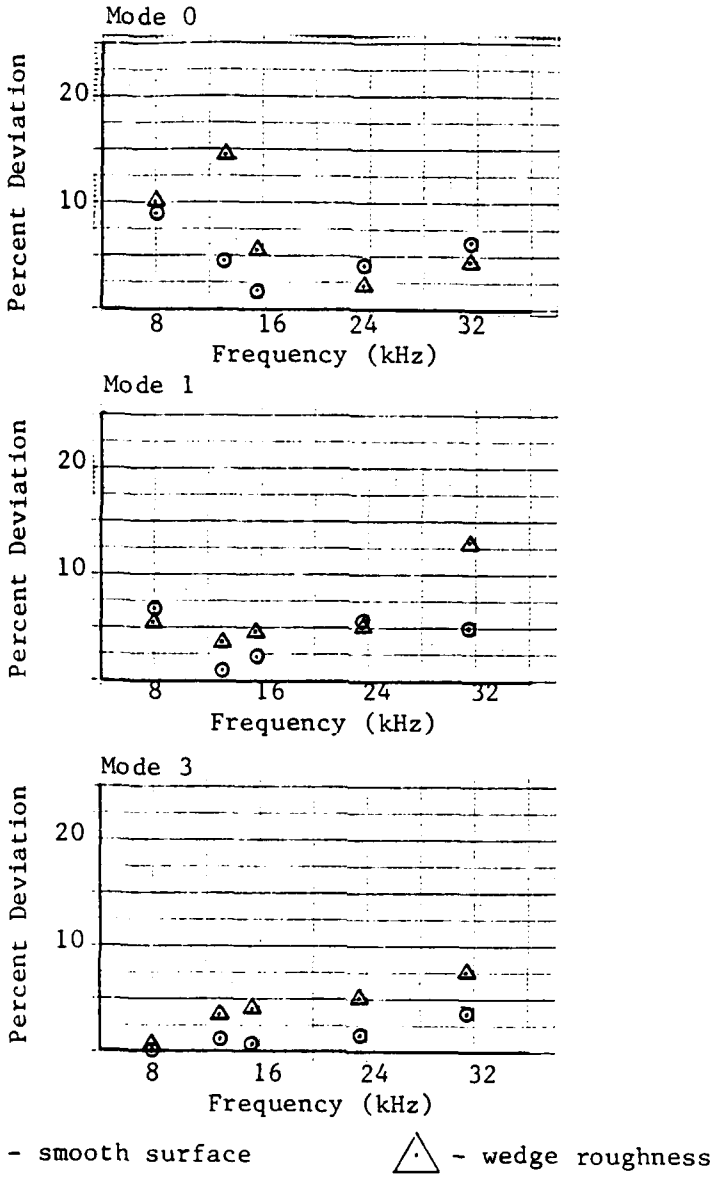

Figure 17b. Standard Deviation in Percent Energy of Modes Adjacent to Modes 2 (Mode 2 Driven).

Average percent energy is the arithmetic mean over all ranges.

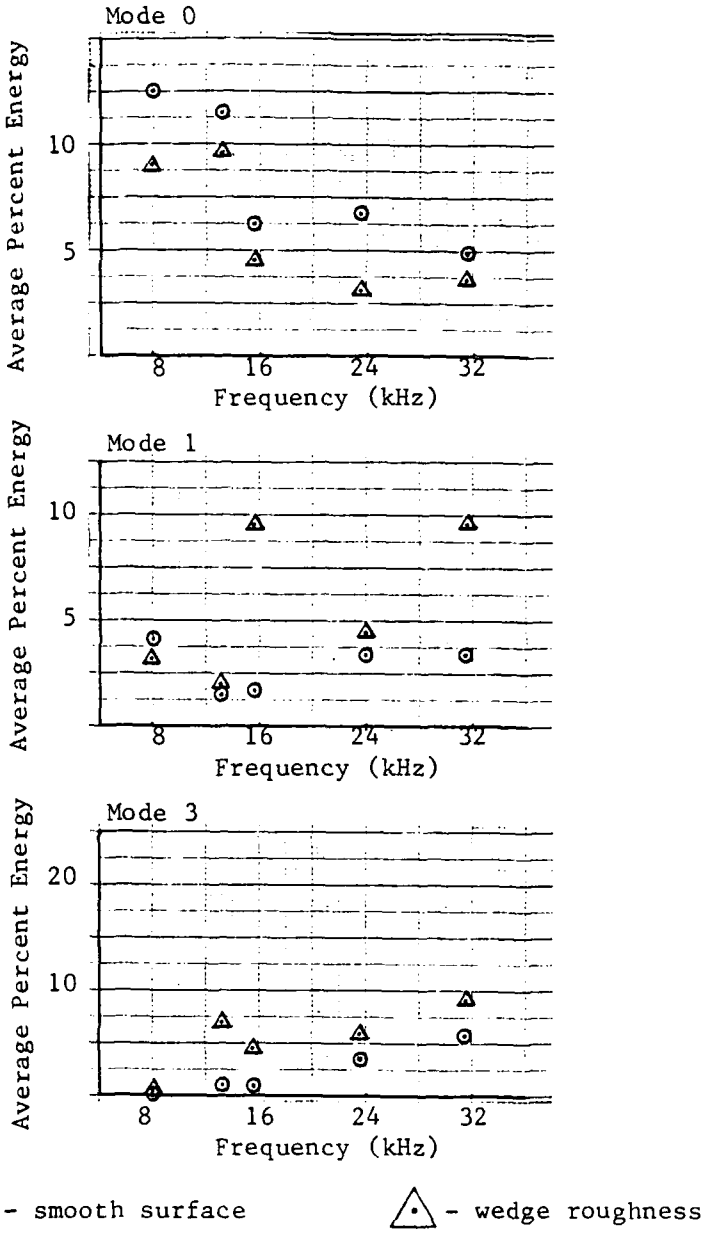

Figure 17a. Average Percent Energy in Modes Adjacent to Mode 2 (Mode 2 Driven).

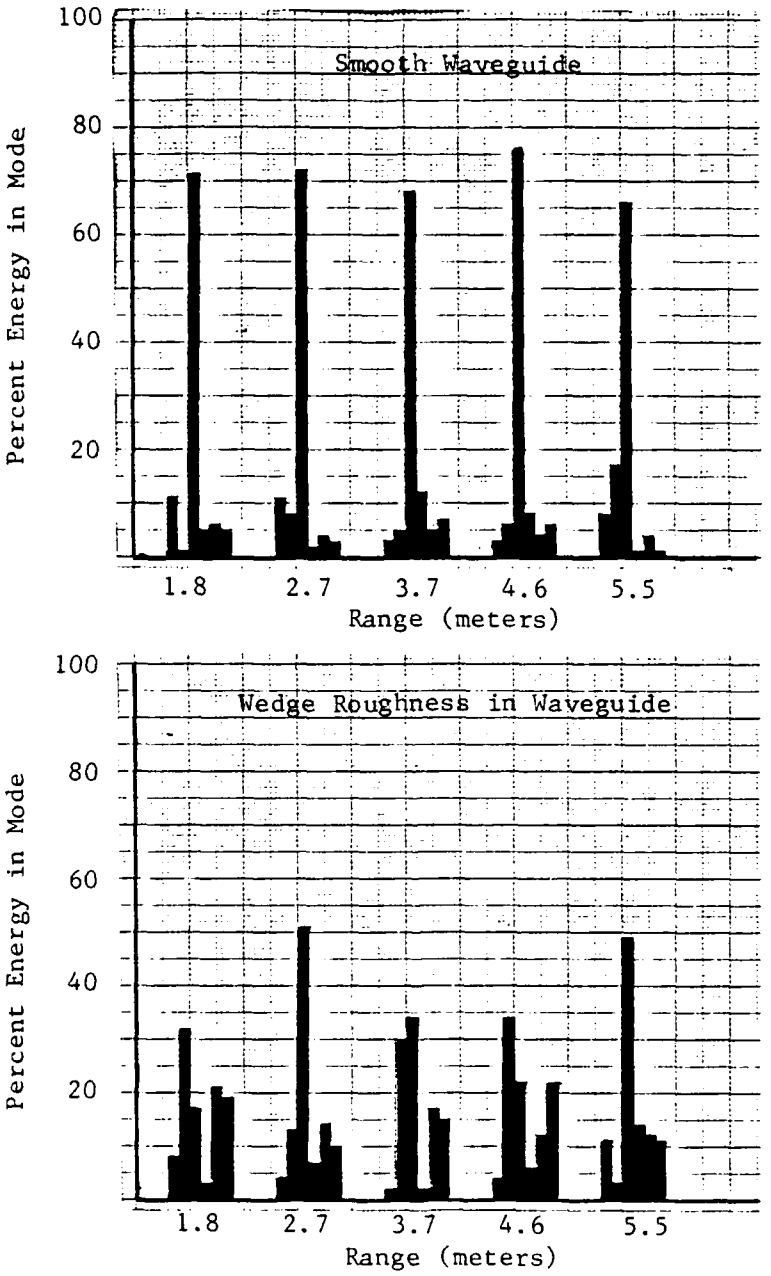

Figure 16d. Energy Distribution vs. Range at 31250 Hz, Mode 2 Driven.

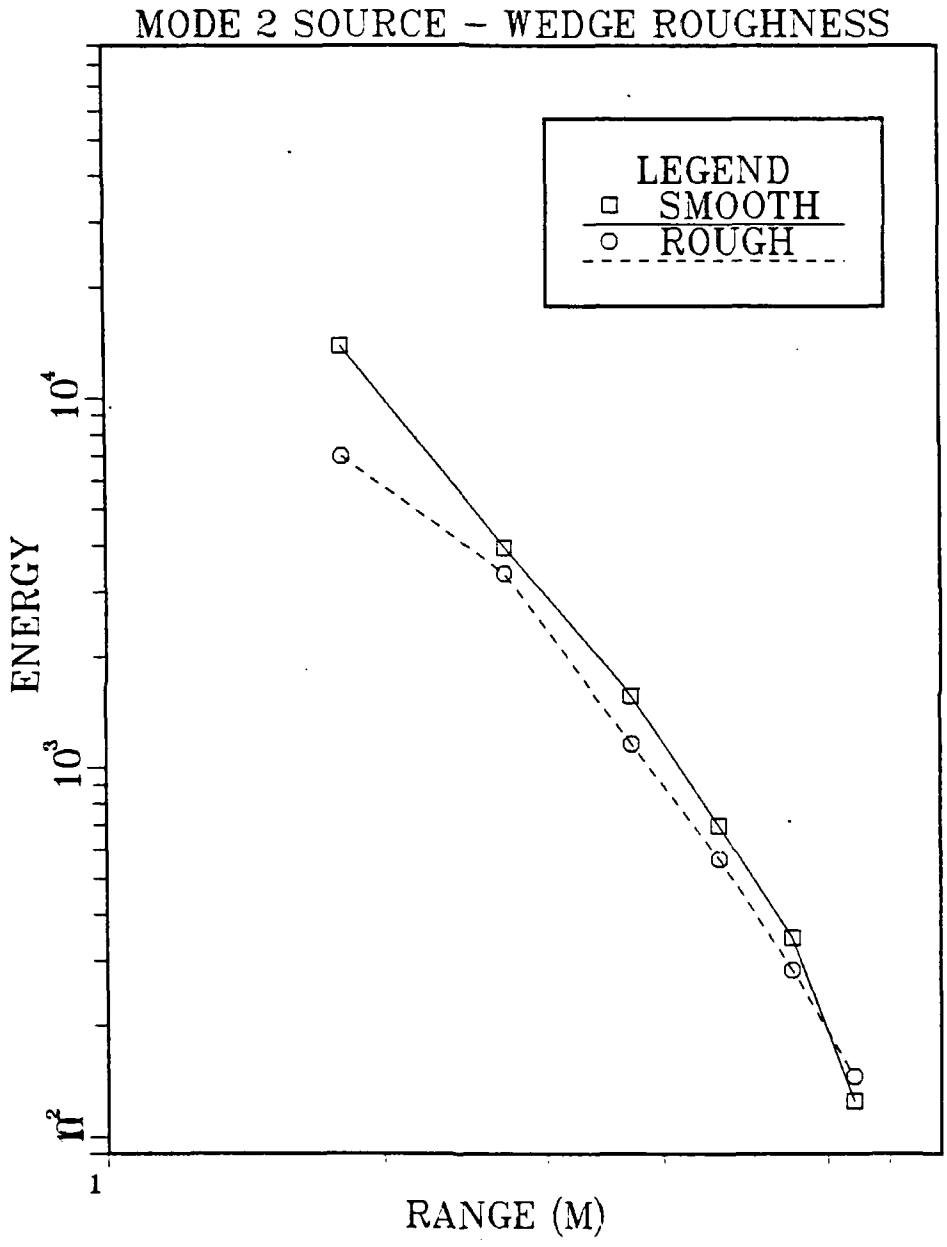

Figure 21b. Total Energy Attenuation at 23500 Hz, Mode 2 Source, Smooth vs. Deterministic Roughness.

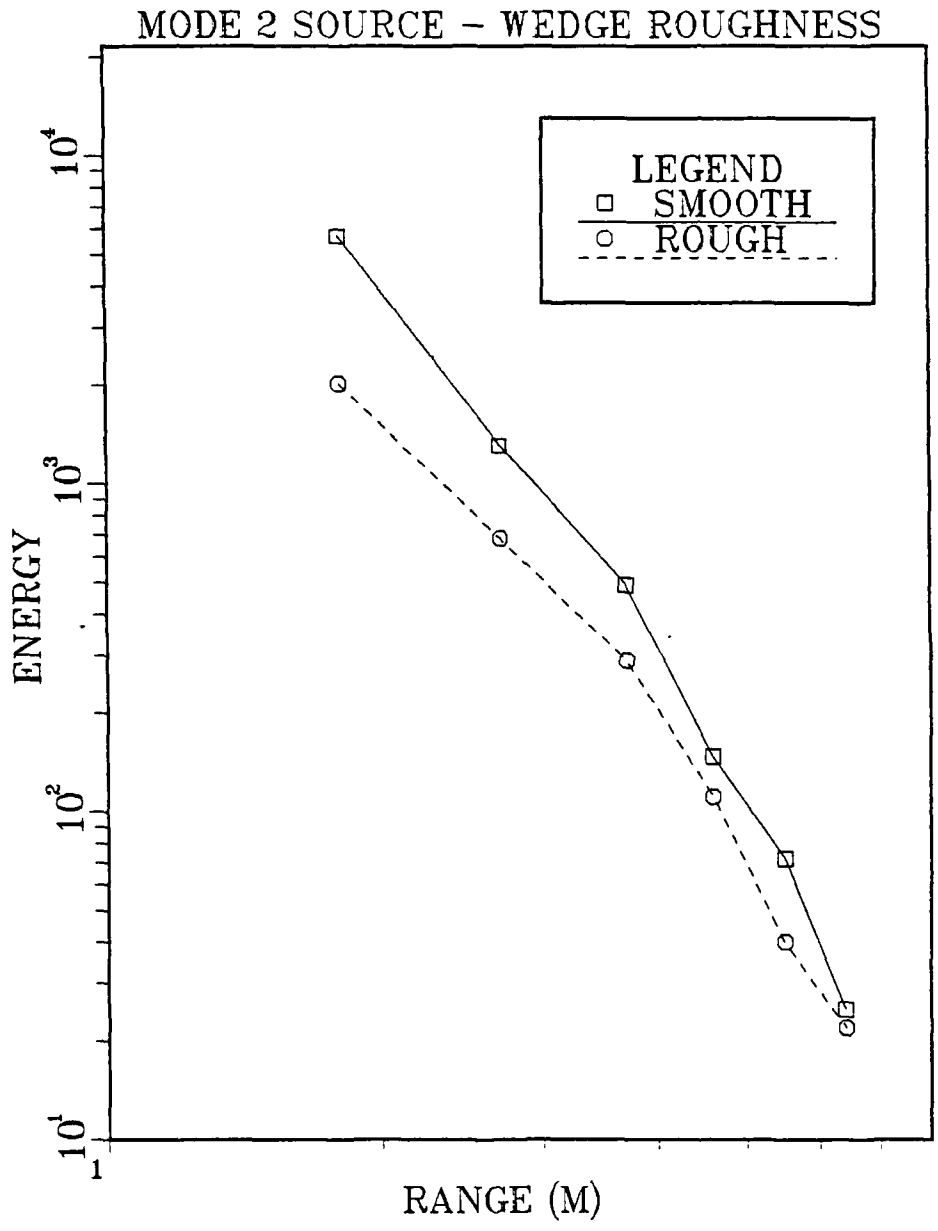

Figure 21c. Total Energy Attenuation at 31250 Hz, Mode 2 Source, Smooth vs. Deterministic Roughness.

Table 11

Energy Attenuation
in Smooth and Wedge Roughness Waveguide,
Mode 2 Driven (dB/m).

Freq (Hz)	7750	15750	23500	31250
Smooth Waveguide	2.28	2.29	2.69	3.98
Wedge Roughness	2.11	1.22	2.24	3.94

factor was used for OPHELEA (Fig. 15 data) than was used for the Nicolet (Fig. 21 data).

2. Phase Analysis

a. Mode 1

The measured phase of the driven mode can be used to determine the phase speeds of the modes and any relative shift in them due to the introduction of the roughness. Only phase information for the driven mode is analyzed since that moda has the largest amplitude and so provided the most reliable data. For a given frequency the phase speed for a mode, m, is given by

$$c_p = c_o/[1-(c_o m/2hf)^2]^{1/2}$$

where f is the frequency in hertz, c_o is the free field speed of sound in meters per second, m is the mode number and h is the height of the waveguide in meters. The most obvious difference between the phase speeds in the smooth versus rough walled waveguide is due to a change in the mean height of the waveguide. The mean height of the smooth waveguide (0.053 m) is greater than the mean height of the rough walled waveguide (0.051 m), the difference being the mean height of the roughness (0.051 m). Since the phase speed is inversely proportional to the mean height, the expected phase speed in the rough walled waveguide is greater than in the smooth waveguide. Using these heights and a free field speed of sound of 345 m/s, the phase speeds in the smooth, c_{ps}, and rough walled waveguide, c_{pr}, are calculated (Table 12). Based on the relation $\phi = \omega t - kr$, where $k = \omega/c_p$, the phase change between measurement positions in the smooth walled waveguide should be greater. The phase gain (relative spatial phase shift) of the smooth over the

	7813 Hz	11719 Hz	15625 Hz
c_{ps} (m/s)	379.50	359.13	352.74
c_{pr} (m/s)	382.72	360.33	353.38
$\Delta\phi_h$ (°)	56.86	35.68	26.34

Table 12. Effect of Waveguide Height on Phase Speed. $\Delta\phi_h$ for a Travel Distance of 0.91 m (Theoretical).

rough waveguide (Table 12) is calculated from

$$\Delta\phi_h = \omega\Delta r[(1/c_{ps})-(1/c_{pr})]$$

where Δr is the distance between measurement positions (0.91m).

$\Delta\phi_h$ is nearly invariant with respect to slight changes in the free field speed of sound, with the greatest changes occurring at frequencies close to cutoff. The stability of $\Delta\phi_h$ with changes in sound speed is calculated for a narrow range of speeds at 7813 Hz (Table 13).

Another factor affecting phase speed is attenuation. For mode 0 in a duct in which viscous losses dominate the total attenuation, Pierce [Ref. 8] gives the apparent phase speed as

$$v_{ph} = c - (c^2\alpha/\omega)$$

Using α = a/8.7 nepers/meter, where a is the attenuation in dB/meter given in Section V-A.1, v_{ph} is calculated for c=345 m/s (Table 14).

While the above formula is for mode 0 rather than mode 1 in a duct different from the waveguide used in this experiment, it does give an estimation of the relative importance of dispersion due to attenuation. Because the attenuation is nearly the same in the smooth waveguide as it is in the waveguide with corrugated roughness, dispersion due to attenuation can account for very little of the relative phase shift between the smooth and rough waveguide. The maximum difference in relative phase speed between the smooth and corrugated rough surface waveguide for mode one due soley to attenuation is 0.02%. The differences in phase speeds due to changes in height therefore dominate over those due to attenuation, although even this cannot explain the changes in the dispersion due to the roughness.

c (m/s)	342	343	344	345	346
c_{ps} (m/s)	375.51	376.84	378.17	379.50	380.83
c_{pr} (m/s)	378.64	380.00	381.36	382.72	384.09
$\Delta\phi_h$ (°)	56.46	56.60	56.73	56.86	57.17

Table 13. Effects of Free Field Speed of Sound on Relative Phase Shift. $\Delta\phi_h$ for a Travel Distance of 0.91 m (Theoretical).

	7813 Hz	11719 Hz	15625 Hz
v_{ph} in Smooth Waveguide	344.54	344.60	344.62
v_{ph} in Rough Waveguide	344.61	344.61	344.68

Table 14. Dispersion Due to Attenuation for Mode 1 and a Free Field Sound Speed of 345 m/s (Theoretical).

The observed values of the phase shifts, $\Delta\phi_{obn}$ have been calculated from the experimental data. If ϕ_{rn} is defined as the phase measured in the rough waveguide at position n (n x 0.91m from the source) and ϕ_{sn} is defined as the phase measured in the smooth waveguide at position n, the measured $\Delta\phi_{obn}$ over one range increment is then

$$\Delta\phi_{obn} = [\phi_{rn}-\phi_{sn}] - [\phi_{r(n-1)}-\phi_{s(n-1)}]$$

These values are calculated for four different data runs for the frequencies 7813 Hz, 11719 Hz, and 15625 Hz (Tables 15, 16, and 17). The average ($\langle\Delta\phi_{obn}\rangle$) and standard deviation for each frequency are computed and are also listed in these tables. These standard deviations are within those expected for a signal to noise ratio of 20 dB, the minimum accepted for reliable data. With a 20 dB signal to noise ratio, the maximum phase error (when signal and noise phases are in quadrature) is $\tan^{-1}1/10 = 5.7$ degrees. The difference of two measured phases has a possible error of 11.4 degrees, but $\Delta\phi_{obn}$ is the difference of two differences and so the possible error induced from noise alone is 22.8 degrees. Data points which are in obvious disagreement with the others at the same frequency are not included in the calculation of the average and are in parentheses in the tables. Data points with an asterisk are 1/2 the phase shift calculated over 1.82 meters. This is necessary in some instances because of a missing reading at a particular range.

Upon comparison of $\Delta\phi_{obn}$ with $\Delta\phi_h$ for each frequency, it is seen that in all cases they differ by more than the standard deviation of $\langle\Delta\phi_{obn}\rangle$. If the assumption is made that the roughness causes a decrease in phase speed, the minimum change in phase speed necessary to

	17 SEP	29 SEP	30 SEP	28 OCT
$\Delta\phi_{ob3}$	12	31	30	16
$\Delta\phi_{ob4}$	42	-22	44	-1
$\Delta\phi_{ob5}$	18	32	(289)	50
$\Delta\phi_{ob6}$	47	51	21	38
$\Delta\phi_{ob7}$		41	12	-28
$\Delta\phi_{ob8}$		-	-	35
$\Delta\phi_{ob9}$		9*	17*	29
$\Delta\phi_{ob10}$		-2	-1	

$\langle\Delta\phi_{obn}\rangle = 22°$

$\sigma = 21.50°$

Table 15. Observed Relative Phase Shifts in Degrees of Mode 1 at 7813 Hz.

	17 SEP	29 SEP	30 SEP	28 OCT
$\Delta\phi_{ob3}$	-46	-45	-72	-37
$\Delta\phi_{ob4}$	-30	-65	-49	-15
$\Delta\phi_{ob5}$	-37	-34	-39	-19
$\Delta\phi_{ob6}$	-47	-32	-72	-39
$\Delta\phi_{ob7}$		-12	-65	-45
$\Delta\phi_{ob8}$		-	-	-
$\Delta\phi_{ob9}$		-27*	-33*	-29*
$\Delta\phi_{ob10}$		(-119)	-79	

$\langle\Delta\phi_{obn}\rangle = -42°$

$\sigma = 18.30°$

Table 16. Observed Relative Phase Shifts in Degrees of Mode 1 at 11719 Hz.

	17 SEP	29 SEP	30 SEP	28 OCT
$\Delta\phi_{ob3}$	-68	-78	-104	-43
$\Delta\phi_{ob4}$	(68)	-114	-119	-55
$\Delta\phi_{ob5}$	-72	-65	-95	-40
$\Delta\phi_{ob6}$	-80	-49	-102	-67
$\Delta\phi_{ob7}$		-72	-76	-64
$\Delta\phi_{ob8}$		-	-	-
$\Delta\phi_{ob9}$		-52*	-104*	-57*
$\Delta\phi_{ob10}$		-54	-67	

$\langle\Delta\phi_{obn}\rangle = -74°$

$\sigma = 22.62°$

Table 17. Observed Relative Phase Shifts in Degree for Mode 1 at 15625 Hz.

account for the observed phase shifts ($\langle\Delta\phi_{obn}\rangle$) can be computed. If a free field speed of sound of 345 m/s is assumed, c_{ps} from Table 12 can be used for each frequency. The observed phase speed in the rough waveguide, $c_{pr'}$ can then be calculated from

$$\langle\Delta\phi_{obn}\rangle = \omega\Delta r[(1/c_{ps}) - (1/c_{pr'})]$$

The results of this calculation are listed in Table 18. The difference between the expected and observed phase speed in the rough walled waveguide can then be computed as a percentage of the expected value. (Table 18) It is apparent that the roughness causes a change in the phase speed of mode 1 that can not be accounted for by the change in waveguide height.

As a check of the percent differences obtained above, the phase data is processed by a second method. The absolute phase speeds are calculated from the average phase change between measurement stations. The phase change between stations is taken to be

$$\Delta\phi_{sn} = \phi_{sn} - \phi_{s(n-1)}$$

and

$$\Delta\phi_{rn} = \phi_{rn} - \phi_{r(n-1)}$$

for the smooth and rough waveguide, respectively. For these calculations only the data of September 29 and 30 are used since it shows the most consistency. Also, the data for the rough waveguide at 15625 Hz showed no consistency and is not used. The values of $\Delta\phi_{sn}$ and $\Delta\phi_{rn}$ are listed in Tables 19, and 20. Their averages ($\langle\Delta\phi_{sn}\rangle$ and $\langle\Delta\phi_{rn}\rangle$) and standard deviations are listed in Table 21. This measured phase shift is equal to

$$\Delta\phi = \omega\Delta r/c_p$$

	7813 Hz	11719 Hz	15625 Hz
c_{pr} (m/s)	382.72	360.33	353.38
$c_{pr'}$ (m/s)	380.72	357.73	350.96
$\frac{c_{pr} - c_{pr'}}{c_{pr}} \times 100(\%)$	0.52	0.72	0.69

Table 18. Observed Effects of Roughness on Phase Speeds for Mode 1.

AD-A154 039 MEASUREMENT OF MODE INTERACTION DUE TO WAVEGUIDE SURFACE ROUGHNESS(U) NAVAL POSTGRADUATE SCHOOL MONTEREY CA S R KASPUTIS ET AL. DEC 84 2/2

UNCLASSIFIED F/G 9/1 NL

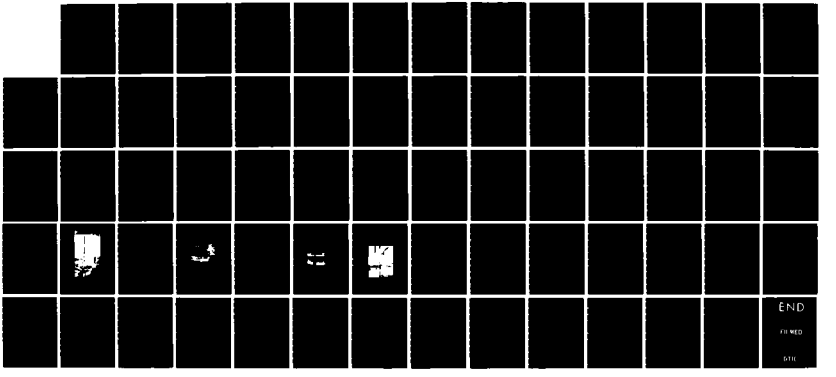

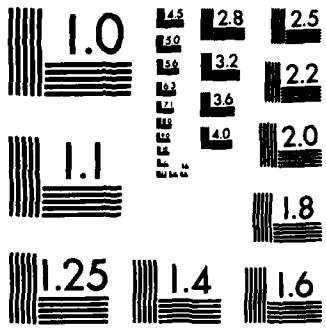

MICROCOPY RESOLUTION TEST CHART
NATIONAL BUREAU OF STANDARDS-1963-A

	7813 Hz 29 SEP	7813 Hz 30 SEP	11719 Hz 29 SEP	11719 Hz 30 SEP	15625 Hz 29 SEP	15625 Hz 30 SEP
$\Delta\phi_{s5}$	1	-6	-4	-21	100	84
$\Delta\phi_{s6}$	1	15	-32	-20	61	79
$\Delta\phi_{s7}$	18	11	-2	0	140	129
$\Delta\phi_{s9}$	2	3	25	25	118	111
$\Delta\phi_{s10}$	8	-11	-4	-10	133	113

Table 19. Phase Change in Degrees Between Stations in Smooth Waveguide for Mode 1.

	7813 Hz 29 SEP	7813 Hz 30 SEP	11719 Hz 29 SEP	11719 Hz 30 SEP
$\Delta\phi_{r5}$	33	(282)	322	300
$\Delta\phi_{r6}$	51	36	296	268
$\Delta\phi_{r7}$	59	22	345	295
$\Delta\phi_{r9}$	10	19	358	340
$\Delta\phi_{r10}$	6	-12	237	271

Table 20. Phase Change in Degrees Between Stations in Wedge Roughness Waveguide for Mode 1.

	7813 Hz	11719 Hz	15625 Hz
$\langle \Delta\phi_{sn} \rangle$	4	-5	107
σ_s	8	16	25
$\langle \Delta\phi_{rn} \rangle$	25	303	-
σ_r	22	38	-

Table 21. Average Phase Shifts and Standard Deviations for Mode 1, Smooth and Wedge Roughness Waveguide.

Since ω, $\Delta\phi$, and Δr are known, a value for c_p can be obtained and the phase speeds calculated for the smooth and rough waveguide (c_{psob} and c_{prob}) (Table 22). The phase speed in the smooth waveguide is then used in the previously stated equation for phase speed to obtain the free field speed of sound, c_o (Table 22). This value for c_o is used to calculate the theoretical phase speed in a waveguide of 0.051 m height ($c_{pr'}$, also in Table 22). The percent difference between c_{prob} and $c_{pr'}$ is calculated (Table 22). When the percent difference in Table 22 is compared to the percent difference listed in Table 18, it is seen that they are in agreement. This comparison demonstrates that the data supports a change in phase speed due solely to the roughness.

It is interesting to note that the calculated free field sound speed, c_o, (Table 22) increases with frequency. Since c_o is in reality the phase speed of mode zero, an increase with frequency is what is expected in an attenuating medium. The increase observed, however, is greater that that expected for the measured attenuation.

There are some qualifications on these conclusions. First is that all of the data used in the above analysis was collected with the use of OPHELEA. It is noted that in data collected by OPHELEA, the total energy of the modes measured repeatedly at any one position under identical conditions decreased with time. It is because of this that OPHELEA's reliability was brought into question and its use suspended. This drift, however, does not seem to affect the measured phase of the modes. Test runs at one position separated by two hours (the approximate time of a data run) showed a measured phase shift of less than 8 degrees. This 8 degree shift is only about two degrees more than that

	7813 Hz	11719 Hz	15625 Hz
c_{psob} (m/s)	375.22	356.05	350.06
c_{prob} (m/s)	376.37	354.37	-
c_0 (m/s)	341.78	342.26	342.49
$c_{pr'}$ (m/s)	378.34	357.22	-
$\frac{c_{prob} - c_{pr'}}{c_{prob}} \times 100(\%)$	0.52	0.81	-

Table 22. Phase Speeds and Free Field Sound Speeds Based upon $\langle \Delta\phi_{sn} \rangle$ and $\langle \Delta\phi_{rn} \rangle$.

which can be explained by noise as discussed earlier. It is felt that any phase shift introduced by the equipment does not significantly affect the above results since the results are consistent from run to run. This assumption remains to be verified however. This can be done by taking data in the smooth waveguide, then the rough, and then the smooth again. If the apparent change in phase speed is real, comparison of each smooth run to the rough should yield the same results.

A second qualification to the above analysis is that the assumption is made that the phase speed in the rough waveguide is slowed by the minimum amount necessary to account for the observed phase. If the number of complete cycles the mode underwent is different from assumed, the phase speed of the mode may decrease more than listed or increase. Tables 23, 24, and 25 show the phase speeds and percent change in phase speeds obtained from the first method discussed if 360 q degrees is added to the observed phase change ($\langle\Delta\phi_{obn}\rangle$) for various values of q. The tables are only calculated to the first value of the percent change greater than five percent. similar results can be obtained using the second method if the assumed number of cycles that mode one in the rough walled waveguide undergoes between stations is changed by q. The actual amount of phase change can be determined if measurements of the sound field are taken at much shorter intervals.

b. Mode 2

The $\Delta\phi$ data for mode 2 is not as consistent as that for mode 1. The only frequency for which the standard deviation of $\langle\Delta\phi_{obn}\rangle$ is less than 30 degrees is 23500 Hz. $\Delta\phi_{obn}$ at 23500 Hz for the two runs

q	$c_{pr'}$ (m/s)	$\frac{c_{pr} - c_{pr'}}{c_{pr}} \times 100(\%)$
-1	361.46	5.55
0	380.72	0.52
1	402.15	-5.08

Table 23. Change in Phase Speed of Mode 1 over Wedge Roughness at 7813 Hz Due to Cycle Error q.

q	$c_{pr'}$ (m/s)	$\frac{c_{pr} - c_{pr'}}{c_{pr}} \times 100(\%)$
-2	335.33	6.94
-1	346.16	3.93
0	357.73	0.72
1	370.07	-2.70
2	383.31	-6.38

Table 24. Change in Phase Speed of Mode 1 over Wedge Roughness at 11719 Hz Due to Cycle Error q.

q	$c_{pr'}$ (m/s)	$\frac{c_{pr} - c_{pr'}}{c_{pr}} \times 100(\%)$
-2	334.53	5.34
-1	342.55	3.07
0	350.96	0.69
1	359.80	-1.82
2	369.09	-4.45
3	378.88	-7.22

Table 25. Change in Phase Speed of Mode 1 over Wedge Roughness at 15625 Hz Due to Cycle Error q.

made with the mode 2 source and the wedge roughness are listed in Table 26 along with $\langle \Delta\phi_{obn} \rangle$ and the standard deviation. The first method of analysis performed on the mode 1 data is performed on this data. The results for c_o assumed as 345 m/s are listed in Table 27. As previously stated, the percent change listed would be different if the actual relative phase shift are 360 q degrees different than that measured.

B. RANDOMLY ROUGH SURFACE

1. Amplitude Effects

The most notable effect of the randomly rough surface is the increased attenuation rate of sound amplitude. The oscillatory effects observed in the deterministically rough surface are not strongly observed and there is a much clearer coupling of energy from higher modes to lower modes.

The dramatic increase in energy attenuation caused by the randomly rough surface is illustrated by table 28 where the attenuation rate AI in dB/m, excluding geometrical spreading, is determined as follows:

$$AI = \frac{-10}{\text{Distance}} \log\left[\left(\frac{\text{Total Energy}}{\text{Total Energy first range}}\right)\left(\frac{\text{first range}}{\text{range}}\right)\right]$$

where distance = range - first range. Recall that for the deterministically rough surface, the energy attenuation rates in the smooth and rough waveguide were nearly identical (Tables 9, 11). This same comparison is presented for the randomly rough surface with mode 1 driven (Fig. 22) and accents the greatly increased attenuation caused by the randomly rough surface.

	8 NOV	12 NOV
$\Delta\phi_{ob3}$	-104	(-270)
$\Delta\phi_{ob4}$	-73	(-242)
$\Delta\phi_{ob5}$	-62	-30
$\Delta\phi_{ob6}$	-42	-90
$\Delta\phi_{ob7}$	-59	-95

$\langle\Delta\phi_{obn}\rangle = -77.26$

$\sigma = 28.47$

Table 26. Observed Relative Phase Shifts in Degrees for Mode 2 over Wedge Roughness at 23500 Hz.

c_{ps} (m/s)	359.05
c_{pr} (m/s)	360.25
$c_{pr'}$ (m/s)	354.38
$\frac{c_{pr} - c_{pr'}}{c_{pr}} \times 100(\%)$	1.63

Table 27. Apparent Change in Phase Speed of Mode 2.

	7750 Hz	15750 Hz	23500 Hz	31250 Hz
$\Delta\phi_{ob3}$	315	194	251	(165)
$\Delta\phi_{ob4}$	302	211	174	257
$\Delta\phi_{ob5}$	313	203	274	227
$\Delta\phi_{ob6}$	300	209	220	252
$\Delta\phi_{ob7}$	310	191	236	274
$\Delta\phi_{ob8}$	313	220	242	244
$\Delta\phi_{ob9}$	314	210	205	254
$\langle\Delta\phi_{obn}\rangle$	310	205	229	231
σ	6.05	10.12	32.56	15.71

Table 34. $\Delta\phi_{obn}$ and $\langle\Delta\phi_{obn}\rangle$ in Degrees for Mode 1 Driven over Randomly Rough Surface.

	7750 Hz	15750 Hz	23500 Hz	31250 Hz
c_{ps} (m/s)	380.15	352.61	348.36	346.89
c_{pr} (m/s)	384.44	353.43	348.71	347.08
$\Delta\phi_h$ (°)	74.69	34.02	22.23	16.19

Table 33. Phase Speeds in the Smooth and Randomly Rough Waveguide for Mode 1 Based upon a Free Field Sound Speed of 345 m/s. $\Delta\phi_h$ for a Travel Distance of 0.91 m (Theoretical).

rough surface is changing the boundary condition toward pressure release. It is not expected that modes 0 and 1 would remain out of phase at the bottom of the waveguide at several consecutive ranges for two frequencies, so an altered boundary condition due to surface roughness is possible.

2. Phase Analysis

Due to the fact that the randomly rough surface could not easily be laid down or removed, there is only one data set for which runs with the randomly rough walled waveguide and smooth waveguide were made on the same day. Phase information was analyzed by the first method discribed in Section V-A. Table 33 shows the phase speeds for waveguides of 5.3 cm and 5.045 cm (c_{ps} and c_{pr}) based upon a free field sound speed of 345 m/s. Also listed is the expected relative phase shift for each frequency for which data is available. Table 34 lists the observed relative phase shifts ($\Delta\phi_{obn}$), the average ($\langle\Delta\phi_{obn}\rangle$), and standard deviation for each frequency. Tables 35 through 38 list some possible values for c_{pr}, the phase speed in the rough waveguide, calculated for c_o = 345 m/s and $\Delta\phi_{obn}$ + 360q degrees for various values of q. Also listed are the percent change in c_{pr}. It is seen that the randomly rough waveguide seems to have a greater effect on phase speed than did the deterministic surface.

An additional consideration with the randomly rough surface in the waveguide is dispersion due to attenuation. The attenuation in the randomly rough waveguide is considerably more than that in the smooth waveguide at the lower frequencies of 7750 Hz and 15750 Hz. Using the equations of section V-A, it is seen that dispersion due to

Table 32

Pressure Spectrum Magnitude (mV) as a Function of Depth for Raw Data, Mode 2 Driven, Randomly Rough Surface.

Signal-to-Noise ratio > 20dB for all data.

Data at 31250 Hz.

	Range (meters)				
Depth	1.8	2.7	3.7	4.6	5.5
0	55.6	12.01	7.31	4.52	2.40
1	52.4	12.89	6.90	4.65	2.56
2	31.3	14.12	6.51	4.26	2.65
3	18.5	7.85	5.61	3.42	2.15
4	38.6	9.96	2.57	3.18	1.99
5	53.4	11.34	2.58	2.63	1.46
6	45.1	10.93	2.04	1.63	0.96
7	52.8	11.30	2.16	0.49	0.66
8	18.1	4.39	1.96	0.56	0.65
9	43.0	9.88	0.73	0.69	0.56

Data at 23500 Hz.

	Range (meters)				
Depth	1.8	2.7	3.7	4.6	5.5
0	188	29.8	10.08	8.20	2.06
1	148	35.3	10.10	4.86	2.22
2	110	20.4	6.14	4.56	2.46
3	29	7.6	4.09	2.33	2.03
4	106	10.5	4.98	2.09	1.38
5	163	22.7	6.87	2.81	0.99
6	206	36.0	7.82	2.96	0.92
7	171	28.5	5.06	1.67	0.76
8	39	14.7	1.30	0.34	0.57
9	110	15.6	3.90	1.84	0.82

Table 31 (cont'd)

Mode 2 at 23500 Hz

Range (m)	Smooth energy in mode (%) 0	1	2	oth	Random Roughness energy in mode (%) 0	1	2	3	oth
1.8	7	4	79	10	4	27	46	11	12
2.7	11	6	77	6	6	43	39	6	6
3.7	11	19	67	3	10	31	53	2	4
4.6	18	4	74	4	42	38	3	9	8
5.5	14	6	74	6	36	54	3	0	7

Mode 2 at 31250 Hz

Range (m)	Smooth energy in mode (%) 0	1	2	3	oth	Random Roughness energy in mode (%) 0	1	2	3	oth
1.8	11	1	72	5	11	5	36	41	7	11
2.7	11	8	72	2	7	5	53	30	3	9
3.7	3	5	68	12	12	9	74	9	2	6
4.6	3	6	76	8	9	34	47	8	1	10
5.5	8	17	66	1	4	56	41	1	0	2

Table 31

Energy Distribution for Mode 2 Driven System,
Smooth and Randomly Rough Surfaces.

Modal energy distribution by percent for ten depth measurements taken by the Nicolet wave analyzer and processed on the IBM 3030.

Signal-to-noise ratio greater than 20 dB for all data.

Mode 2 at 7750 Hz

	Smooth energy in mode (%)				Random Roughness energy in mode (%)			
Range (m)	0	1	2	oth	0	1	2	oth
1.8	23	1	76	0	8	3	84	71
2.7	24	4	72	0	12	19	75	35
3.7	11	3	85	1	15	7	54	24
4.6	22	20	57	1	86	10	3	1
5.5	31	13	54	2	86	9	4	1
6.4	40	9	51	0	93	4	3	0

Mode 2 at 15750 Hz

	Smooth energy in mode (%)				Random Roughness energy in mode (%)			
Range (m)	0	1	2	oth	0	1	2	oth
1.8	13	2	83	2	1	3	85	11
2.7	11	1	84	4	4	4	82	10
3.7	11	6	79	4	3	11	80	6
4.6	12	7	80	1	14	9	61	16
5.5	12	3	83	2	24	51	20	5
6.4	16	1	81	2	38	42	17	3

Table 30 (cont'd)

Mode 1 at 23500 Hz

Range (m)	Smooth energy in mode (%) 0	1	2	3	oth	Random Roughness energy in mode (%) 0	1	2	3	oth
1.8	2	69	8	19	2	36	7	52	3	4
2.7	4	70	1	20	5	41	50	5	2	2
3.7	7	57	2	31	3	49	30	18	0	3
4.6	1	72	1	22	4	53	40	2	2	3
5.5	4	63	0	30	3	51	43	1	1	4
6.4	1	64	2	26	7	65	31	3	1	0
7.3	2	64	5	27	2	64	25	8	1	2
8.2	4	61	2	30	3	66	25	5	0	4

Mode 1 at 31250 Hz

Range (m)	Smooth energy in mode (%) 0	1	2	3	oth	Random Roughness energy in mode (%) 0	1	2	3	oth
1.8	6	62	1	29	2	19	27	38	7	9
2.7	4	66	9	19	2	56	37	1	4	2
3.7	2	69	3	21	5	57	34	6	1	2
4.6	17	36	0	12		57	35	5	0	3
5.5	10	72	3	10	5	63	31	2	0	4
6.4	13	53	2	29	3	70	27	1	0	2
7.3	11	68	2	12		74	17	5	0	4
8.2	5	59	3	29		68	22	4	0	6

Table 30

Energy Distribution for Mode 1 Driven System,
Smooth and Randomly Rough Surface.

Modal energy distributions by percent.
All data processed by Nicolet using ten depth measurements.
Signal-to-noise ratio greater than 20 dB for all data.

Mode 1 at 7750 Hz

	Smooth energy in mode (%)				Random Roughness energy in mode (%)			
Range (m)	0	1	2	oth	0	1	2	oth
1.8	0	96	0	4	1	89	9	1
2.7	2	94	2	2	0	99	1	0
3.7	1	97	2	0	1	98	1	0
4.6	1	99	0	0	1	94	5	0
5.5	1	99	0	0	5	92	2	1
6.4	1	99	0	0	4	90	6	0
7.3	0	100	0	0	2	89	6	3
8.2	1	98	1	0	4	88	6	2

Mode 1 at 15750 Hz

	Smooth energy in mode (%)				Random Roughness energy in mode (%)			
Range (m)	0	1	2	oth	0	1	2	oth
1.8	1	75	3	21	12	79	1	8
2.7	3	73	3	21	22	75	1	2
3.7	2	71	0	27	24	71	1	4
4.6	2	74	0	24	33	58	6	3
5.5	1	40	0	59	15	76	5	4
6.4	3	84	1	12	43	47	6	4
7.3	2	91	1	6	20	68	5	7
8.2	1	98	0	1	34	53	7	6

The attenuation computed using the equation for AI is frequency selective. For either mode 1 or 2, the attenuation rate at 23500 Hz is greater than the rate at 31250 Hz. If the attenuation were a function of kh for kh<1, Rayleigh scatter, attenuation would be expected to increase with frequency. For the rms height of 1.5 mm, kh is tabulated as a function of frequency (Table 29) and is shown to be in the region of Rayleigh scatter (kh<1):

Table 29

kh As a Function of Frequency, h=1.5 mm

	Frequency (Hz)			
	7750	15757	23500	31250
kh	0.21	0.43	0.64	0.86

The coupling of energy to other modes is almost exclusively to lower order modes (Tables 30 and 31) and a dramatic oscillation of percent energy among modes with range is not observed with the randomly rough surface. Energy is almost always removed from the driven mode at each successive range except for the mode 1 driven system at 15750 Hz and the mode 2 driven system at 23500 Hz. The reason for these exceptions is unclear. The mode 1 driven system couples most of its energy to mode 0, but the mode 2 driven system divides the energy between modes 0 and 1 about equally for frequencies from 15750 Hz and up. An interesting point about the mode 2 driven system can be seen in the raw data (Table 32). As the range from the source increases, the magnitude of the observed pressure is always a minimum on the rough surface at the bottom of the waveguide. This, along with the near even distribution of percent energy in modes 0 and 1, suggests that the

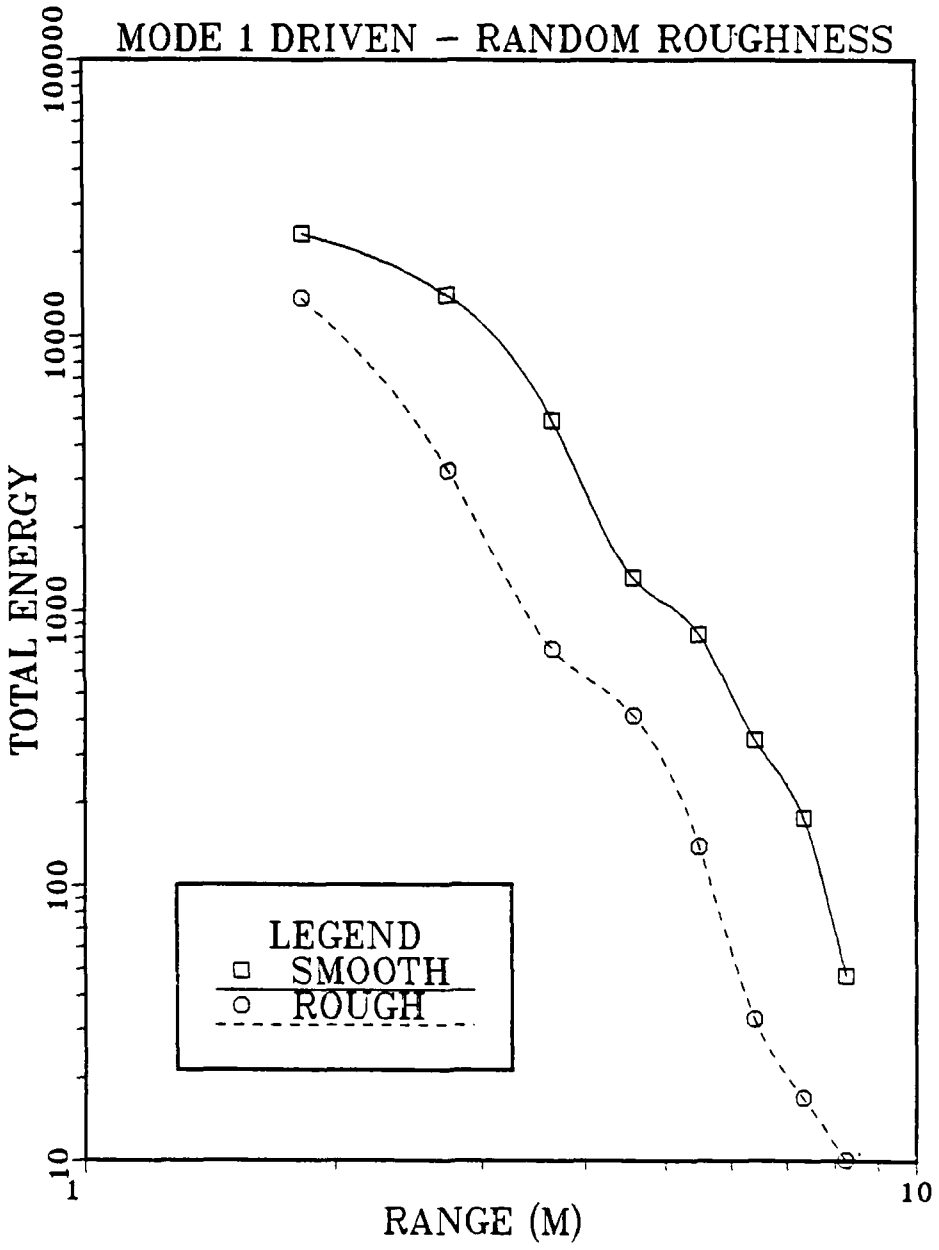

Figure 22d. Energy Attenuation at 31250 Hz, Mode 1 Source, Smooth vs. Randomly Rough Surface.

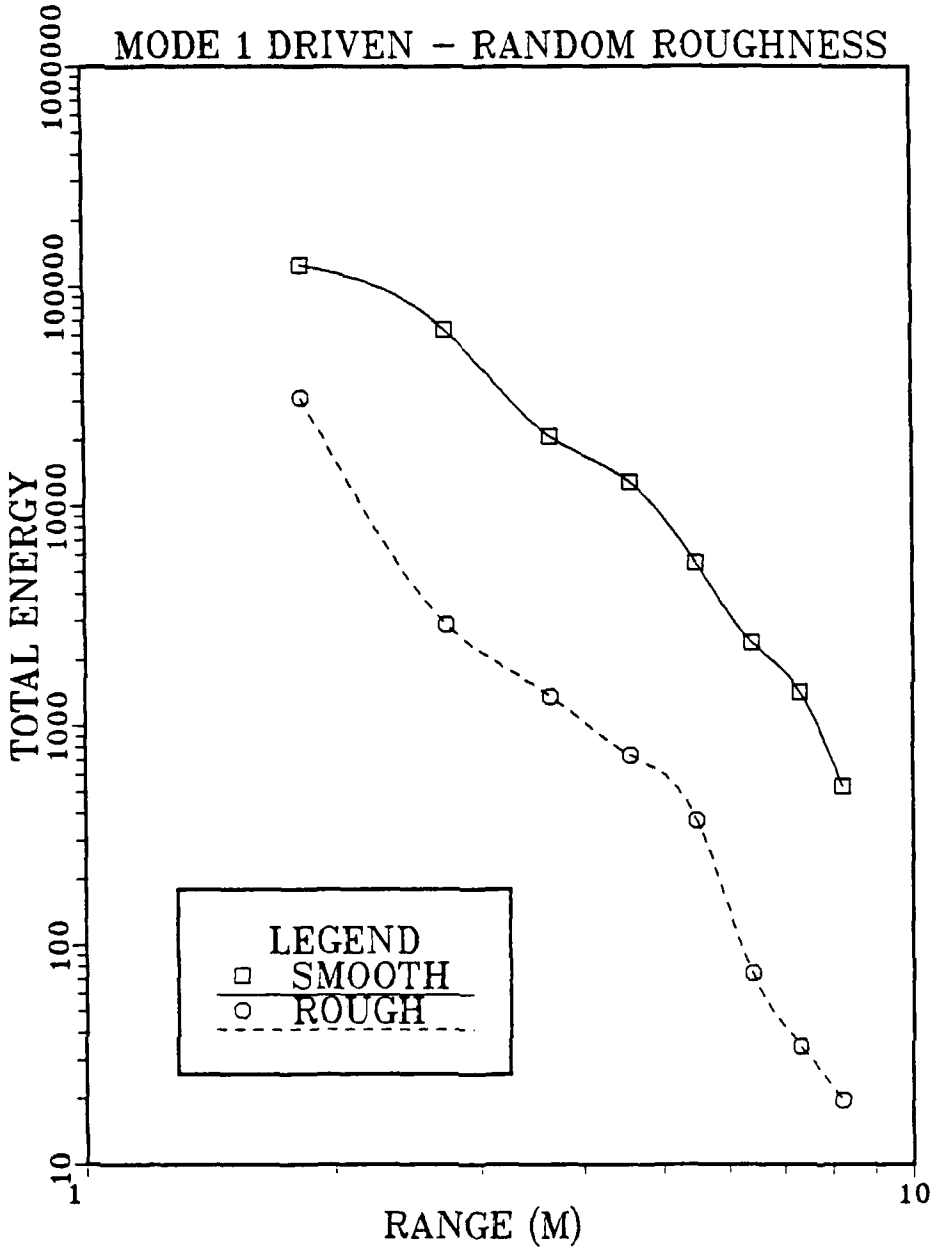

Figure 22c. Energy Attenuation at 23500 Hz, Mode 1 Source, Smooth vs. Randomly Rough Surface.

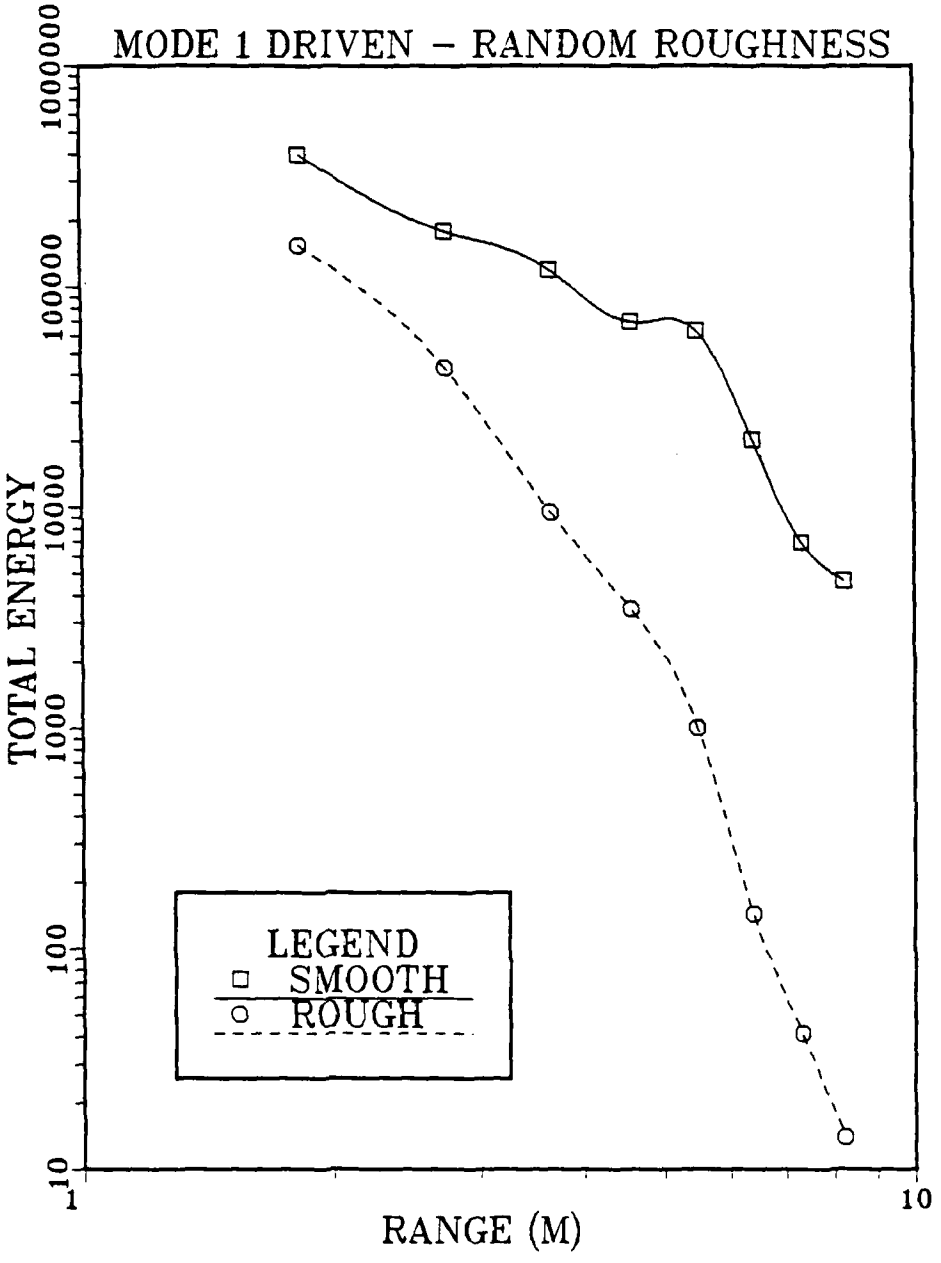

Figure 22b. Energy Attenuation at 15750 Hz, Mode 1 Source, Smooth vs. Randomly Rough Surface.

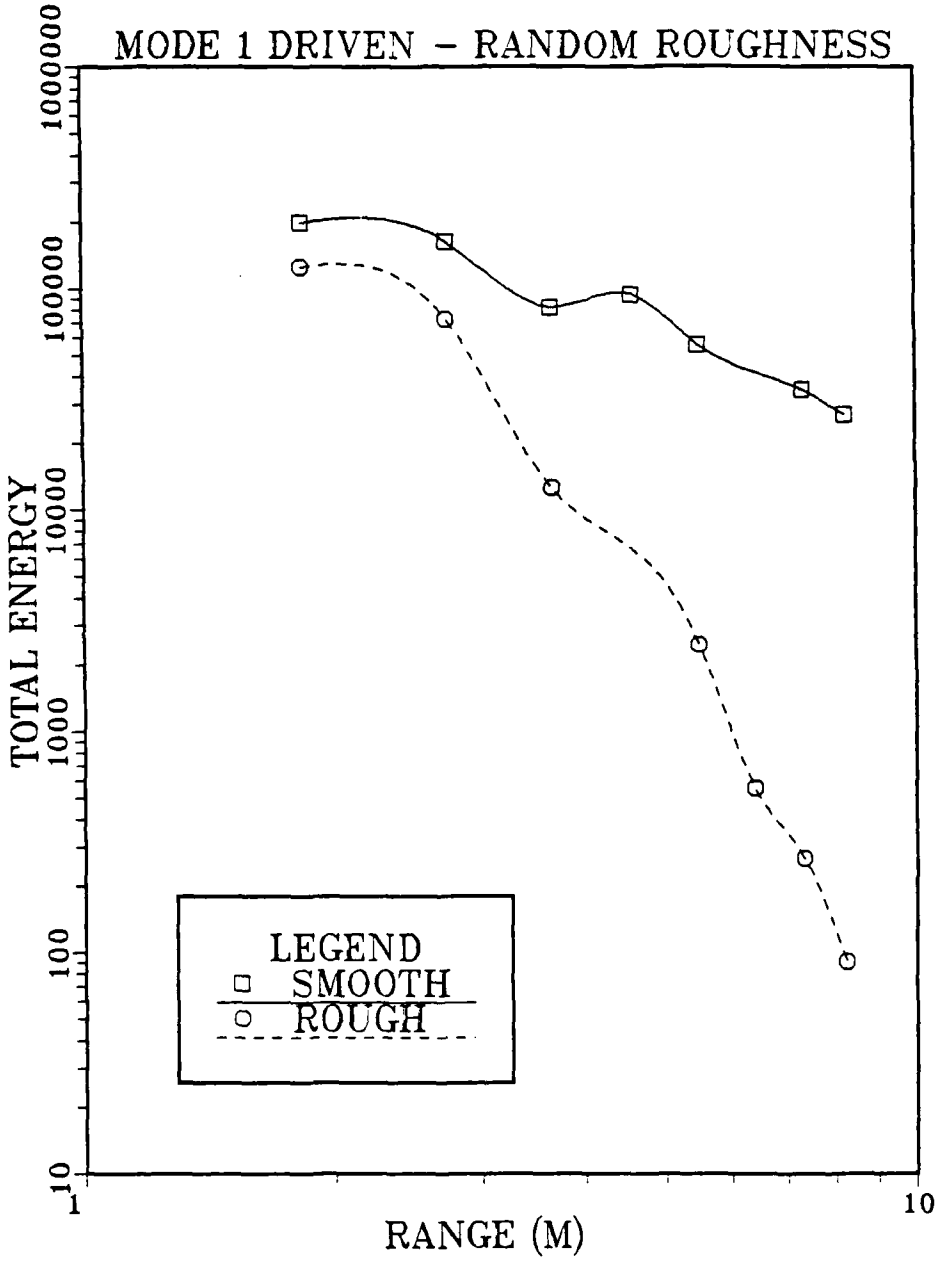

Figure 22a. Total Energy Attenuation at 7750 Hz, Mode 1 Source, Smooth vs. Randomly Rough Surface.

TABLE 28

Randomly Rough vs Smooth Surface Attenuation Rates, Mode 1 Driven

Mode 1 Energy Attenuation

Freq (Hz)	Smooth (dB/m)	Rough (dB/m)
7500	0.5	3.2
15750	1.6	4.8
23500	2.3	5.1
31250	2.5	4.4

Mode 2 Energy Attenuation

Freq (Hz)	Smooth (dB/m)	Rough (dB/m)
7750	2.0	4.8
15750	2.8	10.5
23500	3.5	12.2
31250	4.3	10.1

q	$c_{pr'}$ (m/s)	$\frac{c_{pr} - c_{pr'}}{c_{pr}} \times 100(\%)$
-1	377.30	1.86
0	398.58	-3.68

Table 35. Change in Phase Speed of Mode 1 over Random Roughness at 7750 Hz Due to Cycle Error q.

q	$c_{pr'}$ (m/s)	$\frac{c_{pr} - c_{pr'}}{c_{pr}} \times 100(\%)$
-2	340.68	3.61
-1	348.93	1.27
0	357.62	-1.18
+1	366.72	-3.76

Table 36. Change in Phase Speed of Mode 1 over Random Roughness at 15150 Hz Due to Cycle Error q.

q	$c_{pr'}$ (m/s)	$\frac{c_{pr} - c_{pr'}}{c_{pr}} \times 100(\%)$
-3	335.50	3.79
-2	340.82	2.26
-1	346.31	0.69
0	352.00	-0.94
1	357.86	-2.63
2	363.92	-4.36

Table 37. Change in Phase Speed of Mode 1 over Random Roughness at 23500 Hz Due to Cycle Error q.

q	$c_{pr'}$ (m/s)	$\frac{c_{pr} - c_{pr'}}{c_{pr}} \times 100(\%)$
-4	333.52	3.91
-3	337.46	2.77
-2	341.49	1.61
-1	345.62	0.42
0	349.86	-0.80
1	354.20	-2.05
2	358.65	-3.33
3	363.21	-4.64

Table 38. Change in Phase Speed of Mode 1 over Random Roughness at 31250 Hz Due to Cycle Error q.

attenuation at these frequencies can cause a change in phase speed of 0.24% for 7750 Hz and 0.14% for 15750 Hz. The shift is toward a slower phase speed in the randomly rough walled waveguide due to the increased viscous wall losses. At the higher two frequencies, the difference in attenuation in the rough versus smooth walled waveguide can only account for a slowing of the phase speed in the rough waveguide of less than 0.08%.

VI. SUMMARY

This experiment was the preliminary investigation of mode interaction due to steep sloped roughness elements. It demonstrated the possibility of obtaining effective cylindrical spreading in a long rectangular waveguide with absorbing sides. Using effective single mode transduction, it was shown that attenuation in the waveguide was different for different modes. Measurements of the interaction of low order modes due to the existence of steep sloped roughness demonstrated that the degree of mode interaction in a rough walled waveguide increases with increasing Rayleigh scattering parameter kh. It was also demonstrated that the existence of roughness causes a significant change in the phase speed of the modes investigated. The precise amount of this change and any trends with frequency have yet to be determined. With mode two driven over the randomly rough rigid surface, the data indicated a range dependent change of the rough walled boundry condition from rigid toward pressure release. This too is an area which needs further investigation.

APPENDIX A

MODE SOURCE TRANSDUCERS AND DRIVER SYSTEM

Effective transmission of a single mode in a waveguide [Ref. 7] is possible if the driving elements are located to reinforce the mode pressure maxima with the phase between adjacent segments shifted 180° (Fig. A-1). Using this principle, an amplifier was designed to split a single input into five independent channels with separate amplitude and phase control for each channel. Phase selection between channels is either 0° or 180°. However, at low amplifier gain, the phase between reversed channels is only 170°, as observed on a dual trace oscilloscope. This is the maximum phase error detected and is not observed at high amplifier gain. The design is implemented (Fig. A-2) using 747C dual stage, general purpose operational amplifiers. The first stage of each chip is a buffer to isolate that channel from the others; the second stage provides amplitude control. Phase is controlled by a toggle switch for each channel.

Construction of the mode transducers is straightforward. The transducer measures 5 by 10 cm which covers the entire depth (5 cm) of the waveguide. The guiding design principle is to have no element cross a null of the desired mode and to maximize the element area. The larger the area, the stronger the element's source level. For a mode two source, three elements are imbedded in the lucite backing so that they abut at the two nulls for mode 2, 1/4 depth and 3/4 depth (Fig. A-3). The aluminum elements are bonded to the lucite backing by epoxy. The unit is then ground to make the face of uniform thickness, but

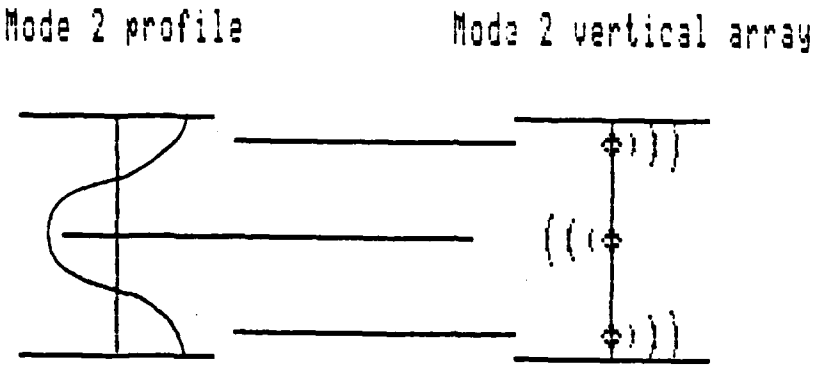

Figure A-1. Driving Mode 2 with a Vertical, Phase Weighted Array.

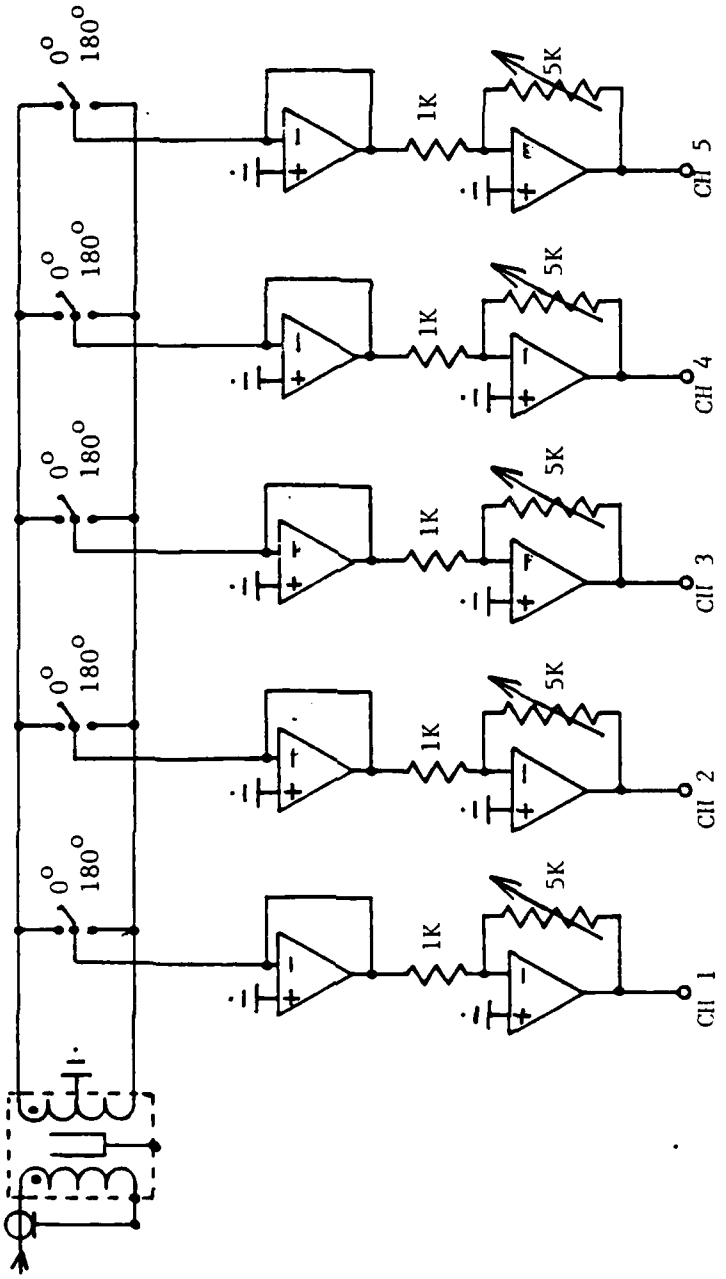

Figure A-2. Amplitude and Phase Control Amplifier.

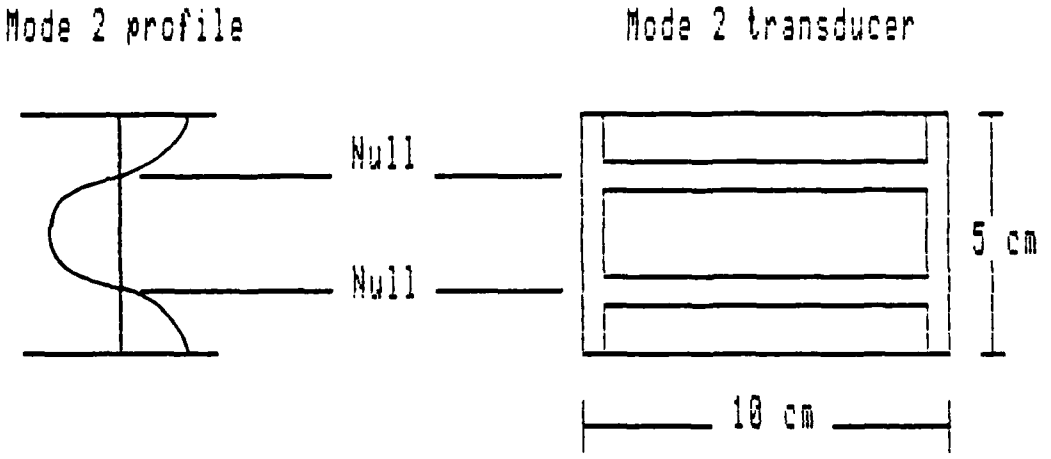

Figure A-3. Mode Transducer Element Placement.

slightly rough. When mylar is stretched over this face, the roughness creates an air space between the face and the mylar, improving the transducer response [Ref. 8]. The mylar is pre-tensioned in a jig to apply a uniform tension across the mylar sheet. The backplate then receives a light layer of quick bonding glue about its perimeter and is pressed against the mylar sheet in the jig. After 30 seconds the glue has bonded and the mylar is released from the jig. A ground lead, common with the center tap on the amplifier, is connected to its aluminized side and provides the zero plane for phase reference (direction of mylar displacement). Curves of the driving response for each element show that this tensioning technique is results in uniform response (Fig. A-4).

The transducer requires a DC bias for proper operation. This bias is provided by an external biasing circuit (Fig. A-5) which can be monitored to ensure consistent transducer response for each data run. Initially, attempts were made to permanantly polarize the mylar with an electric field of 17,000 volts/cm. The polarization uniformity over a large area of mylar was uncertain, however, and had the undesirable property of depolarizing with age [Ref. 8]. Solving this stability problem would greatly simplify the experimental set-up and provide easy-to-use sources.

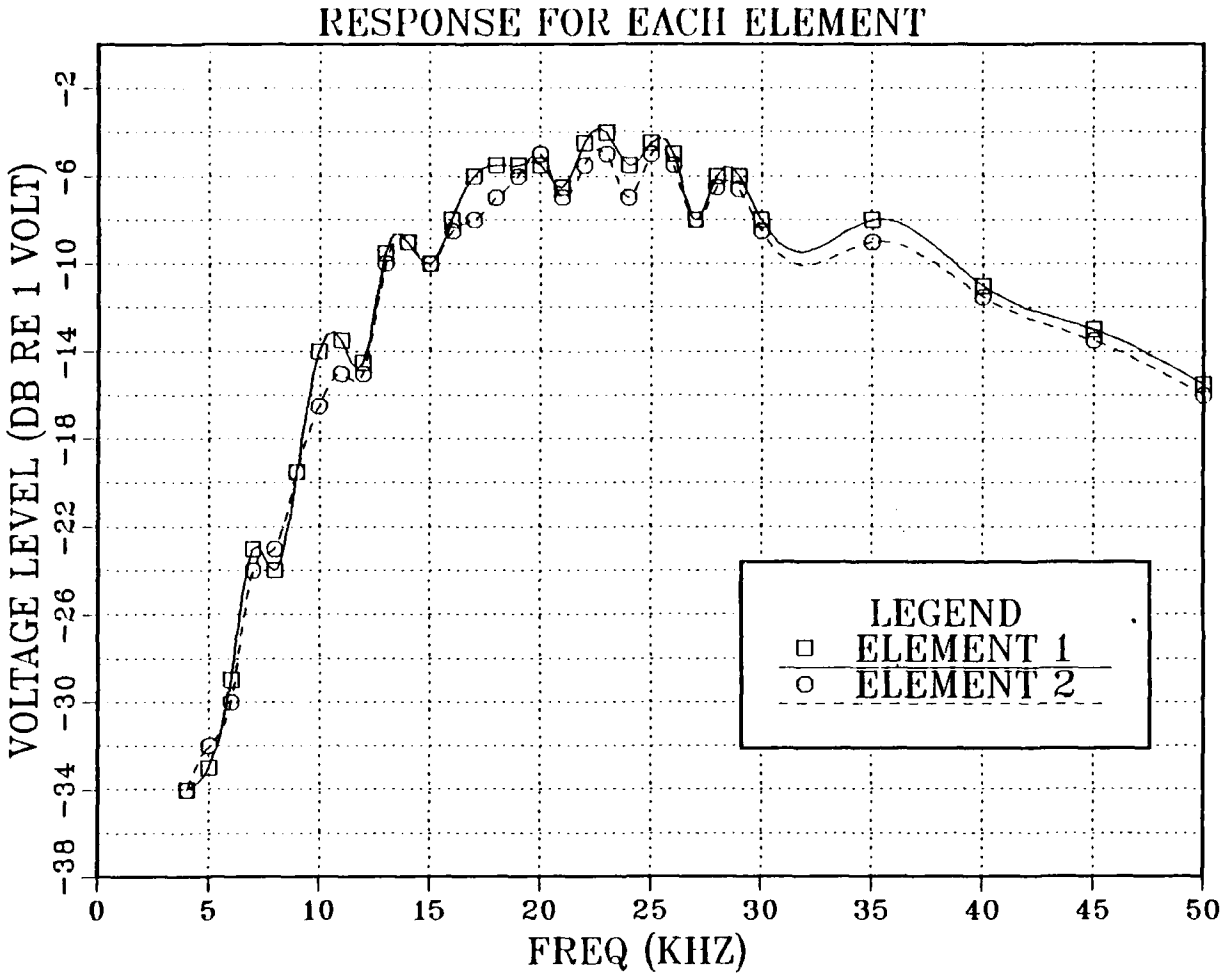

Figure A-4a. Mode 1 Transducer Frequency Response.

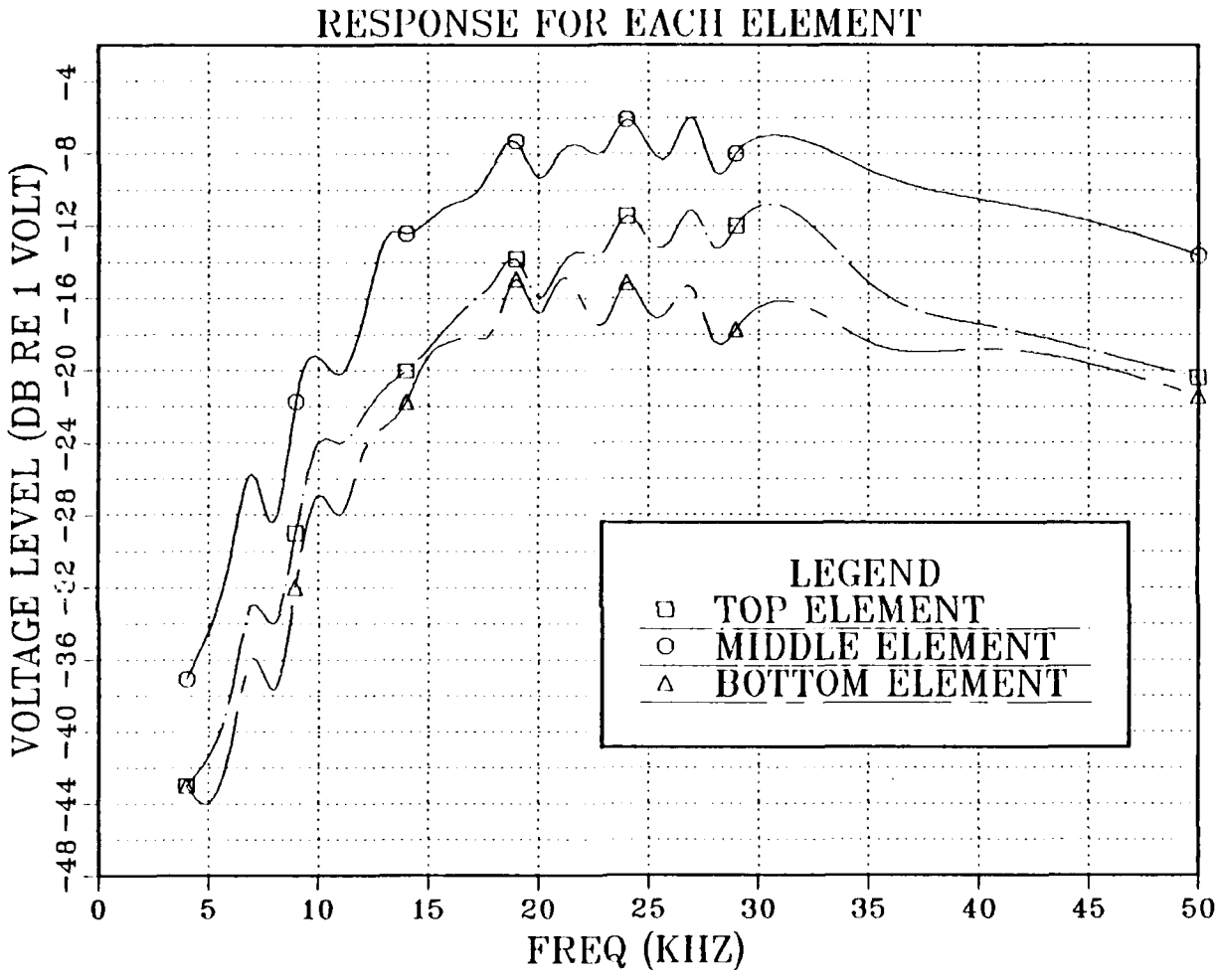

Figure A-4b. Mode 2 Transducer Frequency Response.

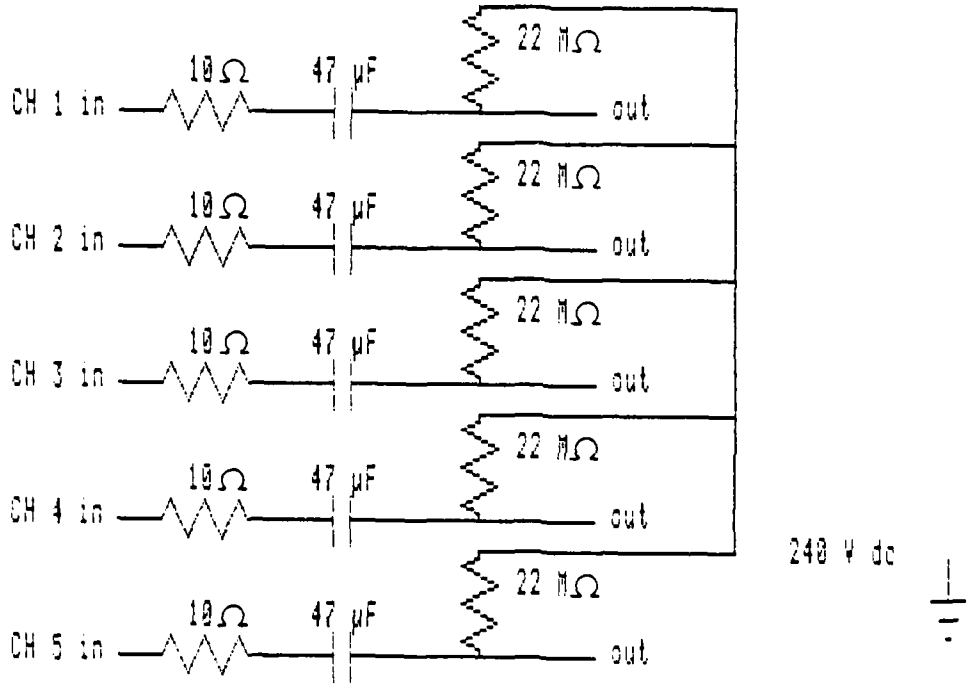

Figure A-5. DC Bias Circuit for Mode Transducers.

2) Wavetek Phaselock Signal Generator (WTK)

a) Mode - gated
b) Attn - dB
c) Sign - sinusoid
d) Freq - as required

C. Polarization Voltage - 230 VDC

D. 5 Channel Amplifier (Voltages measured on RCA WV-98c)

1) Mode 1 source connections

a. Channel 1 - 7.2 volts peak-to-peak, switch up
b. Channel 2 - 7.5 volts peak-to-peak, switch down

2) Mode 2 source connections

a. Channel 1 - 7.0 volts peak-to-peak, switch up
b. Channel 2 - 4.0 volts peak-to-peak, switch down
c. Channel 3 - 7.6 volts peak-to-peak, switch up

E. PARS

1) Gain - 50
2) LF roll off - 100 Hz
3) HF roll off - 100 kHz

F. Kron-Kite Filters

1) High pass - 6 kHz
2) Low pass - 41 kHz

G. Nicolet FFT analyzer

1) Signal enhance
2) Average Time
3) Transient
4) 50-100 averages - AVG N

H. Decade Frequency Synthesizer - 249,999.9 Hz

APPENDIX C

EQUIPMENT SETTINGS

A. Timing Simulator

1) When ARB used as signal generator

Word	Output	Time
0	n.a.	100 msec
1	1 (to ARB)	100 usec
2	n.a.	115 msec
3	9 (to OPHELEA)	5 msec
4	n.a.	100 msec

2) When Wavetek used as signal generator

Word	Output	Time
0	n.a.	100 msec
1	1 (to WTK)	1 msec
2	n.a.	115 msec
3	9 (to OPHELEA & WTK)	5 msec
4	n.a.	100 msec

B. Signal Generators

1) Abitrary Waveform Generator (ARB)

a) Mode - trig
b) Output - on
c) amp - 2.3 V
d) Prst length - 550
e) Block - full
f) Clock - internal
g) func

i. Composite Signals - use block rate of 3906 Hz

RAM 8

X	Y
0	0
16	122
32	0

ii. Sinusoidal Signals - use desired block rate

Table B-1

Equipment Settings for the RSM.

Type and Model	Setting
Wavetek Model 144 HF Sweep Generator	20 KHz Square Wave
PMC Regulated Power Supply	10 Volts, Current Limit Fully Clock-wise
Hewlett Pcakard Model 721A Power Supply (1)	5 Volts, 225mA Short Circuit Current
Hewlett Packard Model 467A Power Amplifier (1)	X1
Hewlett Packard Model 467A Power Amplifier (2)	X1
Power Design Inc. (PDI) Model 3650R Transistorized Power Supply	24 Volts, 4 Amp Current Limit
Hewlett Packard Model 721A Power Supply (2)	14 Volts, 225mA Short Circuit Current

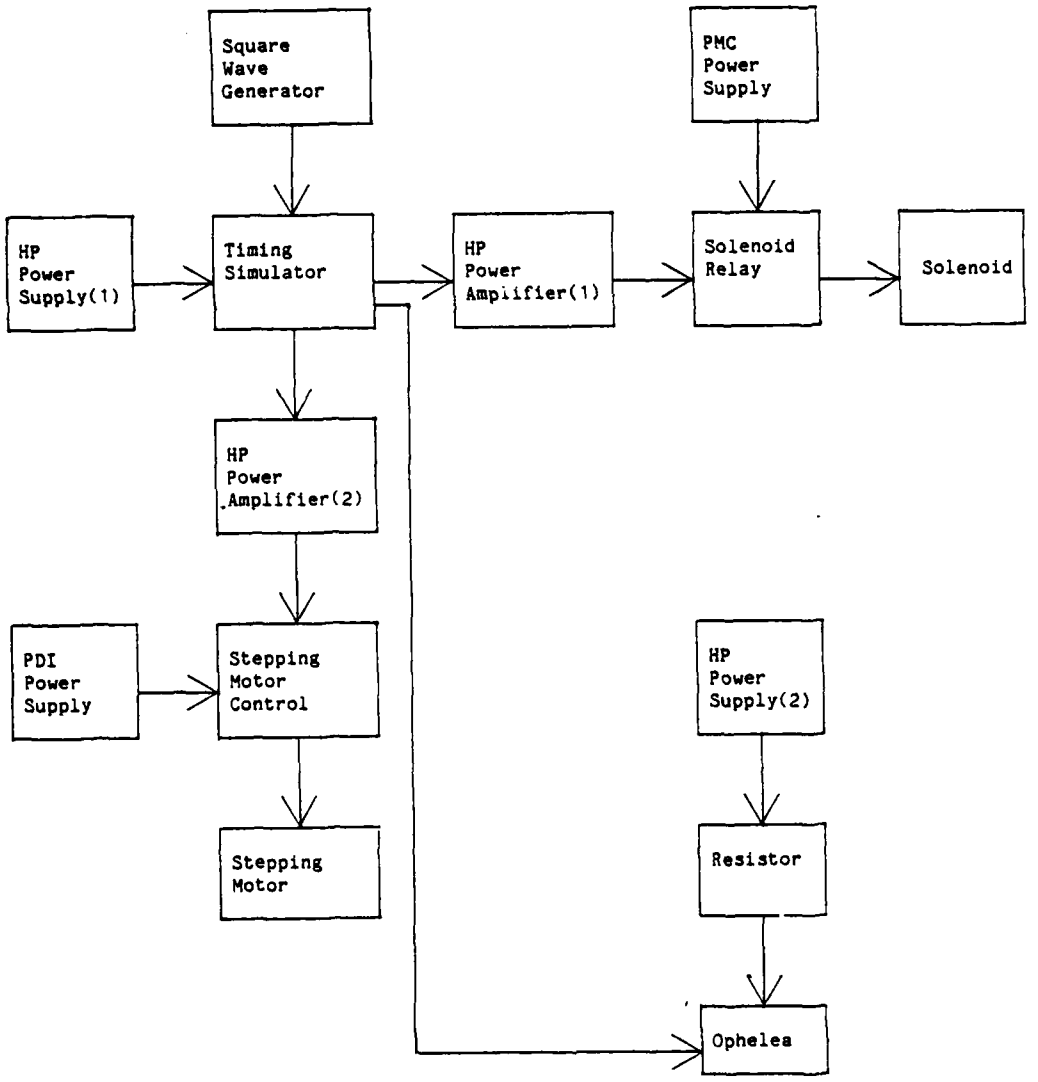

Figure B-7. Equipment Setup.

the number 345 would indicate pin 5 of the chip in the third row and fourth column. A zero indicates that the pin is not connected. Entries at pin locations which are not numbers refer to switches indicated in Figure B-5. SQW stands for the output of the 20 KHz square wave generator.

In addition to the above mentioned equipment, four commercial DC voltage supplies are used to run the device. Two power amplifiers are also needed to step up the output current of the timing simulator for triggering the stepping motor and closing the solenoid relay. A diagram of the equipment setup is given in Figure B-7. Equipment identification and settings are listed in Table B-1.

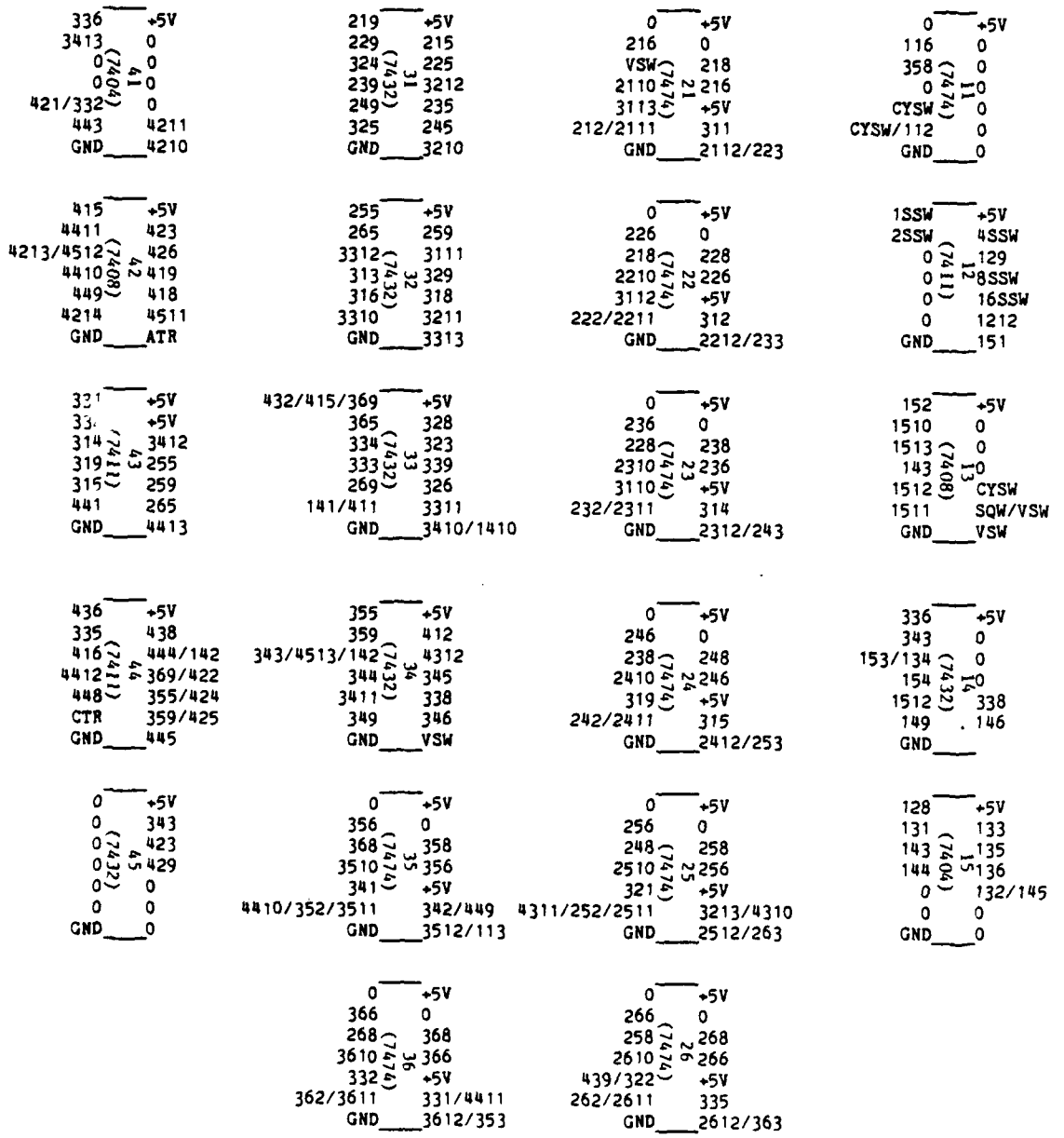

Figure B-6. Pin Connects for Logic Circuit.

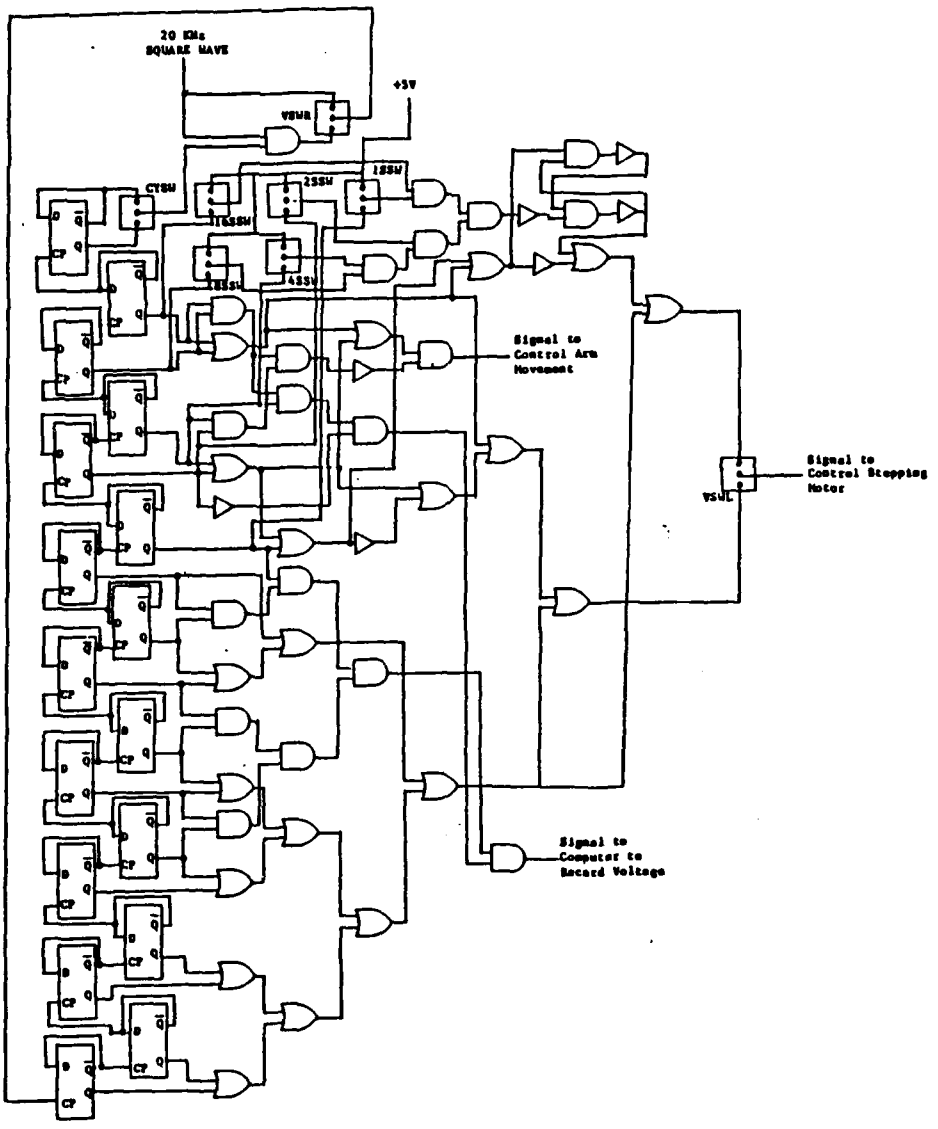

Figure B-5. Logic Circuit to Drive the RSM.

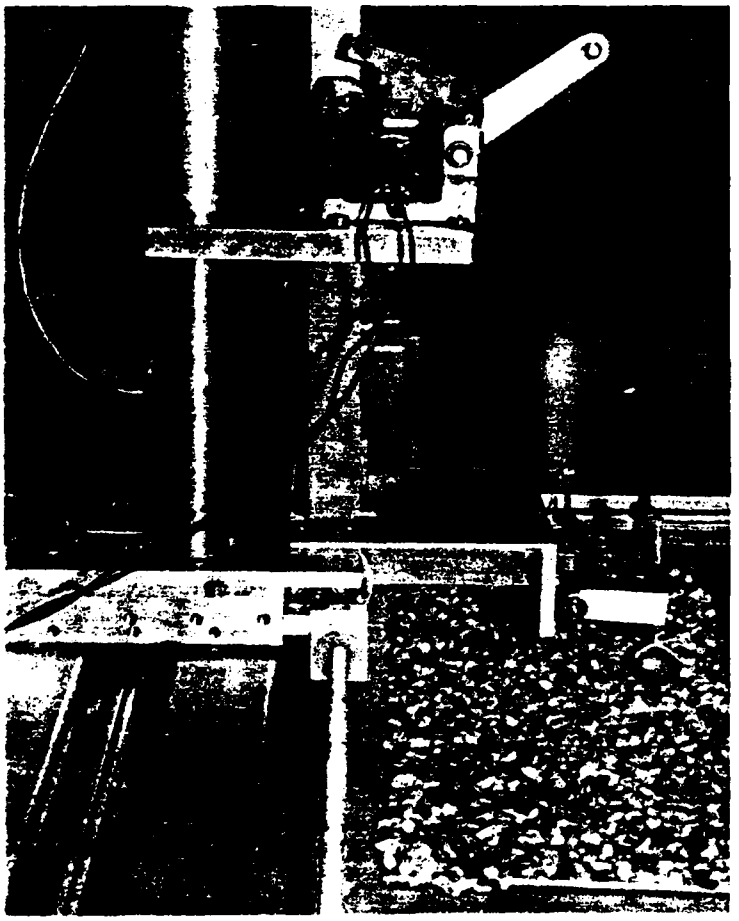

Figure B-4. Solenoid Used to Raise Arm.

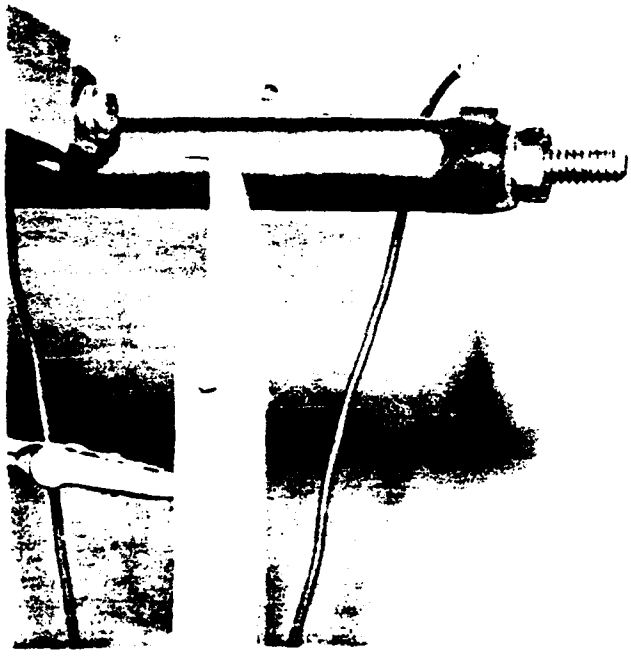

Figure B-3. Wire Wound Resistor and Sliding Contact.

possible needle positions plainly visible. A close up of the wire wound resistor and sliding contact is shown in Figure B-3. Figure B-4 shows the solenoid which raises the arm. The wire connecting the solenoid to the lower part of the arm is visible.

The movement of the arm and stepping motor and data sampling by the computer are sequentially triggered by a logic circuit (Fig. B-5) driven with a 20 KHz square wave. The 16 D type flip-flops are simply used to frequency divide the 20 KHz square wave. (During initial development of the RSM a commercial timing simulator was used in place of the logic circuit and square wave generator.) It should be noted that this timing circuit has a secondary purpose of driving a device not used in this experiment. Consequently additional logic gates and switches are evident in Figure B-5 which are not relevant to the operation of the RSM.

The logic circuit was constructed on standard breadboards with the logic chips arranged in four rows. The pin connections for the chips are given in Figure B-6. Each chip is assigned a two digit number which describes its location on the breadboard. The first digit represents the row the chip is in, the second digit represents its column. This number is located in the center of each chip in the Figure. Below this number is a number indicating the chip type. Each chip has 14 pins. Pin 1 is in the lower left corner for each chip. Pins are numbered successively counter clock-wise around the chip. The numbers at pin locations indicate to which pin(s) that pin is connected. The first two digits indicate the chip, the third (and fourth) digit(s) indicate the pin number of that chip. For example,

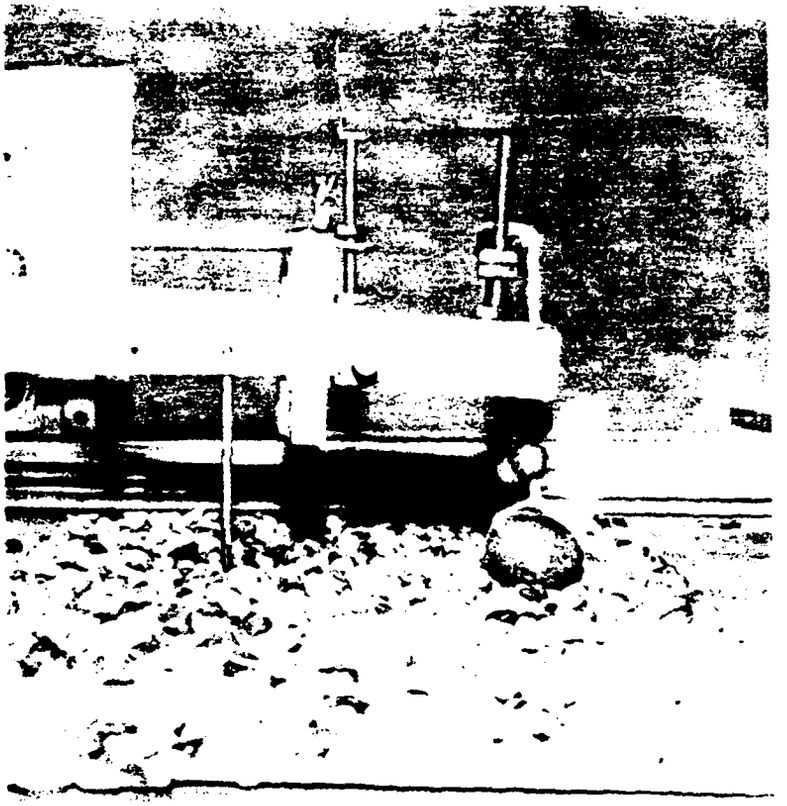

Figure B-2. Needle and Lower Arm.

for placement of the needle for measuring different ranges of roughness. The low end of the range is determined by the minimum height deviation detectable. The high end of the range is determined by the maximum displacement of the needle which will ensure that the sliding contact does not lose contact with the resistor. This is set by the ratio of length of the long arm to length from the pivot point to the needle position. With the needle in the position to provide the greatest resolution, roughnesses in the range of 0.02mm to 2.85mm can be measured. With the needle in the other two positions, the ranges of roughness which can be measured are 0.03mm to 4.28mm and 0.05mm to 5.70mm. Calibration runs were made on a flat glass plate to determine the variance of the readings. Calibration runs along a smooth aluminum wedge were made to determine the voltage to height conversion factors.

After a point is sampled, a relay is closed which energizes a solenoid above the lower section of the arm, raising the arm by a steel wire. A stepping motor is then triggered to turn a threaded positioning rod. The rod moves the arm/needle/resistor assembly over the next point to be sampled. Horizontal spacing between sampled points is 0.0355mm. With only minor changes in the control circuitry, this can be changed to any integral multiple of 0.0071mm.

The surface to be sampled is placed on a flat test bed made of 3/16 inch thick aluminum plate. This plate can be raised or lowered by means of height adjustment screws located at each corner. Downward deflection of the test bed is minimized by inflating the air bladders beneath it.

Figure B-2 is a close up of the needle and lower arm with the three

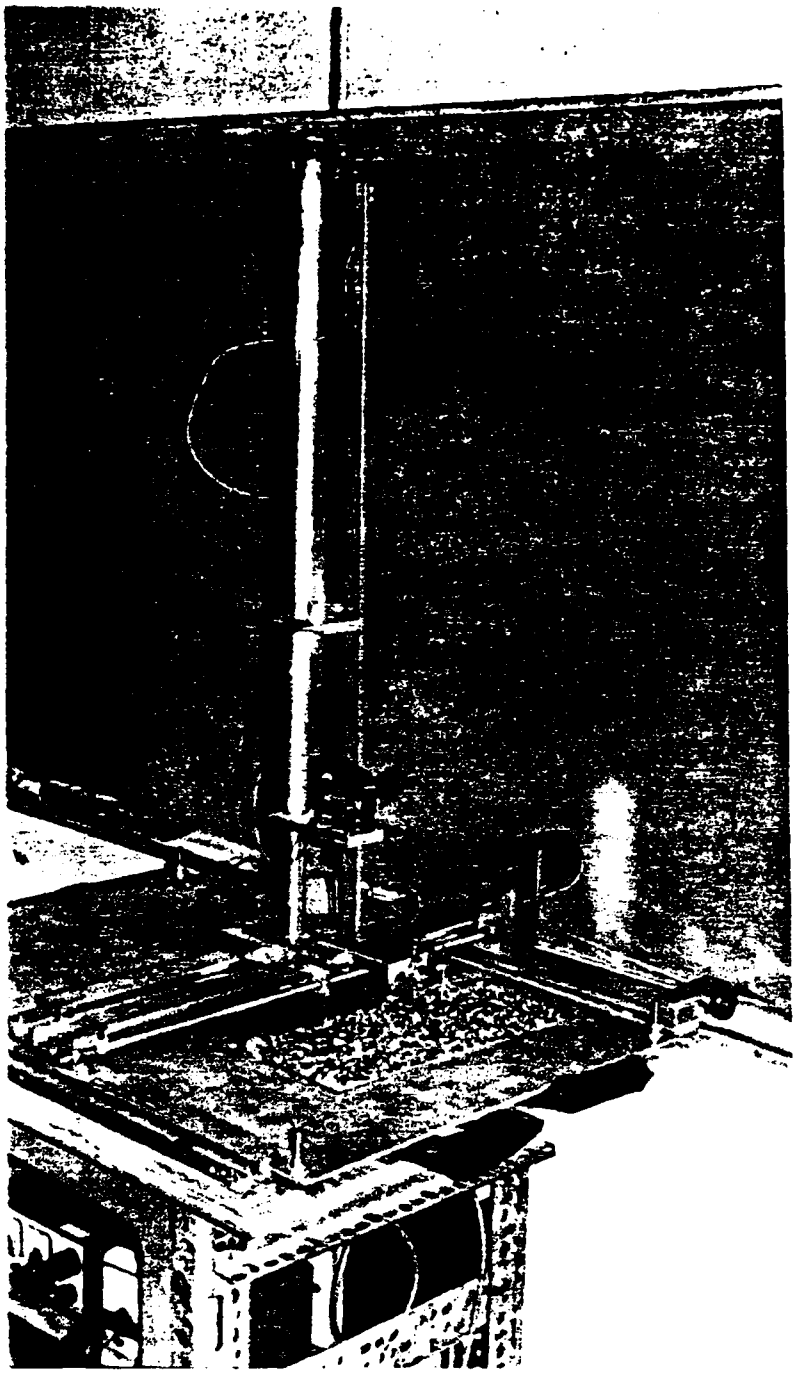

Figure B-1. Random Surface Measuring Device.

APPENDIX B

RANDOM SURFACE MEASURING DEVICE

The random surface measuring device (RSM) measures the height deviation from a mean plane of a surface (roughness) for roughnesses in the range of 0.02mm to 5.7mm with a possible accuracy of 0.02mm. Height measurements are taken at horizontal intervals of 0.0355mm. These height measurements are converted to proportional voltages which are stored directly on OPHELEA's magnetic disk memory. 1024 points, the maximum possible with the software used, are recorded on each data run and processed to give statistics of the surface such as RMS height, RMS slope, and correlation length. The statistics of several runs are then averaged to produce the statistics given in the Section IV which describes the randomly rough surface.

The construction of the RSM is shown in Figure B-1. A constant voltage is applied across the wire wound resistor near the top and can be adjusted with the potentiometer at the base. The "L" shaped arm is the key component with a needle attached under its short section. The long section has an electric contact at its end that slides across the wire wound resistor. The arm pivots freely at the elbow and will rotate by gravity until the needle rests on the rough surface. The voltage difference between the sliding contact and the positive end of the resistor is proportional to the distance the arm has moved for the needle to contact the surface. The voltage is thus a direct measure of the height at that point of the surface.

On the lower part of the arm, there are three possible positions

APPENDIX D

PROGRAM SOURCE CODE

```
FILE: MODES     WATFIV   1                                                    PAGE

$JOB
C$OPTIONS  NOLIST
C PROGRAM MODES   (CREATED BY GLD, 7-30-84)
C    TO DETERMINE THE AMPLITUDE AND PHASE OF N NUMBER OF MODES GIVEN
C    N COMPLEX PRESSURE MEASUREMENTS FROM THE WALL TO THE CENTER IN A
C    HARD-WALLED WAVEGUIDE
C    MAX NUMBER OF MODES THAT CAN BE ANALYZED WITHOUT REDIMENSIONING
C    IS 20
C
      IMPLICIT REAL*8(D),CHARACTER*40(S)
      REAL*4 DIM
      DIMENSION S(20,2),P(20,2),A(20,2)
      DOUBLE PRECISION DCO(20,20),DCOIN(20,20),DWKAREA(460)
      DPI=3.14159265
C INPUT A TITLE TO THE OUTPUT
      READ 5,STUG
      PRINT 6,STUG
    5 FORMAT(A40)
    6 FORMAT(/,3X,A40)
C
C INPUT NUMBER OF FREQUENCIES
C
      READ 10,NFF
C
C  INPUT NUMBER OF RANGES AT WHICH DEPTH MEASUREMENTS WERE MADE
C
      READ 10,NR
   10 FORMAT(I3)
C
C INPUT NUMBER OF MODES N WHICH MUST ALSO EQUAL THE NUMBER OF PRESSURE
C    MEASUREMENTS FROM THE RIGID WALL TO THE CENTER
      READ 10,N
      NN=N-1
C
C INPUT MODE OF LARGEST AMPLITUDE
C
      READ 10,M
      MM=M+1
C
C GENERATE THE COSINE (EIGENFUNCTION) MATRIX
C
      DO 15 I=1,N
      DO 16 J=1,N
      DTEMP=DFLOAT((I-1)*(J-1))/DFLOAT(NN)
      DCO(I,J)=DCOS(DPI*DTEMP)
   16 CONTINUE
   15 CONTINUE
C
C
C
C     PRINT 20
C  20 FORMAT(/,3X,'COSINE MATRIX')
C     DO 21 I=1,N
C     PRINT 22, (DCO(I,J),J=1,N)
C  21 CONTINUE
C  22 FORMAT(20(3X,F5.4))
```

```
C
C  MATRIX INVERSION
C
      IDGT=0
      CALL LINVDF(DCO,N,20,DCOIN,IDGT,PARAM,IER)
C
      PRINT 23,IER
   23 FORMAT(/,5X,' ERROR CODE = ',I4)
C
C
      PRINT 25
   25 FORMAT(/,54,'INVERSE OF COEFF. MATRIX')
      DO 26 I=1,N
      PRINT 27, (DCOIN(I,J),J=1,N)
   26 CONTINUE
```



```
C   27 FORMAT(20(3X,E8.5))
C
      IR=1000
C
      DO 300 IER=1,NER
C
C  INPUT MEASUREMENT FREQUENCY
C
      READ 30,F
   30 FORMAT(F5.0)
C
      PRINT 33,F
   33 FORMAT(///,5X,' MEASUREMENT FREQUENCY = ',F5.0,' HZ')
C
C  INITIALIZE MATRIX BA
C
      DO 35 I=1,N
      BA(I,1)=0.
      BA(I,2)=0.
   35 CONTINUE
C
      DO 99 ISA=1,NP
C
C
C  READ IN RANGE AND N CORRELF EXPOSURE MEASUREMENTS
C   CAUTION: THE REAL AND IMAGINARY VALUES OF THE RECEIVED MUST BE
C   RIGHT-JUSTIFIED TO COL. 12 AND COL. 27 IN THE DATA FILE
C
      READ 10,IR1
      IDB=IR1-IP
      IR=IR1
```

```
C
   40 FORMAT(E12.6,1X,F12.6)
      DO 45 I=1,N
      READ 40, (P(I,J),J=1,2)
      PRINT 46, P(I,1), P(I,2)
   45 CONTINUE
C
C  PRE-MULTIPLY PRESSURE RATIOS BY INVERSE TO GET FINAL RESULT
C
      DO 52 K=1,N
      DO 51 I=1,2
      ST=0.0
      DO 50 J=1,4
      ST=ST+DCOIN(K,J)*P(I,I)
   50 CONTINUE
      S(K,I)=ST
   51 CONTINUE
   52 CONTINUE
C
C  CALCULATE AMPLITUDE AND PHASE
C
      DO 60 I=1,N
      P(I,1)=SQRT(S(I,1)*S(I,1) + S(I,2)*S(I,2))
      P(I,2)=180.*ATAN2(S(I,2),S(I,1))/PI
   60 CONTINUE
C
C  CALCULATE AMP AND PHASE DIFFERENCE IN MODE 3 AND TOTAL ENERGY
C
      ET=0.
      DO 65 I=1,N
      S(I,1)=P(I,1)/P(1,1)
      S(I,2)=P(I,2) - P(1,2)
      ET=ET + P(I,1)*P(I,1)
   65 CONTINUE
C
C
      PRINT 70,N
   70 FORMAT(/,' RANGE = ',I4)
      PRINT 75,N,N
   75 FORMAT('  MODE',I4,'  AMPLITUDE',I4,'  MODE (1-3)',I4,'  E = 1.0E ',
```

FILE: MODES WAVIV A PAG

```
     1I1,54,'% OF TOTAL ENERGY',5X,'PHASE DIFF RE MODE ',I1)
   80 FORMAT(3X,I2,4X,E14.6,3X,F5.4,4X,F7.5,12X,F5.2,13X,F9.4)
      DO 81 I=1,N
      A2=P(I,1)*P(I,1)*100./ET
      PRINT 80,I,P(I,1),P(I,2),S(I,1),A2,S(I,2)
   81 CONTINUE
      PRINT 82, ET
   82 FORMAT(' TOTAL ENERGY FOR A SET OF PRESSURES SQUARED = ',E12.2)
C
      IF (IDR.EQ.0) GO TO 37
```

```
C AMP AND PHASE OF PREVIOUS RANGE
C
C     DO 99 I=1,N
C     RA(I,1)=R(I,1)/PA(I,1)
C     RA(I,2)=S(I,2) - PA(I,2)
C  99 CONTINUE
C
C     FACT=1./(FLOAT(ZER)*F*10.**)
C
C     PRINT 91,FACT
C  91 FORMAT(' MODE',5X,'AMP TO LAST RANGE',5X,'CHANGE OF PHASE LIFE WE
C    1 LAST RANGE',3X,'FACTOR = ',E15.6)
C  92 FORMAT(3X,I2,12X,F6.4,11X,F5.1,3X,F10. )
C     DO 96 I=1,N
C     CIN=RA(I,2)*FACT/360.
C     PRINT 92,I-1,RA(I,1),RA(I,2),CIN
C  96 CONTINUE
C
   97 DO 98 I=1,N
      PA(I,1)=R(I,1)
      PA(I,2)=S(I,2)
   98 CONTINUE
C
C
   99 CONTINUE
  300 CONTINUE
C
C
      STOP
      END
C
C
C
      SUBROUTINE LINV2F (A,N,IA,AINV,IDGT,WKAREA,IER )
C
      DOUBLE PRECISION    A(IA,4),AINV(IA,4),WKAREA(1),ZERO,ONE
      DATA                ONE/1.0D0/,ZERO/0.0D0/
C                                 FIRST EXECUTABLE STATEMENT
C                                 INITIALIZE IER
      IER=0
C                                 SET AINV TO THE 4 X 4
C                                 IDENTITY MATRIX
      DO 100 I = 1,4
         DO 50 J = 1,4
            AINV(I,J) = ZERO
   50    CONTINUE
         AINV(I,I) = ONE
  100 CONTINUE
C                                 COMPUTE THE INVERSE OF A
      CALL LEQT2F (A,4,4,IA,AINV,IDGT,WKAREA,IER)
      IF (IER.EQ.0) GO TO 9005
 9000 CONTINUE
      CALL UERTST (IER,6HLINV2F)
 9005 RETURN
      END
REWIND
```

```
        $JOB
        OPTIONS  NOLIST

        $ENTRY

    NOVEMBER 19 - RANDOMLY ROUGH - MODE 2

     RANGE CODE =    0


     MEASUREMENT FREQUENCY =   7750. HZ
-37.000000      -37.699990
-40.100000      -30.300000
  2.700000       -3.210000
 30.000000       23.699990
 49.699990       58.100000
 51.699990       58.699990
 31.699990       47.300000
  5.400000       15.199990
-36.300000      -31.500000
-54.100000      -11.000000

RANGE =    0
MODE      AMPLITUDE        PHASE (DEG)       RATIO MODE 2        % OF TOTAL ENERGY      PHASE DIFF RE MODE 2
  0        14.452870          99.1622            3.21329              4.16                195.0676
  1        9.285290          -95.8642            2.06473              1.71                 70.1411
  2        67.324180        -155.1034            1.00000             91.84                  0.0000
  3        3.906292          46.5746            0.08679              0.76                202.4880
  4        3.858026          10.7.2138            0.08575              0.73                262.8259
  5        4.308310          -23.3198            0.09580              0.91                242.2854
  6        4.414516          113.0037            0.09816              0.95                249.2090
  7        2.263330          -90.7771            0.05031              0.27                244.0282
  8        5.256336          33.4456             0.03800              0.04                216.0485
  9        4.145026        -111.5695             0.03178              0.03                 24.0354
TOTAL ENERGY FROM SUM OF PRESSURES SQUARED =        4992.11
 32.699990       -13.099990
 29.100000        -7.200000
 14.699990         4.800000
 -5.500000        15.000000
-20.800000        20.499990
-23.100000        17.300000
 -8.400000         2.500000
 15.100000       -10.100000
 38.000000       -24.300000
 46.899990       -47.000000

RANGE =    1
MODE      AMPLITUDE        PHASE (DEG)       RATIO MODE 2        % OF TOTAL ENERGY      PHASE DIFF RE MODE 2
  0         9.187256          -19.4699            0.22607              1.34                 17.4123
  1        14.969510          104.9013            0.36833             11.85                140.3431
  2        40.643990          -36.7615            1.00000             85.44                  0.0000
  3         3.176209          153.1601            0.07815              0.18                196.0425
  4         1.429420         -101.4774            0.03517              0.04                -64.5964
  5         0.327636           78.2584            0.00806              0.00                113.1779
  6         1.207307          -36.4217            0.02970              0.01                -53.5401
  7         0.544308          167.1171            0.01339              0.00                144.0286
  8         0.334229         -142.7764            0.00822              0.00                -97.0377
  9         0.170111          109.6551            0.00422              0.00                146.7367
TOTAL ENERGY FROM SUM OF PRESSURES SQUARED =        1914.75
```

-2.360000	23.100000
-2.560000	18.500000
3.340000	8.780000
11.199990	-3.430000
17.300000	-11.399990
-6.560000	4.750000
-5.130000	3.000000
9.010000	2.630000
3.100000	13.300000
9.370000	19.300000

RANGE = 12

MODE	AMPLITUDE	PHASE (DEG)	AMP RE MODE 2	% OF TOTAL ENERGY	PHASE DIFF RE MODE 2
0	7.231711	59.5082	0.59904	14.54	-37.7853
1	1.446773	113.3785	0.11903	3.57	21.3850
2	12.135620	37.3935	1.00000	40.52	0.0000
3	3.413905	154.4566	0.65233	19.42	57.0631
4	2.434175	101.6284	0.20139	1.65	7.2349
5	7.559299	-37.7034	0.62185	15.67	-135.0960
6	0.810402	128.3327	0.06741	0.16	30.9992
7	4.471429	140.2573	0.36814	5.49	43.8635
8	2.516664	-3.5717	0.20727	1.74	-100.8652
9	0.579880	-78.1513	0.07165	0.21	-175.5745

TOTAL ENERGY FROM SUM OF PRESSURES SQUARED = 584.67

6.743000	4.400000
6.230000	4.310000
6.150000	5.020000
5.430000	4.560000
4.950000	3.920000
4.830000	3.450000
4.370000	3.130000
5.000000	3.440000
5.560000	3.140000
6.130000	2.630000

RANGE = 15

MODE	AMPLITUDE	PHASE (DEG)	AMP RE MODE 2	% OF TOTAL ENERGY	PHASE DIFF RE MODE 2
0	4.704642	35.5964	4.08420	95.54	28.3302
1	1.152344	62.3533	1.53132	2.82	55.1257
2	0.738055	7.2682	1.00000	1.16	0.0000
3	0.264139	-147.1780	0.35829	0.15	-154.4462
4	0.302667	-61.4325	0.41003	0.13	-68.7007
5	0.085689	147.3614	0.11610	0.02	140.0932
6	0.159540	-104.5290	0.21615	0.05	-111.7082
7	0.098324	15.3376	0.13322	0.02	8.0394
8	0.147356	-8.1166	0.20047	0.05	-15.3848
9	0.038626	-139.6669	0.05233	0.00	-146.9351

TOTAL ENERGY FROM SUM OF PRESSURES SQUARED = 47.05

MEASUREMENT FREQUENCY = 15750. HZ

-12.199990	-102.000000
-3.200000	-45.199990
-0.347000	30.100000
-2.500000	14.600000
-6.370000	33.600000
-1.730000	66.800000
14.199990	59.300000
25.100000	18.600000

```
 25.000000      -46.000000
  9.480000      -71.190000

RANGE =   6
MODE      AMPLITUDE       PHASE (DEG)      ARE BE MODE 2      % OF TOTAL ENERGY      PHASE DIFF BE MODE 2
  0          5.012805        12.5778          1.07277              0.41                  98.8194
  1         20.345416      -137.1197          3.24375              5.19                 -50.8777
  2         77.127500       -38.4420          1.00000             77.64                   0.0000
  3          3.510386       -94.5412          0.04549              0.14                 150.7832
  4         27.175360      -133.5568          0.43239              5.94                 -19.3548
  5         10.303360       -33.3568          0.13359              1.33                   3.1952
  6          8.007047      -152.7795          0.10411              1.01                 -16.5373
  7          5.434251        62.6235          0.07111              0.33                 168.8755
  8         14.137340        97.7067          0.18291              2.60                 105.9887
  9         10.254160        67.3015          0.13295              1.37                 173.7435
TOTAL ENERGY FROM SUM OF PRESSURES SQUARED =        7701.31
 12.000000      -16.133330
 14.190000      -15.930000
  7.200000       -9.720000
  2.320000       -6.541200
 -1.510000        5.850000
 -3.630000       12.600000
-11.395330        8.840000
 -4.560000       -0.859030
  3.260000      -14.300000
 10.000000      -23.590000

RANGE =   9
MODE      AMPLITUDE       PHASE (DEG)      ARE BE MODE 2      % OF TOTAL ENERGY      PHASE DIFF BE MODE 2
  0          4.234634        -6[illegible]          0.41910              4.61                  -5.9442
  1          4.670581        -2[illegible]          0.24331              4.63                  28.2203
  2         12.[illegible]       -[illegible]          1.00000             79.79                   0.0000
  3          6.025773       139.6372          0.34135              9.32                 133.0992
  4          2.736737       -27.7[illegible]          0.15[illegible]              1.61                  34.2075
  5          1.373674       113.4653          0.07033              0.41                 173.7573
  6          0.492204      -101.4041          0.02533              0.05                 -46.1122
  7          1.102103       132.[illegible]          0.05711              0.26                 186.5284
  8          0.162431       177.3790          0.02487              0.05                 231.6719
  9          0.361195       130.4436          0.02340              0.05                 190.7356
TOTAL ENERGY FROM SUM OF PRESSURES SQUARED =         771.39
 -3.260000       -6.310[illegible]
  1.770000       -5.630000
  1.100000       -1.060000
  4.170000        2.360000
  5.890000        3.720000
  6.110000        3.120000
  3.770000        1.650000
 -0.457000       -0.63[illegible]000
 -3.770000       -2.930000
 -5.420000       -3.110000

RANGE =   12
MODE      AMPLITUDE       PHASE (DEG)      ARE BE MODE 2      % OF TOTAL ENERGY      PHASE DIFF BE MODE 2
  0          1.011150       -15.[illegible]          0.25403              0.29                 120.9144
  1          1.[illegible]       -[illegible]          0.25513              7.15                 109.1962
  2          0.[illegible]      -135.2720          1.00000             12.01                   0.0000
  3          1.07[illegible]       -[illegible]          3.16[illegible]              2.26                  31.4525
  4          0.327[illegible]       -7[illegible]          0.0[illegible]              0.21                  43.5889
  5          0.[illegible]       141.[illegible]          0.04[illegible]              0.17                 308.2275
  6          0.167[illegible]       141.[illegible]          0.07231              0.43                 281.2590
```

7	0.336233	173.4376	0.73611	0.61	309.7302
8	0.891956	173.7916	0.13803	1.56	300.0642
9	0.393505	174.1332	0.36022	0.33	310.4058

TOTAL ENERGY FROM SUM OF PRESSURES SQUARED = 50.68

0.351000	0.231000
0.305000	0.115000
0.686000	-0.452000
1.490000	-0.884000
2.210000	-1.960000
2.200000	-0.757000
1.730000	-0.576000
0.251000	-0.167000
-1.270000	0.317000
-1.830000	1.180000

RANGE = 15

MODE	AMPLITUDE	PHASE (DEG)	AMP RE MODE 2	% OF TOTAL ENERGY	PHASE DIFF RE MODE 2
0	0.825098	-22.1154	0.47672	15.33	-176.0846
1	0.651068	-20.7582	0.37560	9.34	-174.7290
2	1.730803	153.9708	1.00000	69.31	0.0000
3	0.421399	1.4052	0.24338	4.03	-152.5656
4	0.152132	91.6160	0.08791	0.52	-62.3549
5	0.131135	-59.9946	0.07570	0.13	-213.9655
6	0.093852	46.7271	0.05368	0.20	-107.2437
7	0.063363	-126.7719	0.03707	0.03	-280.7427
8	0.058363	81.0460	0.03333	0.33	-72.9248
9	0.060114	-68.2477	0.03438	0.08	-222.2186

TOTAL ENERGY FROM SUM OF PRESSURES SQUARED = 4.41

MEASUREMENT FREQUENCY = 25000. HZ

-31.000000	-19.000000
-31.699930	-30.300000
-18.129990	-27.800000
2.970000	3.420000
29.000000	10.800000
37.399990	21.300000
33.800000	20.100000
34.399990	-9.700000
2.490000	-6.710000
-25.899990	7.569000

RANGE = 6

MODE	AMPLITUDE	PHASE (DEG)	AMP RE MODE 2	% OF TOTAL ENERGY	PHASE DIFF RE MODE 2
0	11.733020	-11.9074	0.33297	4.91	138.3971
1	28.909250	-156.1051	0.81981	23.17	-6.7705
2	35.263369	-149.3375	1.00000	43.40	0.0000
3	16.485210	6.9722	0.46719	9.43	156.3697
4	13.551540	130.2409	0.38429	6.41	239.6384
5	8.651792	-5.7306	0.24533	2.62	143.6069
6	10.411030	98.7475	0.29524	3.78	248.1450
7	2.335402	139.7766	0.06623	0.17	289.1741
8	1.554011	-3.9534	0.05026	0.14	145.4941
9	0.319336	-31.8096	0.00991	0.00	117.5279

TOTAL ENERGY FROM SUM OF PRESSURES SQUARED = 2005.33

7.760000	6.970000
9.370000	6.160000
5.640000	2.690000
-0.477000	1.960000

-3.960000	0.567000
-7.250000	-1.790000
-10.399990	-1.170000
-8.520000	1.370000
-2.810000	2.670000
2.860000	2.590000

RANGE = 9

MODE	AMPLITUDE	PHASE (DEG)	AMP RE MODE 2	% OF TOTAL ENERGY	PHASE DIFF RE MODE 2
0	2.283327	127.4246	0.34667	4.84	100.2344
1	7.030577	14.5455	1.07876	46.35	-12.5447
2	6.553456	27.1362	1.00000	39.33	0.0000
3	2.177505	-179.2773	0.33176	4.36	-206.4080
4	1.401553	14.8811	0.21354	1.82	-12.2488
5	1.041717	149.8234	0.21364	1.92	122.6982
6	0.533334	-150.7053	0.08121	0.28	-177.8401
7	0.731525	-155.4096	0.11142	0.49	-182.5398
8	0.133145	-103.1175	0.02025	0.02	-130.2477
9	0.313304	177.4249	0.04781	0.09	150.2938

TOTAL ENERGY FROM SUM OF PRESSURES SQUARED = 106.17

-2.800000	0.386400
-2.540000	0.250000
-1.170000	0.952000
0.233000	1.520000
1.360000	1.360000
1.710000	1.970000
1.740000	2.000000
1.510000	1.080000
0.101000	-0.362000
-1.330000	-0.537000

RANGE = 12

MODE	AMPLITUDE	PHASE (DEG)	AMP RE MODE 2	% OF TOTAL ENERGY	PHASE DIFF RE MODE 2
0	1.110604	64.2735	0.46164	13.27	225.9851
1	1.504676	175.9246	0.62606	24.23	320.7354
2	2.097351	-145.7116	1.00000	57.20	0.0000
3	0.355375	55.0294	0.13393	1.45	200.7410
4	0.402269	-143.8817	0.11230	2.12	1.8300
5	0.276150	4.3956	0.13207	1.33	149.7112
6	0.160357	131.5500	0.07647	0.33	277.3015
7	0.150515	-47.9393	0.07177	0.29	97.7723
8	0.070532	78.4930	0.03352	0.06	224.2007
9	0.045396	21.4305	0.02055	0.02	167.1425

TOTAL ENERGY FROM SUM OF PRESSURES SQUARED = 7.69

0.052700	0.918000
-0.211000	1.170000
-0.362000	1.010000
0.016100	0.672000
-0.067300	0.332000
-0.142000	0.430000
-0.513000	0.432000
-0.261000	0.221000
0.034500	-0.157000
0.255000	0.005200

RANGE = 15

MODE	AMPLITUDE	PHASE (DEG)	AMP RE MODE 2	% OF TOTAL ENERGY	PHASE DIFF RE MODE 2
0	0.335785	105.8421	5.66344	33.37	83.8999
1	0.551338	93.8971	5.61409	49.31	71.3549
2	0.074151	21.9422	1.00000	1.27	0.0000

4	0.413337	14.6247	2.47427	0.57	120.6020
5	0.205534	-31.4126	3.13354	2.36	-55.5848
6	0.137038	-94.1330	1.48132	0.72	-75.0758
7	0.342781	35.7255	0.456433	0.25	13.8533
8	0.091185	-31.6603	0.57912	1.22	-56.6230
9	0.004050	131.7732	0.04280	0.30	131.8370
10	0.059754	-138.3450	0.03466	0.51	-158.5281

TOTAL ENERGY FROM SUM OF PRESSURES SQUARED = 0.70

MEASUREMENT FREQUENCY = 11330. Hz

6.630000	19.360010
5.430000	11.030160
5.000000	14.000000
-8.530000	4.230000
-9.710000	-17.100100
-14.300000	-14.300000
-13.000000	-11.300300
-15.691990	-15.190000
-8.000000	2.500300
1.650000	15.190000

RANGE = 0

MODE	AMPLITUDE	PHASE (DEG)	AMP RE MODE 2	% OF TOTAL ENERGY	PHASE DIFF RE MODE 2
0	5.370105	172.3607	0.52851	5.12	111.7845
1	13.496328	61.2403	0.81536	32.12	-13.3360
2	10.477040	74.5762	1.00000	43.01	0.0000
3	4.613340	-162.3475	0.24192	3.82	-188.1437
4	2.486273	11.2267	0.11853	1.06	-56.3475
5	5.421439	-111.7000	0.34516	3.20	-179.3622
6	3.109374	-7.0553	0.13347	1.80	30.2796
7	2.047363	165.4956	0.17291	1.44	96.3194
8	2.397246	-62.0913	0.12753	0.76	-120.2676
9	1.335395	-21.7711	0.11147	0.60	-88.3474

TOTAL ENERGY FROM SUM OF PRESSURES SQUARED = 363.67

4.810000	1.660000
4.110000	1.290000
3.020000	-1.770000
-0.020700	-3.030720
-1.970000	-2.100000
-4.070000	0.200000
-4.570000	-0.420000
-3.810000	-0.910000
-1.150000	0.330000
-1.010000	2.570000

RANGE = 9

MODE	AMPLITUDE	PHASE (DEG)	AMP RE MODE 2	% OF TOTAL ENERGY	PHASE DIFF RE MODE 2
0	0.855094	-173.0557	0.30775	4.00	-137.1367
1	3.517511	-2.3422	1.25533	54.27	-26.7139
2	2.713334	26.0311	1.00000	32.29	0.0000
3	0.933510	157.3440	0.30721	4.00	133.7632
4	0.737576	37.4480	0.27151	2.53	64.3633
5	0.206722	-133.8101	0.07931	0.32	-147.0512
6	1.719183	111.0616	0.21434	0.25	90.7837
7	0.212492	-33.1033	0.07831	0.20	59.0288
8	0.324004	-120.2930	0.11975	0.46	-145.0440
9	0.625753	-7.1024	0.23061	1.72	-96.1840

TOTAL ENERGY FROM SUM OF PRESSURES SQUARED = 22.60

0.324000	1.110000
0.041600	1.400000
0.348000	1.389000
0.345000	0.237000
-0.110000	0.324000
-0.135000	-0.754000
-0.035400	-0.697000
-0.117000	-0.335000
-0.432000	-0.602000
-0.415000	-0.145000

RANGE = 12

MODE	AMPLITUDE	PHASE (DEG)	AMP RE MODE 2	% OF TOTAL ENERGY	PHASE DIFF RE MODE 2
0	0.120343	137.1235	0.28681	0.83	4.3659
1	1.131725	71.5704	2.82337	78.01	-32.1873
2	0.118351	102.7577	1.00000	9.79	0.0000
3	0.223040	-112.2160	0.54483	2.30	-214.9737
4	0.099250	177.6575	0.23715	0.35	74.8399
5	0.137793	-111.5033	0.32921	1.06	-204.3215
6	0.175308	-18.4974	0.42846	1.30	-121.2554
7	0.276283	-70.9508	0.66174	4.29	-172.8484
8	0.017584	49.6040	0.04201	0.02	-53.1537
9	0.110081	31.7683	0.26255	0.75	-10.7887

TOTAL ENERGY FROM SUM OF PRESSURES SQUARED = 1.75

-0.426000	0.489000
-0.378000	0.428000
-0.323000	0.518000
-0.201000	0.127000
0.053800	0.343000
0.012700	0.484000
0.117000	0.027000
0.087700	-0.223000
-0.031800	-0.039170
-0.055700	0.157000

RANGE = 15

MODE	AMPLITUDE	PHASE (DEG)	AMP RE MODE 2	% OF TOTAL ENERGY	PHASE DIFF RE MODE 2
0	0.252215	115.3016	1.62707	25.05	277.4366
1	0.341261	127.0921	2.20083	45.95	289.2271
2	0.155060	-162.1351	1.00000	9.47	0.0000
3	0.040392	-15.9371	0.26011	0.66	146.1980
4	0.137769	90.3455	0.88861	7.47	252.4806
5	0.133324	-78.7706	0.85985	7.53	83.3645
6	0.057431	-90.7373	0.37036	1.30	71.3481
7	0.068006	140.2128	0.44133	1.85	302.3477
8	0.040100	67.7330	0.25861	0.63	229.8081
9	0.022947	77.6469	0.14214	0.15	239.7820

TOTAL ENERGY FROM SUM OF PRESSURES SQUARED = 0.25

STATEMENTS EXECUTED= 141135

CORE USAGE OBJECT CODE= 19576 BYTES,ARRAY AREA= 10664 BYTES,TOTAL AREA AVAILABLE= 371056 BY

DIAGNOSTICS NUMBER OF ERRORS= 0, NUMBER OF WARNINGS= 0, NUMBER OF EXTENSIONS= 2

COMPILE TIME= 0.17 SEC,EXECUTION TIME= 1.52 SEC, 3.33.22 WEDNESDAY 21 NOV 84 WATF

C$STOP

LIST OF REFERENCES

1. Twersky, V., "On the Non-specular Reflection of Plane Waves of Sound," The Journal of the Acoustical Society of America, V. 22 pp. 539-546, September 1950.

2. Biot M., "Reflection on a Rough Surface from an Acoustic Point Source," The Journal of the Acoustical Society of America, V. 29, pp. 1193-1200, November 1957.

3. Tolstoy, I., "Smoothed Boundary Conditions, Coherent Low-frequency Scatter, and Boundary Modes" The Journal of the Acoustical Society of America, V. 75, pp. 1-22, January 1984

4. Tolstoy, I., "Coherent Modes and Boundary Waves in a Rough Walled Acoustic Waveguide,"The Journal of the Acoustical Society of America, V. 75, pp. 1192-1199, April 1983.

5. Dozier, L., "PERUSE: A Numerical Treatment of Rough Surface Scattering for the Parabolic Equation," The Journal of the Acoustical Society of America, V.75, p. 1415-1431, May 1984.

6. McDaniel, S., "Mode Conversion in Shallow-water Sound Propagation," The Journal of the Acoustical Society of America, V. 62, pp. 320-325, August 1977.

7. Medwin, H. and others, "Low-frequency Grazing Propagation over Periodic Steep-sloped Rigid Roughness Elements," The Journal of the Acoustical Society of America, (To be published).

8. Pierce, A., Acoustics, p.534, McGraw-Hill, 1981.

9. Gazanhes, C. and Garnier, J., "Experiments on Single Mode Excitation in Shallow Water Propagation," The Journal of the Acoustical Society of America, V.64, pp. 963-969, April 1983.

10. Sessler, G. and West, J., "Electret Transducers: a Review," The Journal of the Acoustical Society of America, V.53, pp. 1589-1598, 1973.

INITIAL DISTRIBUTION LIST

		No. Copies
1.	Defense Technical Information Center Cameron Station Alexandria, Virginia 22314	2
2.	Library, Code 0142 Naval Postgraduate School Monterey, California 93943	2
3.	Professor H. Medwin, Code 61Md Department of Physics Naval Postgraduate School Monterey, California 93943	5
4.	Dr. J. C. Novarini Av. Cordoba 4190 Cap. Fed. 1188 Buenos Aires Argentina	1
5.	Dr. J. M. McKisik Code 4250A Office of Naval Research 800 N. Quincy Arlington, Virginia 22217	1
6.	Professor C. S. Clay University of Wisconsin 1215 W. Dayton St. Madison, Wisconsin 53706	1
7.	Lt. Stephen R. Kasputis 308 Lake Cliff Dr. Erie, Pennsylvania 16511	1
8.	Lt Paul D. Hill Naval Underwater Systems Center Newport, Rhode Island 02840	2

END

FILMED

6-85

DTIC